2012

Capture and Characterization of Dioxygen Reactive Intermediates in CYP51 Catalysis

Gareth Kent Jennings
Virginia Commonwealth University

School of Pharmacy
Virginia Commonwealth University

This is to certify that the dissertation prepared by Gareth K. Jennings titled "Capture and Characterization of Dioxygen Reactive Intermediates in CYP51 Catalysis" has been approved by his or her committee as satisfactory completion of the dissertation requirement for the degree of Doctor of Philosophy.

John C Hackett, School of Pharmacy

Keith Ellis, School of Pharmacy

Darrell Peterson, School of Medicine

Martin Safo, School of Pharmacy

Tonie Wright, School of Medicine

Richard A. Glennon, Graduate Chair, Medicinal Chemistry

Victor A. Yanchick, Dean, School of Pharmacy

F. Douglas Boudinot, Graduate Dean

Date

Capture and Characterization of Dioxygen Reactive Intermediates in CYP51 Catalysis

A dissertation submitted in partial fulfillment of the requirements for the degree of Doctor of Philosophy at Virginia Commonwealth University.

by

Gareth K. Jennings
Doctor of Philosophy

Director: John C Hackett, Assistant Professor
Department of Medicinal Chemistry

Virginia Commonwealth University
Richmond, Virginia
December 2012

Acknowledgment

Without anyone on this list, I could not have achieved this goal. Thank you. John Hackett, Anuja Modi, Caroline Ritchie, Kakali Sen and Justin Elenewski. Keith Ellis, Darrell Peterson, Martin Safo, Tonie Wright. Tamara Zarubica, Maria Palesis, Shirley Taylor, Richard Moran. Hilda Meth. Dan Tassone, Kim Tassone, Nick Tassone, Nora Tassone, Satjit Brar, Heidi Brar, Anika Brar, Sean Cassidy, Leon Bosch, Sharon Bosch, Jarred Arendse and Esteban Jenkins. Lyndon Aguiar. Geraldine Jennings, Wayne Jennings, Ewan Jennings, Kenneth Jennings, Dellen*é* Jennings and Catherine Bell.

Contents

List of Tables

List of Figures

List of Schemes

Abstract

CAPTURE AND CHARACTERIZATION OF DIOXYGEN REACTIVE INTERMEDIATES IN CYP51 CATALYSIS

By Gareth K. Jennings

A dissertation submitted in partial fulfillment of the requirements for the degree of Doctor of Philosophy at Virginia Commonwealth University.

Virginia Commonwealth University, 2013.

Director: John C Hackett, Assistant Professor, Department of Medicinal Chemistry.

The cytochromes P450 (CYPs) are a superfamily of biological catalysts that are ubiquitous throughout the biological domain. CYPs are heme-*b* containing monooxygenases which oxidize substrates with the help of accessory redox partners. CYP substrates include endogenous compounds required for many biological functions and homeostasis, such as steroids, as well as the majority of clinically used drugs and environmental xenobiotics. The majority of studies that have been performed to date are on P450cam (CYP101) from *Pseudomonas putida*. Of the numerous reactions catalyzed by CYPs, unactivated carbon-carbon bond cleavage, is one of particular versatility. Being unique in their catalytic mechanisms, the C-C bond cleaving enzymes and in particular CYP51 from *Mycobacterium tuberculosis* are though to be capable of utilizing multiple reactive oxygen intermediates. During the process of C-C bond cleavage, CYP51 catalyzes two classical hydroxylation reactions. The final reaction culminates in an enigmatic third step which cleaves a C-C bond, liberates formate, and

installs a 14,15 double bond within its steroid substrate. The mechanism of CYP51s final step is still unclear and the exact activated oxygen species has yet to be observed. CYP51 is also distinct from most CYPs owing to the fact that the acid functionality of the conserved active site "acid-alcohol pair" found in most CYPs, is replaced by a histidine. This study aimed to trap and characterize dioxygen reactive intermediates, and elucidate the role of the unique acid-alcohol pair in the formation and stabilization of these intermediates. This study demonstrates our success in generating, stabilizing, and spectroscopically characterizing reactive dioxygen intermediates in Mtb CYP51. As the life-time of the oxyferrous intermediate in Mtb CYP51 is extremely short at ambient temperatures, this work has shown the laboratory's expertise in being able to generate reduced oxyferrous intermediates at cryogenic temperatures. These intermediates have only been generated in a handful of cytochromes P450 and as such this work adds critical information to the small body of work currently reported.

Introduction

1.1 The Cytochromes P450

1.1.1 Background

The cytochromes P450 (CYPs) are a superfamily of biological catalysts that are ubiquitous throughout the biological domain. CYPs are heme-*b* containing monooxygenases which oxidize substrates with the help of accessory redox partners. Using two reducing equivalents, the CYPs are capable of catalyzing oxygen atom insertion into otherwise unactivated C-H bonds of a substrate (R-H) [1] by the reaction:

$$R - H + \mathrm{O}_2 + NAD(P)H + H^+ \rightarrow R - OH + \mathrm{H}_2\mathrm{O} + NAD(P)^+ \qquad (1.1)$$

The term "cytochrome" refers to proteins that contain a heme prosthetic group that participates in electron transport. In cytochromes P450, "P450" refers to pigment that absorbs at 450 nm in the UV-visible (UV-vis) spectrum following reduction and binding to carbon monoxide [2]. This terminology is still used today even though the preferred naming by the Nomenclature Committee of the International Union of Biochemistry (NCIUB) nomenclature is in fact, "heme-thiolate protein" [3]. The nomenclature applied today, as summarized by Nebert [4, 5], designates the CYP by its gene family denoted by a number, subfamily (if there are more multiple subfamilies) denoted by a letter, and individual gene denoted by a number. The arbitrary cutoff of amino acid identity required for a CYP within a particular family is 40% and

within a particular subfamily is 55% [5]. The enzyme CYP3A4, for example, is part of the CYP3 family, which plays a role in drug and steroid (including testosterone) metabolism. CYP3A4 is also part of the only subfamily of the CYP3 family, namely subfamily A and is expressed from a human gene, denoted in this particular example as 4.

The superfamily can be divided into two classes, based on their electron donor proteins. Type I CYPs are mitochondrial/bacterial proteins which acquire electrons from an iron-sulfur ferredoxin containing an [Fe-S] cluster which has been reduced by an NADH-dependent FAD-containing reductase. All drug and xenobiotic metabolizing proteins are Type II CYPs which utilize an FAD-FMN to reduce a NADPH-cytochrome P450 reductase, which in turn shuttles electrons to the CYP [6]. In both classes, interaction with the CYP and its electron donor is a prerequisite for catalytic activity.

CYP substrates include endogenous compounds required for many biological functions and homeostasis, such as steroids, as well as the majority of clinically used drugs and environmental xenobiotics. As much as 75% of all known drugs encounter CYPs at some point during their metabolism in humans [7, 8]. The documentation and understanding of xenobiotic metabolites is of great importance, owing to the fact that metabolites can be toxic and carcinogenic.

1.1.2 The Cytochrome P450 Catalytic Cycle

As previously stated the in Section 1.1 the CYPs are capable of activating O_2 to a number of reactive oxygen species capable of oxidizing their substrates. The CYPs utilize an iron protoporphyrin IX with a cysteine thiolate axial ligand. As depicted in Scheme 1.1, **A** the resting state of the enzyme is widely accepted as the aquaferric species (the iron is in the ferric (Fe^{3+}) form, and is hexacoordinated with a water molecule as a ligand). In general, as the substrate binds to the enzyme (Scheme 1,

RH) , the water molecule is displaced and the spin state shifts from a hexacoordinated low-spin (LS) state ($S = 1/2$) to a pentacoordinated high-spin (HS) state ($S = 5/2$) (Scheme 1.1, **B**) . This spin shift is accompanied by an increase in the redox potential of the enzyme. In the case of camphor binding to P450cam, the redox potential shifts from -300 mV to -170 mV [9, 10]. In the case of CYP51 from *Mycobacterium tuberculosis*, upon binding estriol, the potential shifts from -375 mV to -225 mV [11]. The ligand-induced shift in spin-state results in a shift of the Soret from 412 - 417 nm in the LS form to 391 - 395 nm in the HS form [1]. The change in conformation of the enzyme on ligand binding has also been implicated in the increased affinity of the P450 for its redox partner [12].

The increase in redox potential affords the first electron transfer from nicotinamide cofactors(NADH or NADPH). This results in the reduction of the heme iron from Fe^{3+} to ferrous (Fe^{2+})**C** (Scheme 1.1). It is at this point of the cycle that O_2 binds to the P450 (Scheme 1.1, **D**). It is speculated that the this species (Fe^{2+}-O_2) has another resonance form (Fe^{3+}-$O_2{}^{-}$) [13, 14] in P450cam. It is important to note that all the species to this point of the catalytic cycle have been observed and characterized experimentally, without excessive challenges in the laboratory.

At this point the oxyferrous species is capable of accepting another electron from its redox partner and forms a ferric peroxo species (Fe^{3+}-$O_2{}^{2-}$) (Scheme 1.1,**E**), which is in turn able to accept a proton and form the hydroperoxo ferric species (Scheme 1.1, **F**) also known as Compound 0 (Cmpd 0). Cmpd 0 is capable of undergoing a second protonation that cleaves the O-O bond releasing water to yield a high-valent iron-oxo complex **G** (Scheme 1.1) known as Compound I (Cmpd I) [15–19]. Cmpd I is an oxoferryl π-cation radical species and is considered to be the most prominant oxidant in CYP catalysis and is recognized as nature's most powerful oxidant. Cmpd I mediates the hydroxylation reaction via a hydrogen atom abstraction/hydroxyl radical

rebound mechanism (Scheme 1.1, **H**) [20]. As the hydroxylated product leaves the active site, it is replaced by a water molecule completing the cycle and regenerating the resting state enzyme.

The catalytic cycle also has three pathways known as uncoupling pathways, which are unproductive with regards to hydroxylation of substrate and ultimately result in the return of the enzyme to the ferric resting state. The first uncoupling is referred to as "autoxidation" (Scheme 1.1, **1**) and occurs when the oxyferrous species (Scheme 1.1, **D**) undergoes a release of a superoxide anion ($O_2^{\cdot -}$) [21]. The second uncoupling occurs when peroxide is released from Cmpd 0 known as a "peroxide shunt"(Scheme 1.1, **2**). Cmpd I is also capable of undergoing a shunt referred to as the "peroxidase shunt" (Scheme 1.1, **3**) and occurs when the oxo-ferryl species undergoes two electron reductions with concomitant protonation of the oxygen, resulting in the aquaferric species. The majority of the uncoupling reactions that occur are autoxidations as result of no substrate being present in the active site [22–24].

1.2 **Cytochrome P450 Structure**

1.2.1 Ligand Recognition and Binding

The majority of studies that have been performed to date are on P450cam (CYP101) from *Pseudomonas putida* owing largely to the fact that it was the first CYP that could be purified in large enough quantities for such studies as it was soluble and highly expressed in *P. putida*. The first crystal structure of CYP101, solved by Poulos [25] in 1985, contributed greatly in the understanding of the active site structure of CYPs. In the last decade, numerous crystal structures have permitted larger generalizations to be made about CYPs with regard to overall structure and active-site architecture. When comparing the crystal structures of these enzymes, it is evident that although

Scheme 1.1

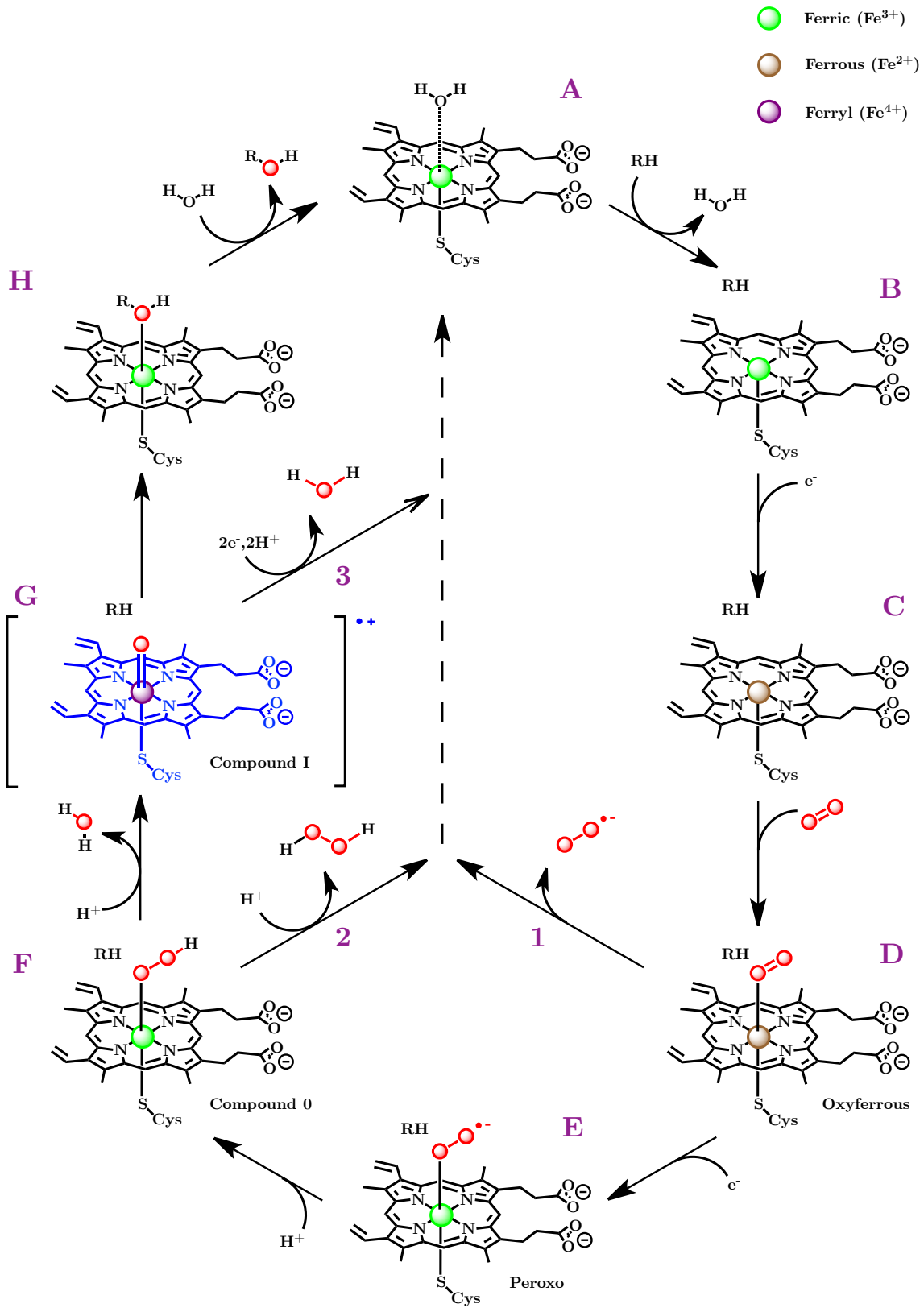
Ferric (Fe^{3+})
Ferrous (Fe^{2+})
Ferryl (Fe^{4+})
A
B
C
D
E
F
G
H
RH
Cys
Compound I
Compound 0
Oxyferrous
Peroxo
1
2
3
e^-
$2e^-,2H^+$
H^+

there is generally low sequence homology ($\sim$ 20%) between members of the CYP superfamily all exhibit similar topology and overall fold [26, 27]. The CYP fold can be divided into α-helical and β-strand-rich domains as seen in Figure 1.2. The inner core of the protein is made up of the N-terminal half of the protein which wraps around the heme and C-terminal half. However, the N-terminal begins in the β-domain (Figure 1.2) and crosses into the helical domain after which as it follows the I-helix it returns to the β-domain [28]. This criss-crossing of the polypeptide has implications in the folding of the protein and incorporation of the heme prosthetic group, since the entire polypeptide must be released from the ribosome prior to protein folding, which complicates expression of the protein in non-native environments [29].

The conserved structures include 11 α-helices (A-K) as well as 5 pairs of β-strands in antiparallel conformation. The variations in the length and shape of these secondary structural elements, affords the variable architecture of the CYP superfamily active sites. This in turn allows for promiscuity in substrate recognition and the diversity of the reactions catalyzed by the enzymes. There are six sites in the CYP structure that are important for substrate recognition and binding known as the "substrate recognition sites" (SRS1-6). The first SRS is found in the loop between the B and C helices (SRS1) and is positioned over the heme. The second and third sites are in segments of the F (SRS2) and G helices (SRS3) which are involved in allowing substrate access to the active site as well as interactions with the membrane, if the enzyme is membrane associated. Another protein segment found to extend over the heme pyrrole ring is part of the I helix (SRS4). The β-turn of the β4 (SRS5), and the K helix-β2 loop (SRS6) are also involved in substrate recognition [30]. These regions confer specificity for substrates and have been shown to drastically alter specificity when mutated [31]. This is also evident in naturally occurring variations as seen in CYP2A4 (testosterone hydroxylation) and CYP2A5 (coumarin hydroxylation), from

the mouse, which differ only in a few amino acids in SRS2 [32–35].

The environment immediately surrounding the heme, which includes the D, E, L and I helices, is the most strongly conserved among members of the CYP superfamily [22,36]. The heme group is is found between the I and L helices and is bound to a loop which has a conserved sequence -Phe-Xaa-Xaa-Gly-Xaa-(His/Arg)-Xaa-Cys-Xaa-Gly-, where the Cys is the cysteine-thiolate which contributes the fifth ligand of the iron of the iron-protoporphyrin IX heterocycle. Prior to the availability of any CYP crystal structures, Dawson confirmed the cysteine-thiolate ligand using magnetic circular dichroism (MCD) spectroscopy [37]. This Cys is critical in mediating CYP chemistry. Structurally, the peptide NH of this Cys residue donates an anti-parallel β strand type hydrogen-bond with an oxygen of the carbonyl of an adjacent residue [25, 28]. This helps form an environment that orients the Cys amongst multiple peptide NH groups with no hydrogen-bond acceptors other than that of the Cys-thiolate as shown in Figure 1.1. These hydrogen-bonds between the peptide NH's and Cys-thiolate are generally accepted as being needed in order to modulate the redox potential of the Fe. With hydrogen-bonds being donated to the Cys, its negative charge is decreased, effectively increasing the redox potential of the system, allowing NAD(P)H or other reductants to reduce the Fe [38, 39]. It is speculated that if these peptide NH hydrogen-bond donors were not present, the Fe would remain in the oxidized Fe(III) state. Density Functional Theory (DFT) calculations have confirmed the ability of these hydrogen-bonds to play a role not only in redox potential of the Fe but also in tuning the reactivity of Cmpd I. The thiolate exhibits radical character during the formation of Cmpd I in these calculations [40]. On the addition of a hydrogen-bond donor to the Cys-thiolate of the model, the radical character shifts to the the porphyrin, this in turn, increases the reactivity of Cmpd I [41, 42].

Another conserved feature amongst CYPs is the disruption of the α-helical

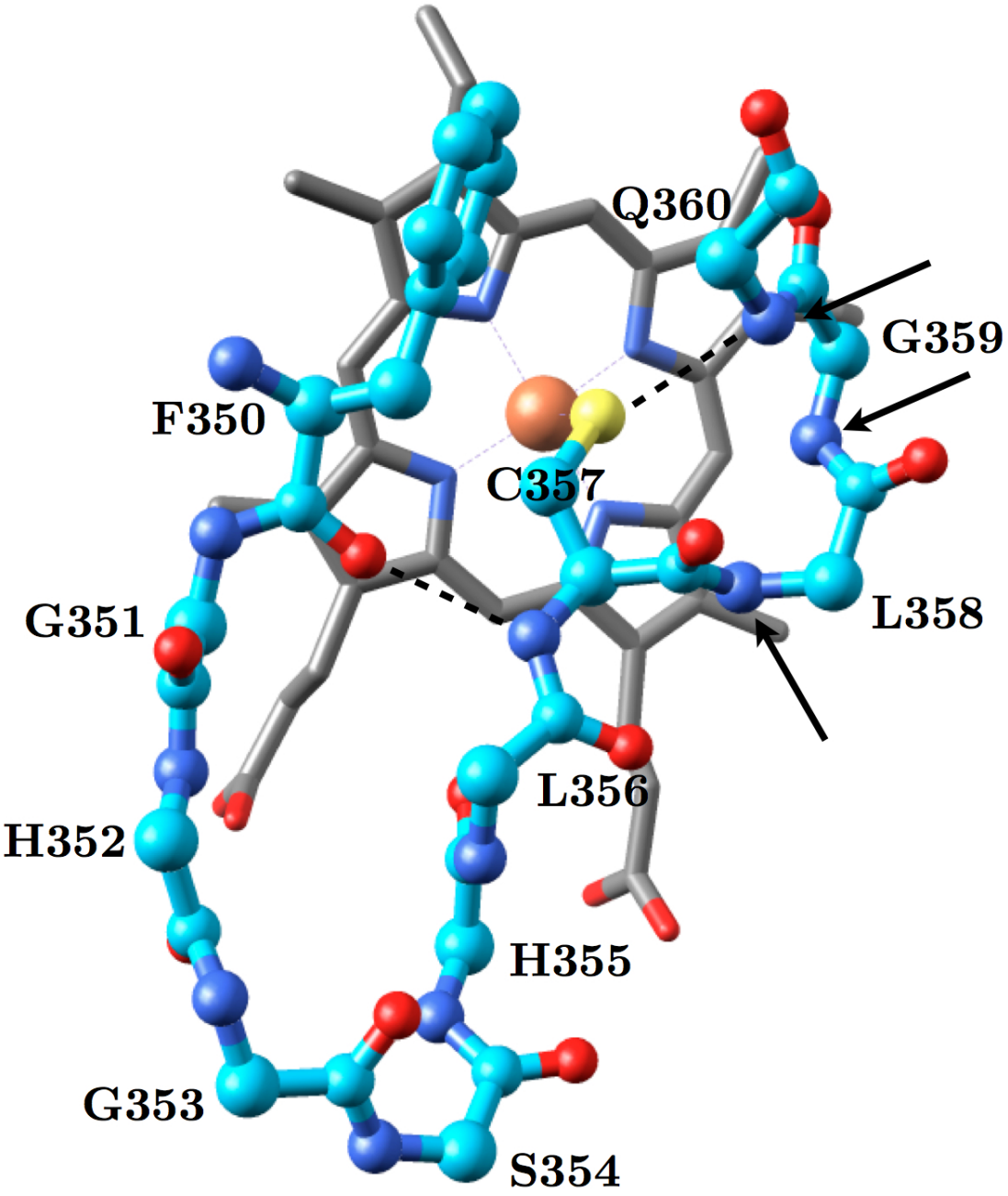

Figure 1.1: The cysteine thiolate ligand loop of CYP101. Arrows point to the peptide N that are oriented around the cysteine thiolate. Dotted lines represent hydrogen bonding.

hydrogen-bonding in the I-helix. This disruption or "kink" occurs near the conserved "acid-alcohol" and creates an opening required for solvent accessibility [43]. Both the distortion in the I-Helix and the resulting solvent accessibility are required in O_2 activation. In the case of CYP51, it too has a "kink" in the I-helix, however there it is unique in that the I-helix is bent by ∼45 degrees [44], which has been implicated as an alternative opening for substrate binding and product release.

1.2.2 The CYP Active Site

When the first crystal structure of CYP101 was published by Poulos [25] in 1985, it became evident that no residues could be definitively assigned as playing a role in proton conduction to the active site [10] as the residues were predominantly hydrophobic and no apparent acid-base catalytic residues were present. It would take alignments of multiple CYP amino acid sequences to determine that within the P450 superfamily two highly conserved residues were present [5, 45]. These were two sequential amino acids that have become known as the conserved "acid-alcohol pair" of the P450 superfamily. In CYP101, Asp251 and Thr252 are oriented directly over the heme plane in the I-helix (Figure 1.4). The "kink" of the I-helix, brought about by the loss of α-helical hydrogen-bonding consists of the conserved sequence -Gly-Gly-Leu-Asp-Thr-. Together, these conserved sequences play a critical role in CYP molecular oxygen activation and catalysis. A number of mutations aimed at the acid-alcohol pair have revealed insight into their function. Due to the Asp251 and Thr252 residues' ability to transfer protons, as well as their close proximity to the heme, it was prudent to determine the role of these amino acids in stabilizing the oxygen complex and mediating proton transfer to the peroxo anion, as shown in Figure 1.5.

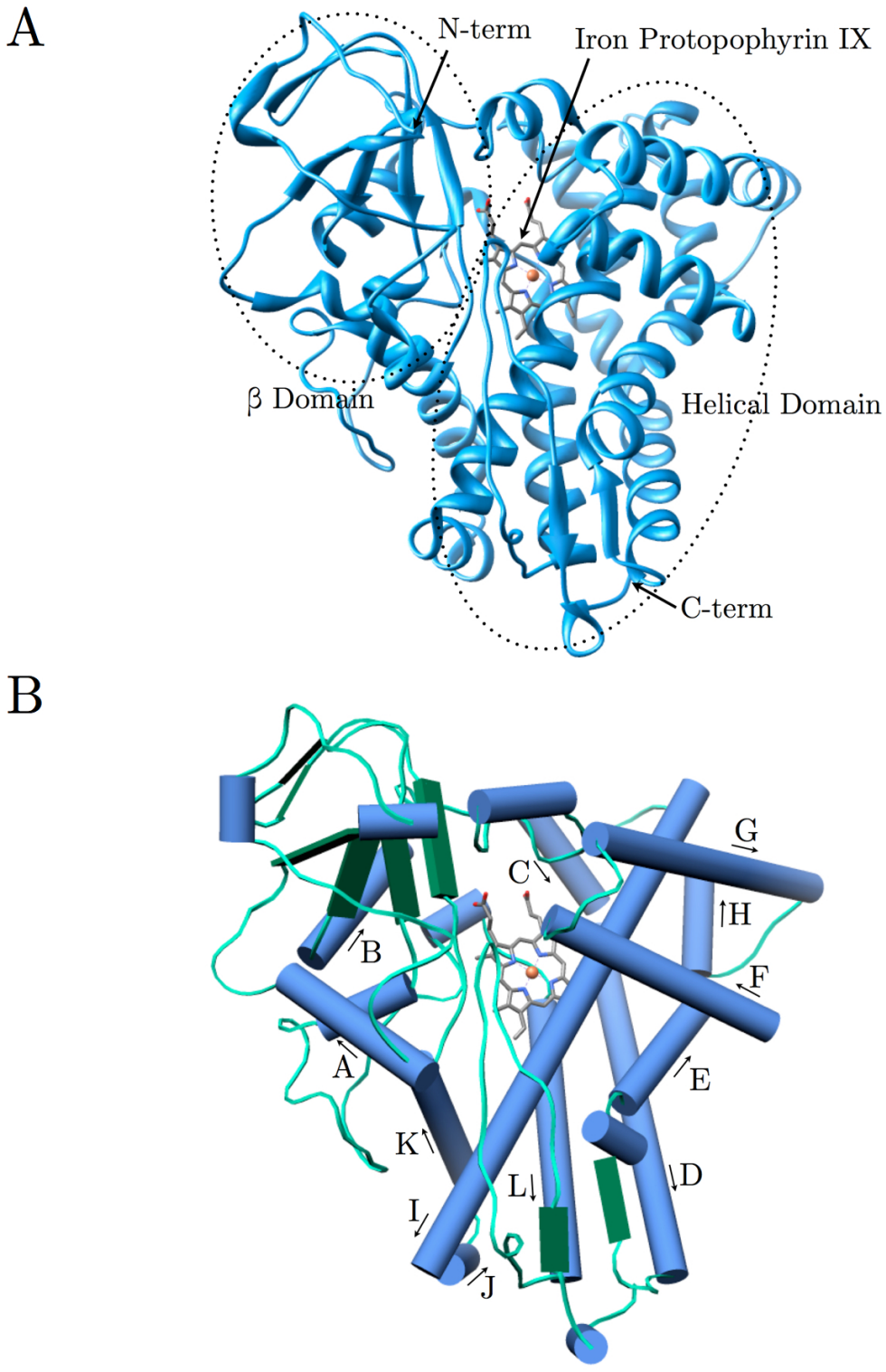

Figure 1.2: A) The general topology of CYP101 (PDB:1DZ8) with helical and β domains. B) Pipe and Plank rendering of CYP101 (PDB:1DZ8). Letters label α helices A through K of the protein with arrows pointing in the direction of N-terminus to the C-terminus.

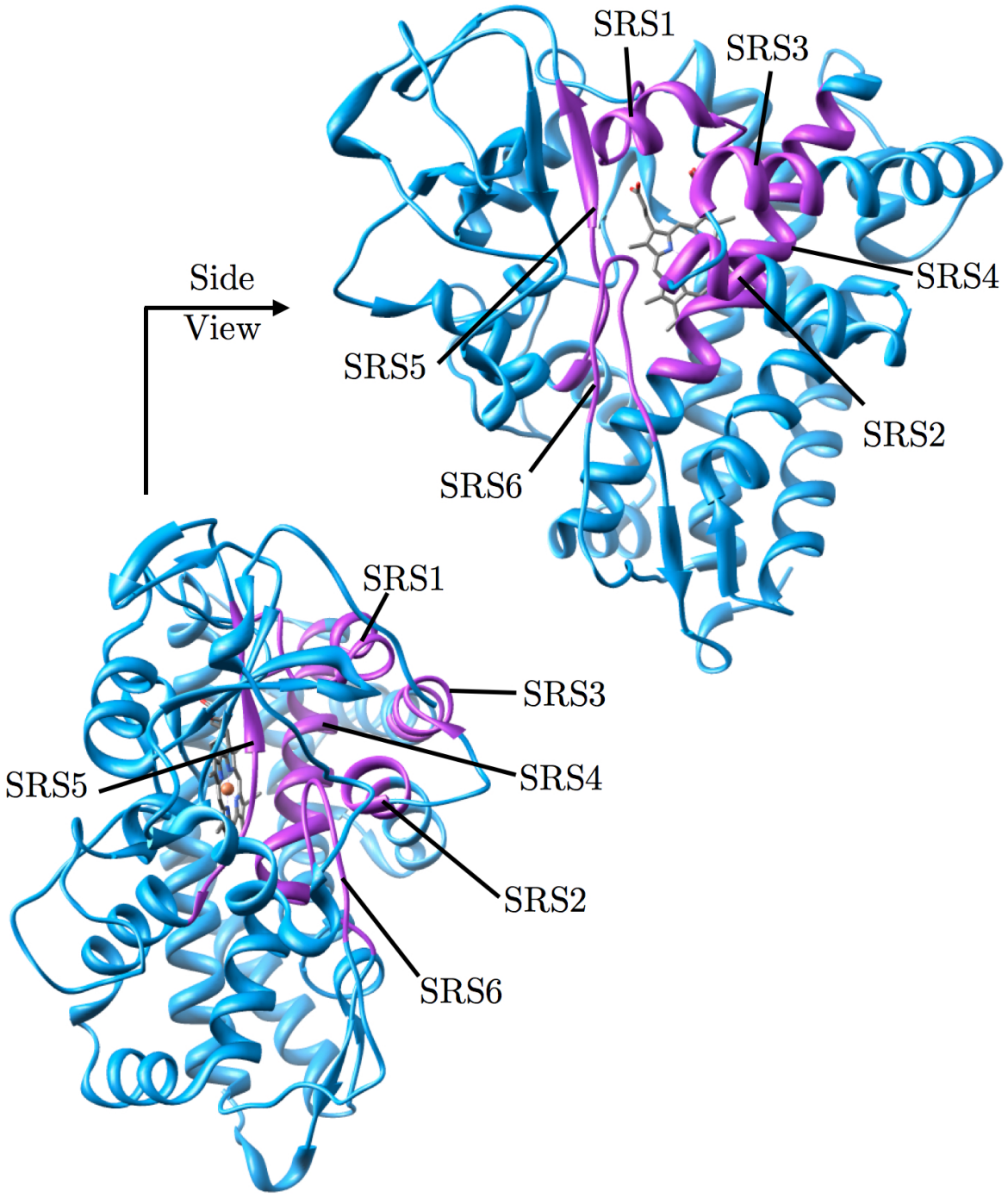

Figure 1.3: Substrate Recognition Sites (SRS) 1 through 6 of the CYP101 crystal structure (PDB:1DZ8). SRS are colored in Purple

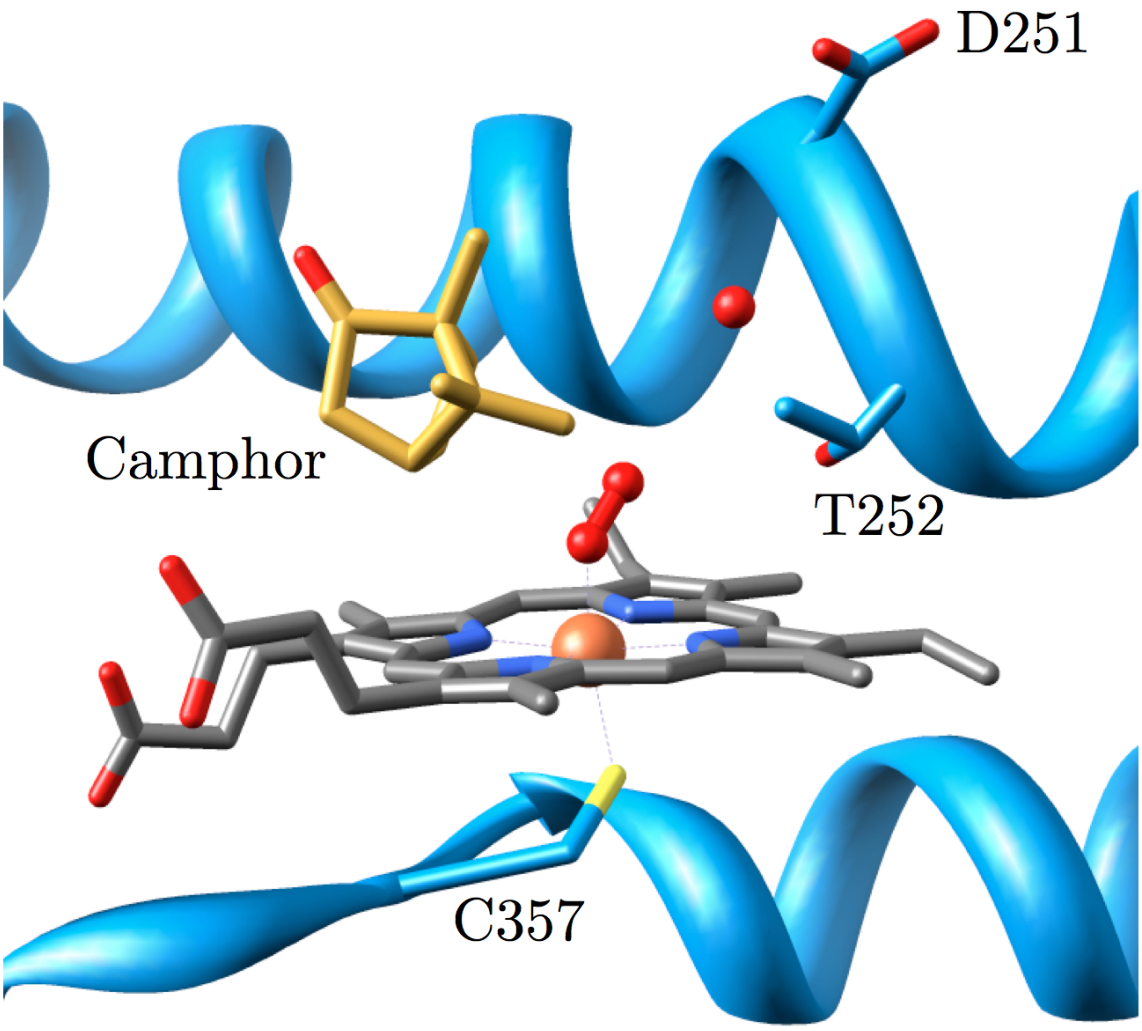

Figure 1.4: The active site structure of CYP101 (PDB:1DZ8), with its subtrate, camphor, bound in the presence of the O_2 bound ferrous heme.

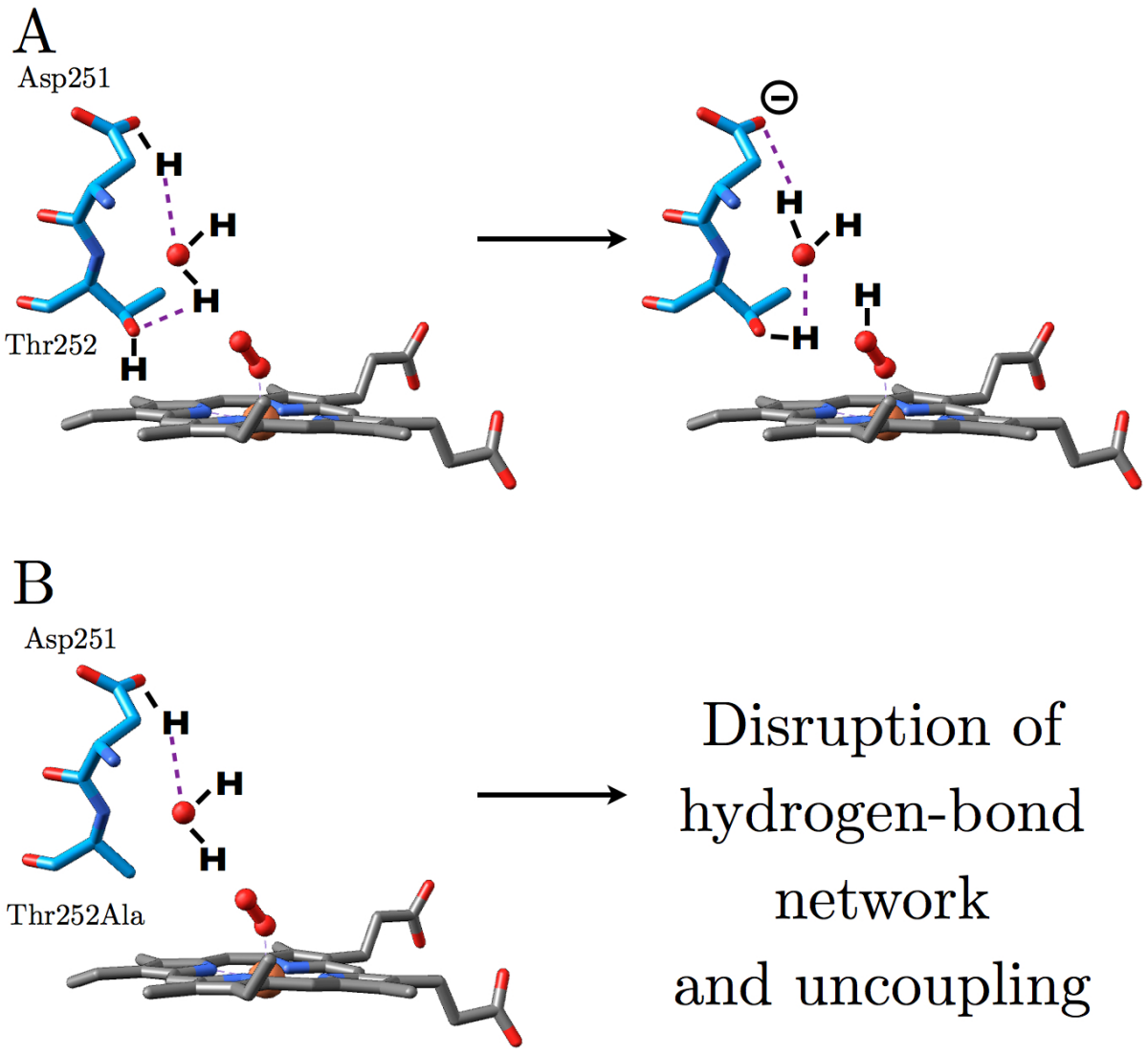

Figure 1.5: A)Schematic of the proposed role of the acid-alcohol pair of CYP101. B) Schematic of uncoupling in the Thr252Ala mutant of CYP101.

When Thr252 was mutated to an Ala an uncoupling of the catalytic cycle occurred, with no evidence of the hydroxylated product (camphor to 5-hydroxycamphor)[46, 47]. However, CYP101 was still capable of accepting two reducing equivalents from NADH, without any significant change to the kinetics of both electron transfer steps. The uncoupling was a result of the enzyme's inability to cleave the O_2 bond and ultimately lead to the release of hydrogen peroxide [47]. These results were explained by the authors in the crystal structure of the mutant [47] where a new water molecule was found to hydrogen-bond to the backbone N-H of the Thr252Ala residue. This was said to play a role in destabilizing the oxyferrous complex. In other mutagenesis studies [48, 49] when Thr252 was replaced with a residue capable of hydrogen-bonding (such as Ser) the extent of uncoupling was diminished. Regardless of the size of the mutant sidechain or its pK_a the requirement was not proton transfer but rather, its ability to hydrogen-bond with a potential secondary proton donor [22]. Unnatural amino acids have also been utilized to study the role of Thr252, with a Thr252Thr-O-methyl being incorporated into the protein, which retained the ability to hydroxylate camphor [50]. This work implied once again that Thr252 was not directly transferring protons to the peroxoanion intermediate, but rather maintaining a water molecule network that was involved in transferring protons. This work however did not address the ability of CYPs to demethylate substrates, potentially removing the methyl group of the unnatural methoxy-Thr effectively rendering the wild type enzyme [10, 22, 51]. In CYP107, this alcohol functionality is not present and is replaced by an Ala. In the crystal structure of CYP107 shown in 1.6 it was seen that an OH of the ligand 6-deoxyerythronolide B (6-DEB) was oriented such that it provided the only direct hydrogen-bond to the distal O_2 atom. It was speculated that this OH of 6-DEB was the most likely candidate as the direct proton donor to the peroxo species [52, 53], in a process referred to as"substrate-assisted catalysis" [54, 55]. This mechanism was

further substantiated by mutation of this Ala to a Thr [55], resulting in loss of product formation (thought to be due to the overlapping of the respective hydroxyls) however the mutant enzyme was now capable of metabolizing other substrates it was previously unable to [10, 56].

The acid residue Asp251 had also been implicated in proton transfer during catalysis, however mutagenesis studies revealed that the role of Asp251 is different to that of Thr252. The bio-isosteric Asp251Asn mutant of CYP101 showed a decrease in the rate of electron transfer from NADH, however 5-hydroxycamphor formation was still occurring, albeit slower, and was shown to be due to the decreased rate of the second electron transfer as well as proton transfer after the formation of the oxyferrous complex [57]. The Asp251Ala and Asp251Gly mutants also produce a similar phenotype to the Asp251Asn mutant [49], implying that the chemical properties of the side chains are less important. Kinetic solvent isotope effect (KSIE) studies of the Asp521Asn mutant [58] showed a drop in turnover by $\sim$5 fold as a result of D_2O addition, implying proton transfer from solvent is the rate limiting step in catalysis of the mutant. In the same study, examination of the influence of pH on the mutant's catalysis was performed, with a linear increase in catalytic rates with the increase of solvent protons being observed, pointing to bulk solvent being the proton donor. This notion was strengthened by the observation of increased accessibility of bulk solvent to the distal pocket due to new salt bridge contacts being formed in the mutant which subjects the heme and distal pocket to greater access from outside of the protein [22, 58]. Combined, these studies point to a general understand that the Asp251 plays a critical role in proton transfer, either directly or indirectly.

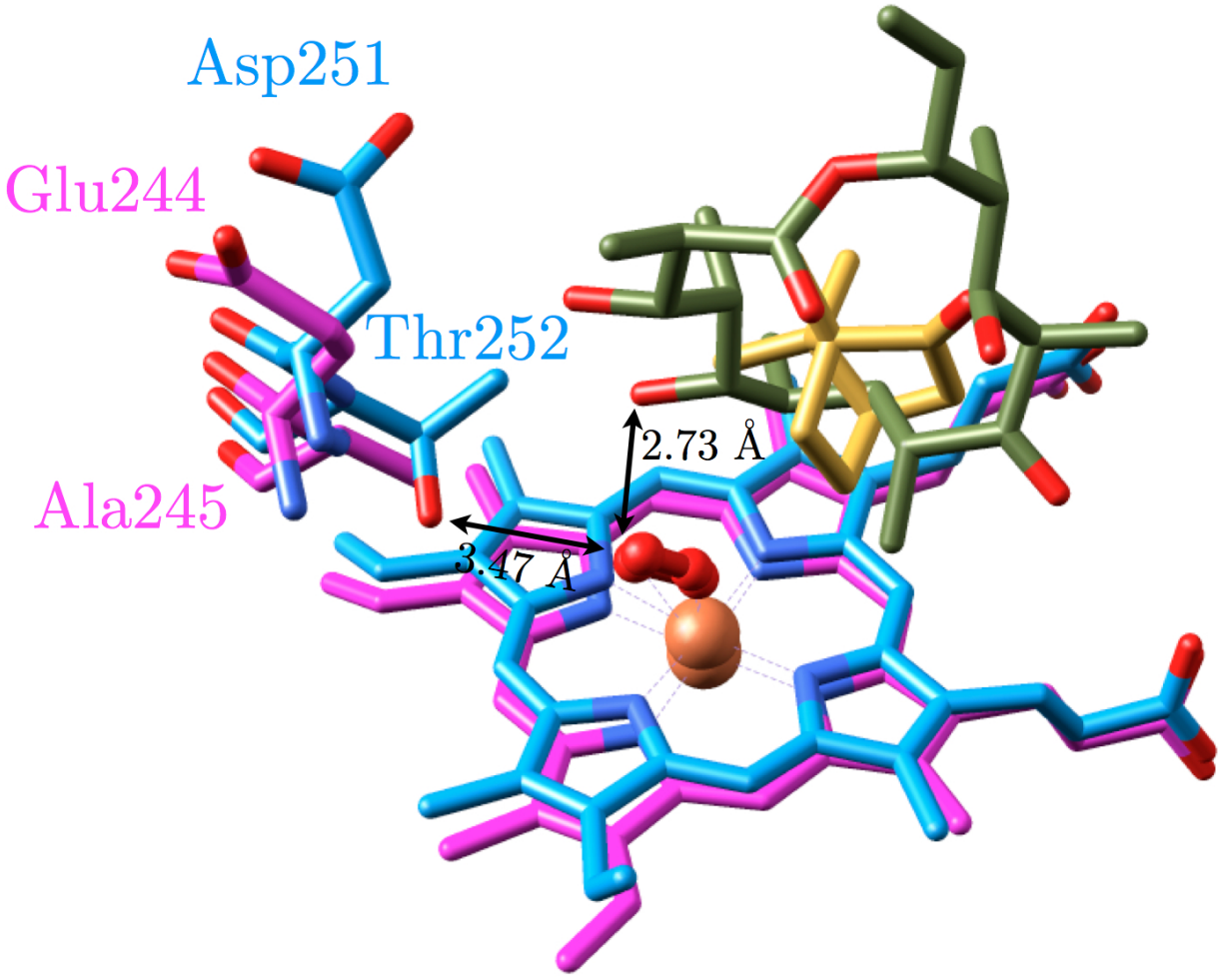

Figure 1.6: The structure of the acid-alcohol pair of CYP101 (blue, PDB:1DZ8), with its substrate, camphor (gold), overlaid with the structure of CYP107 (magenta, PDB:1Z8O), with bound 6-deoxy-erythronolide B (dark green). The double headed arrows indicate the distances between the OH of Thr252 in CYP101 and the distal O atom (3.47 Å) and the OH of 6-deoxy-erythronolide B and the distal O atom (2.73 Å) of their respective structures.

1.3 **Carbon-Carbon Bond Cleaving Enzymes**

1.3.1 Carbon-Carbon Bond Cleaving Reactions

Of the numerous reactions catalyzed by CYPs, unactivated carbon-carbon (C-C hereafter) bond cleavage, illustrates the versatility of the CYP catalytic cycle. This reaction is a critical step in many steroid biosynthetic pathways. These reactions can require multiple passes through the catalytic cycle for C-C bond scission. The C-C cleaving CYPs are capable of tuning the active site to use multiple reactive intermediates. The final C-C cleavage step that is catalyzed can occur between two oxygenated Cs, a C α to an oxygenated C and a C α to a C bearing an N. These final scission steps can occur on substrates which already bear these chemical features or these chemical groups could be a result of previous oxidations by the enzyme.

CYP11A1 ($P450_{scc}$) is a CYP which catalyzes the cleavage of the C20-C22 bond of cholesterol resulting in pregnenalone, the common intermediate in steroid hormone biosynthesis(Scheme 1.2 **A**) [59]. CYP11A1 performs two oxidations on the side chain of cholesterol in typical fashion of CYP oxidation, first hydroxylating C22 of cholesterol resulting in 22R-hydroxycholesterol. The second step hydroxylation step occurs on C20 resulting in 20R,22R-dihydroxycholesterol as the product. The final step results in the cleavage of the side chain between C20 and C22, releasing pregnenolone and 4-methylpentanal [60]. Mass spectrometry studies performed by Burnstein [61] in bovine adrenocortical mitochondria preparations using cholesterol and $^{16}O_2$ and $^{18}O_2$ environments showed the sequential oxidation of the C22 and C20 positions. As each intermediate does not accumulate during catalysis, and both have higher binding affinities for the CYP11A1 than cholesterol, it is expected that these oxidations occur in a sequential manner without the subtrate leaving the active site during each turn of the catalytic cycle [62] and that there is increasing stability of the oxyferrous state

with each intermediate [63]. While the first and second reactions are accepted to proceed through the hydrogen atom abstraction/hydroxyl radical rebound mechanism, the mechanism of the final step is poorly understood. Two mechanisms have been proposed for this final step. The first would require the formation of a hydroperoxide on one of the hydroxyl groups with a CYP activated oxygen intermediate, with this intermediate undergoing heterolytic cleavage as a result of the other hydroxyl group losing a proton, to form two keto-products (Scheme 1.2 **B1**). The second potential pathway is the result of Cmpd I hydrogen atom abstraction from one of the hydroxyl groups resulting in a radical species forming which causes a homolytic C-C cleavage to occur forming a product with a hydroxyl group and a radical situated on the carbon, and an aldehyde group. The Fe(IV)=OH will effectively react with the radical forming the other product (Scheme 1.2 **B2**) [1, 64].

Of particular mechanistic interest is CYP17A, a mammalian CYP involved in pregnenolone and progesterone metabolism [65, 66]. During the metabolism of pregnenolone, the most favored pathway within this enzyme is the initial hydroxylation of C17, followed by the attack of the C20 ketone by the ferric peroxoanion. Homolytic cleavage of the of the peroxo O-O bond then occurs with concomitant release of an acetic acid and formation of an alkoxy radical. Radical rebound occurs onto an Fe(IV)O species with subsequent dehydration of the geminal diol complex resulting in a ketone product (Scheme 1.3 **B1**) [67]. CYP17A is also capable of catalyzing C17-C20 cleavage in pregnenolone through an alternative pathway, resulting in two different products (Scheme 1.3 **B2**). This pathway requires that pregnenolone does not undergo the initial C17 hydroxylation, but rather peroxyanion attack of the carbonyl C20 resulting in the release of acetic acid and a radical product. This can undergo either oxygen rebound forming a hydroxylated product or a dismutation resulting in an alkene product [67]. Mutation of the alcohol (Thr306Ala) of the acid alcohol pair in

Scheme 1.2

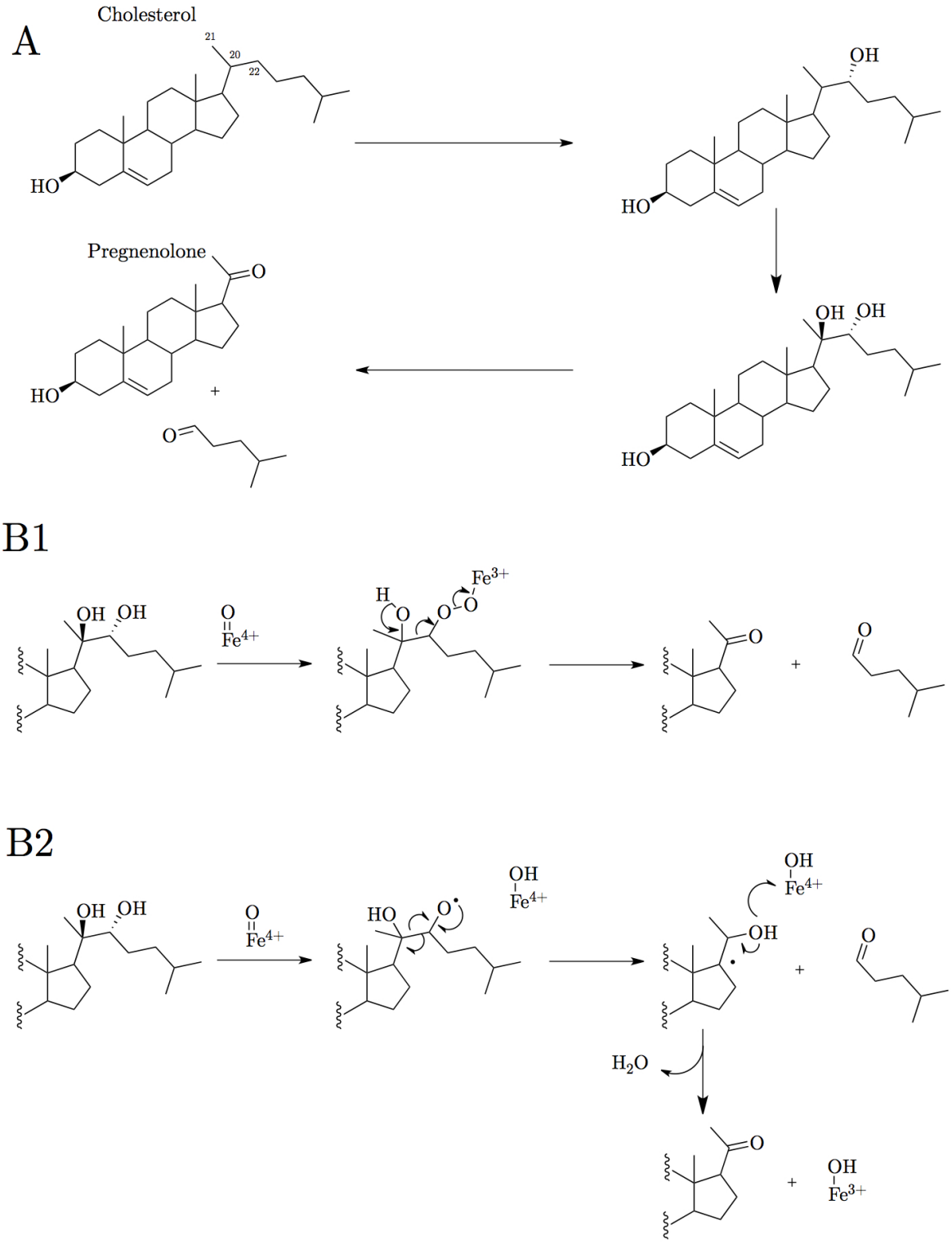
A
Cholesterol
21
20
22
HO
OH
OH
OH
HO
Pregnenolone
O
HO
+
O
B1
OH
OH
O
Fe4+
H
O
O
O
Fe3+
O
+
O
B2
OH
OH
O
Fe4+
HO
O
OH
Fe4+
OH
Fe4+
OH
+
O
H2O
O
+
OH
Fe3+

CYP17A[68], resulted in a drastically decreased formation of the initial hydroxylation step of C17 in pregnenolone and is thought that this mutation disrupts the proton delivery mechanism required for the formation of Cmpd I which is required in the initial hydroxylation reaction [1, 64].

Two examples of enzymes which cleave C-C bonds adjacent to aldehydes are CYP51 and CYP19. Both are steroid biosynthetic enzymes which perform three sequential oxidations in order to perform bond scission. As CYP51 will be discussed in more detail in following sections, the focus will immediately shift to CYP19. CYP19 also known as aromatase, catalyzes the aromatization of androstenedione to estrone (Scheme 1.4 **A**) [69–71]. Drugs targeting CYP19 in humans, called aromatase inhibitors, have been developed for the treatment of estrogen-positive breast cancers [72, 73]. It should be highlighted using CYP19 as a pertinent example that understanding the mechanistic details of its specific catalytic pathway is critical for the design of such inhibitors. The importance of this understanding extends to any CYP protein that could be considered a therapeutic target, so as to develop drugs with high specificity and efficacy.

In trying to understand the catalytic mechanism of CYP19 it is important to identify the products of the three oxidative steps and their reactive oxygen intermediates operative in each step. The aldehyde in Scheme 1.4 **B1**, is a good candidate for oxidation by a ferric peroxide intermediate, this mechanism was used to rationalize the observation of the fate of $^{18}O_2$ and $^{16}O_2$ during CYP19 catalysis in the work of Akhtar and coworkers [74]. In summary their work showed that that formic acid which is released in the third catalytic step bears oxygen atoms from the first and third oxidation steps. This work is summarized in Scheme 1.5. This evidence allows for a much smaller set of possible reaction mechanisms with the generally accepted mechanism being the reaction of the ferric peroxide attack on the C19 carbonyl yielding a peroxohemiacetal intermediate. This intermediate undergoes fragmentation

Scheme 1.3

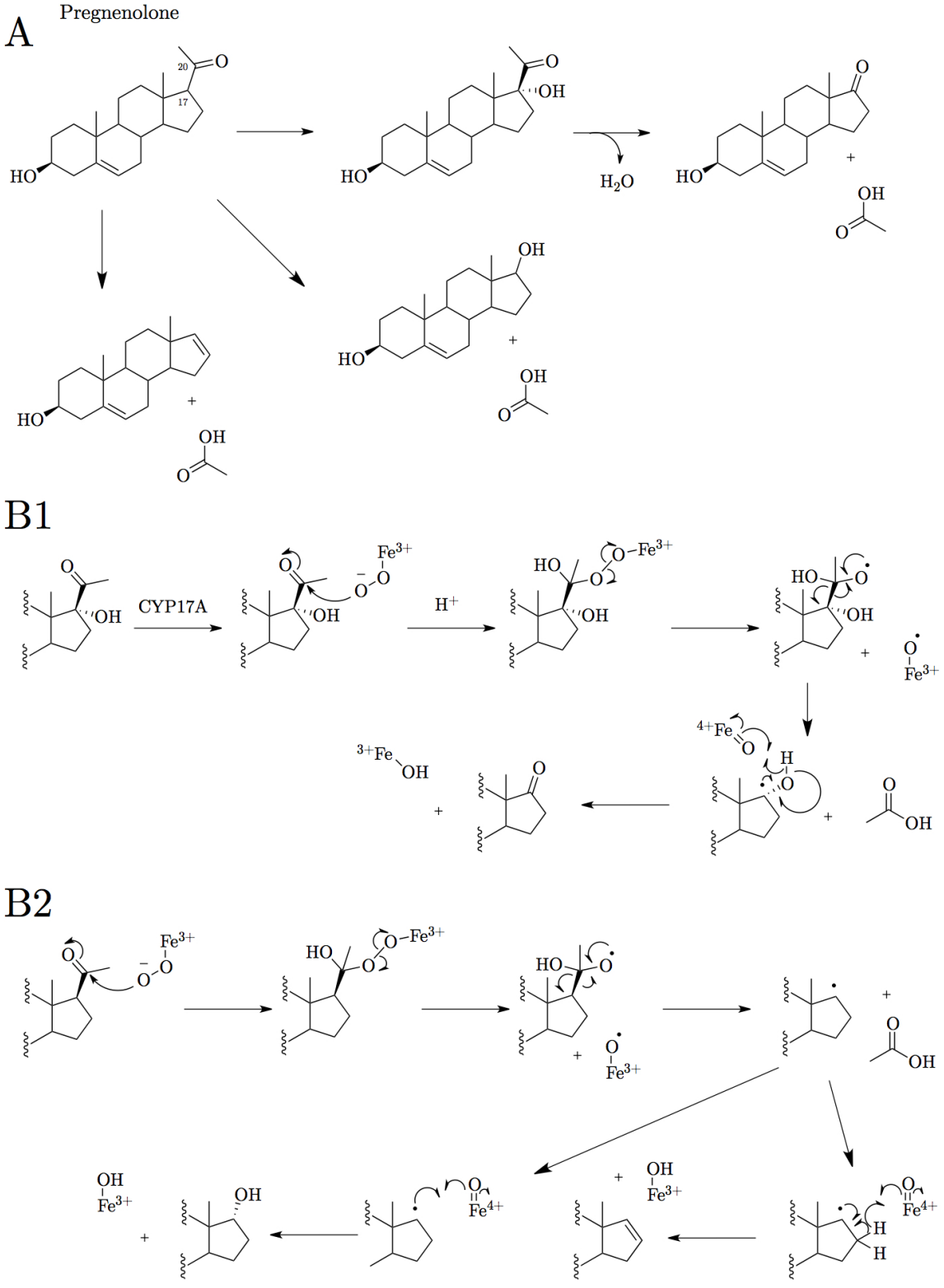

forming an alkoxy radical, which ultimately is released as formic acid after enolization, resulting in a C10 radical. After hydrogen atom abstraction of the 1βH, aromatization occurs [1, 64, 75, 76].

Delving deeper into details pertaining to the exact Iron-oxo species performing catalysis, Sen and Hackett, using molecular dynamics simulation and hybrid quantum mechanics/molecular mechanics in combination with the recently published CYP19A1 crystal structure (PDB ID: 3EQM [77]) showed a kinetic advantage of one mechanism (Scheme 1.4 **B2**) over that of any other proposed mechanisms, which supported the formation of a peroxohemiacetal and C-C cleavage occurring as a concerted step, after which formate is released. Cmpd II will perform hydrogen atom abstraction followed by stereoselective enolization where Fe(III)-OH deprotonates the 2β-position. The authors highlight key intermediates which would be experimentally observable (within current laboratory means) and offer explanations as to why the proposed intermediates have yet to be observed due to such transient lifetimes. They also highlight the role of critical amino acids in stabilization of catalytic intermediates. These theoretical insights into CYP catalytic mechanism illustrate the synergism afforded by the cooperation between theory and experiment.

Numerous catalytic mechanisms have been proposed for the final catalytic step of CYP19 [78–80]. The aldehyde which is formed through two turns of the CYP19 catalytic cycle (Scheme 1.4 **A**) has been generally accepted as being the intermediate through which ferric-peroxo can oxidize the carbonyl carbon.

1.3.2 Sterol 14α-Demethylases as Models of C-C Bond Cleaving Enzymes

Of particular interest, within the group of CYPs catalyzing C-C bond cleavage, are the sterol 14α-demethylases (CYP51). These homologs are among the most ubiquitous and ancient of the CYP superfamily and found in the all biological domains [81–83]. As

Scheme 1.4

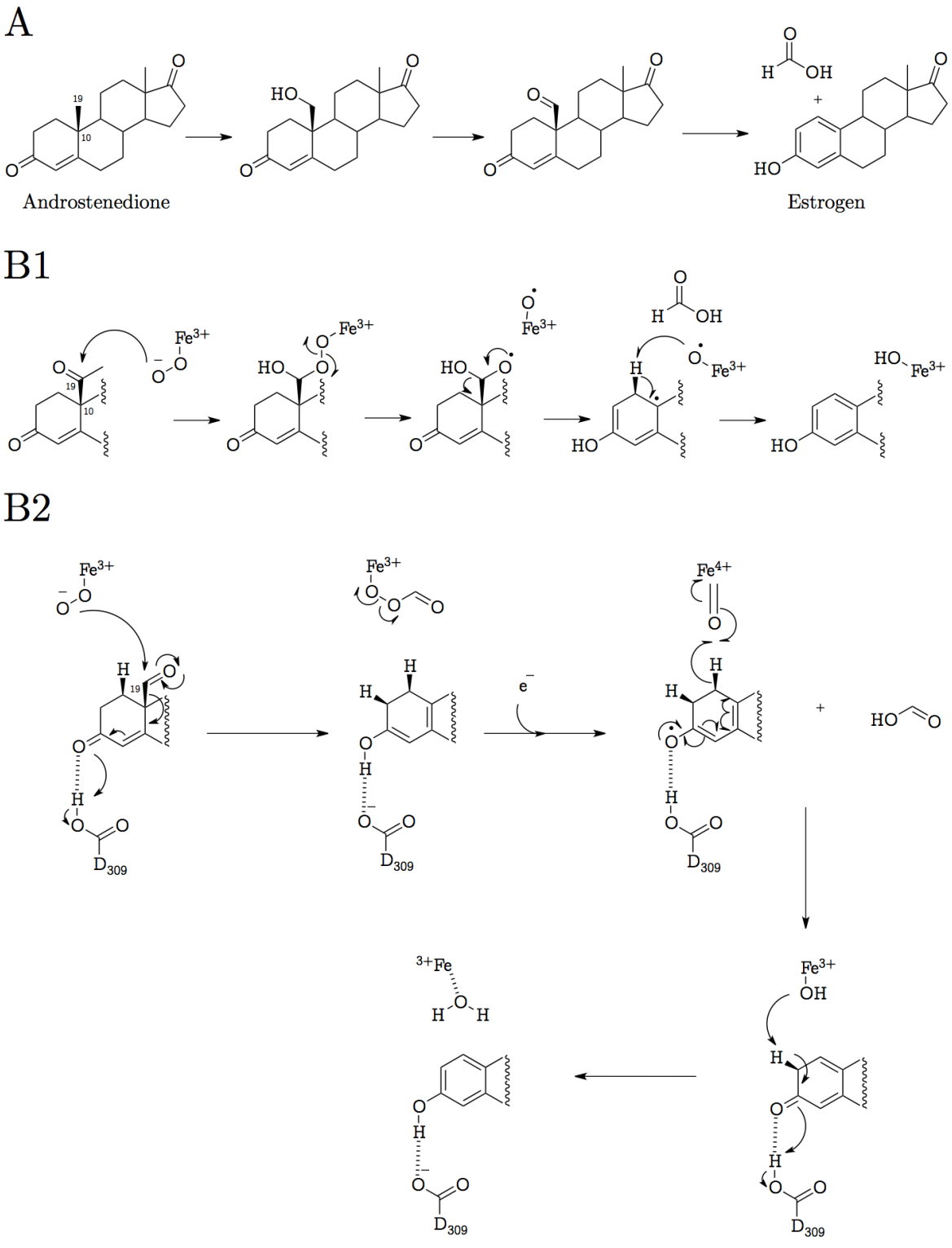

Scheme 1.5

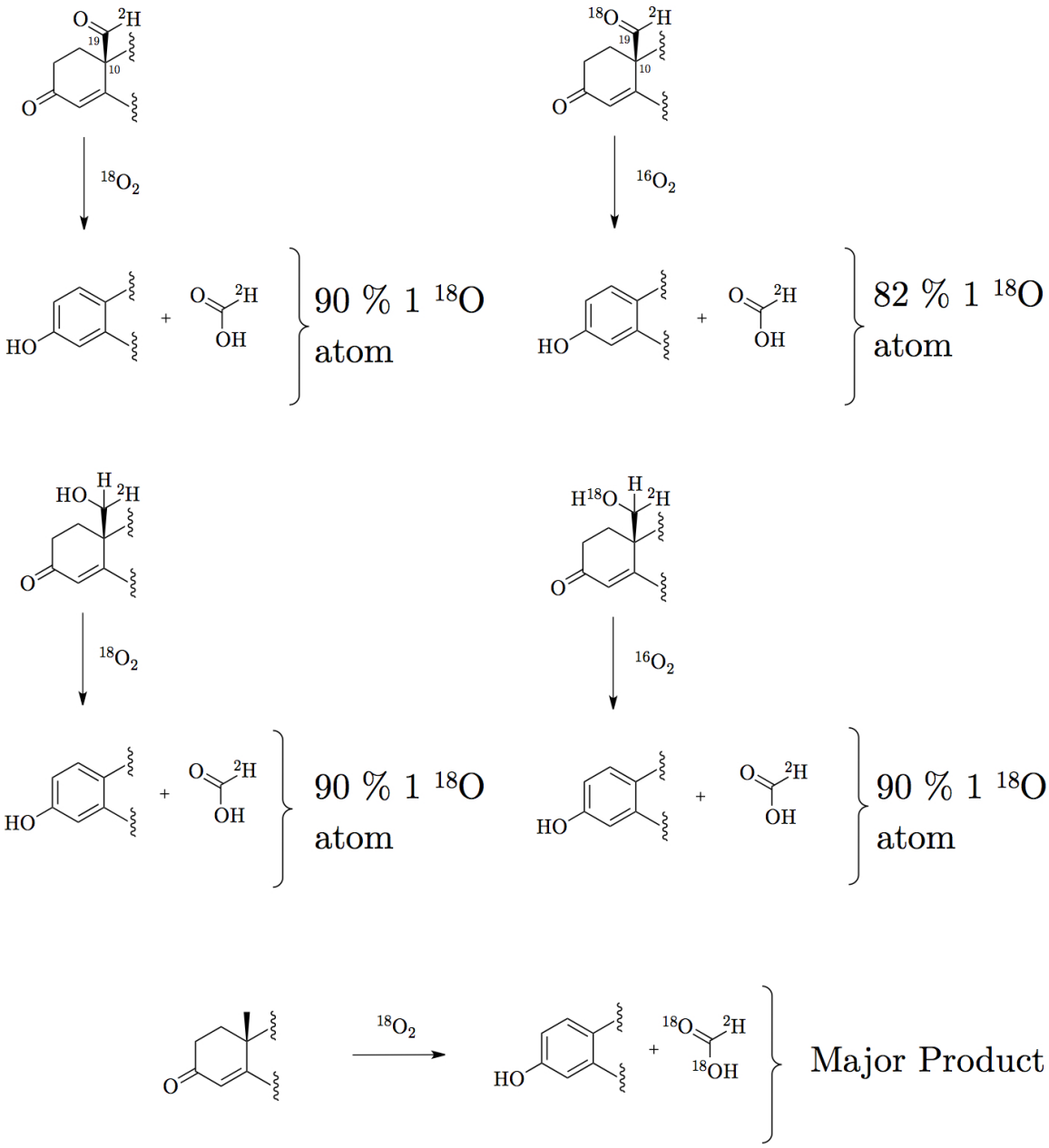
$^{18}O_2$
$^{16}O_2$
90 % 1 ^{18}O atom
82 % 1 ^{18}O atom
90 % 1 ^{18}O atom
90 % 1 ^{18}O atom
Major Product

shown in Scheme 1.6, using dihydrolanosterol (DHL) as an exmple, it has been shown that the reaction occurs in three turns of the catalytic cycle, each using one molecule of O_2 and two reducing equivalents supplied by NADPH. The first two turns of the cycle are simple monooxygenation reactions, with the first product being a geminal diol as seen in Scheme 1.6 and the second being a geminal diol. The geminal diol may undergo a dehydration step ultimately resulting in an aldehyde product [74, 84, 85]. During the final step, formate is released and the 15α hydrogen atom is removed from the substrate. The mechanism of this final step is still unclear and the exact activated oxygen species has yet to be observed. Some mechanistic insight was provided by studies conducted by Shyadehi and coworkers using *Candida albicans* CYP51 and 32-^{18}O and 32-^{16}O labeled aldehyde intermediates [84]. Unfortunately, however, a number of catalytic mechanisms could be postulated that are consistent with the observed isotope ditributions in the products. Although the proposed mechanism was mediated by peroxo or Cmpd 0, there is still the possibility that the C-C cleavage step may be Cmpd I mediated.

1.4 *Mycobacterium tuberculosis* CYP51 as a model of C-C bond cleaving

1.4.1 Structure

The sequencing and annotation of the entire genome of *Mycobacterium tuberculosis* (*M. tuberculosis*, Mtb) strain H37Rv [86, 87] was an important step in determining drug targets for this bacterial pathogen. The information acquired from this study was the starting point for researchers to understand proteins within *M.tuberculosis*. Sequencing revealed that *M.tuberculosis* genome codes for up to 20 putative Cytochromes P450, including a CYP51-like (gene *Rv0764c*). CYP51 is a known target of azole drugs such as clotrimazole and fluconazole in the treatment of fungal infections,

Scheme 1.6

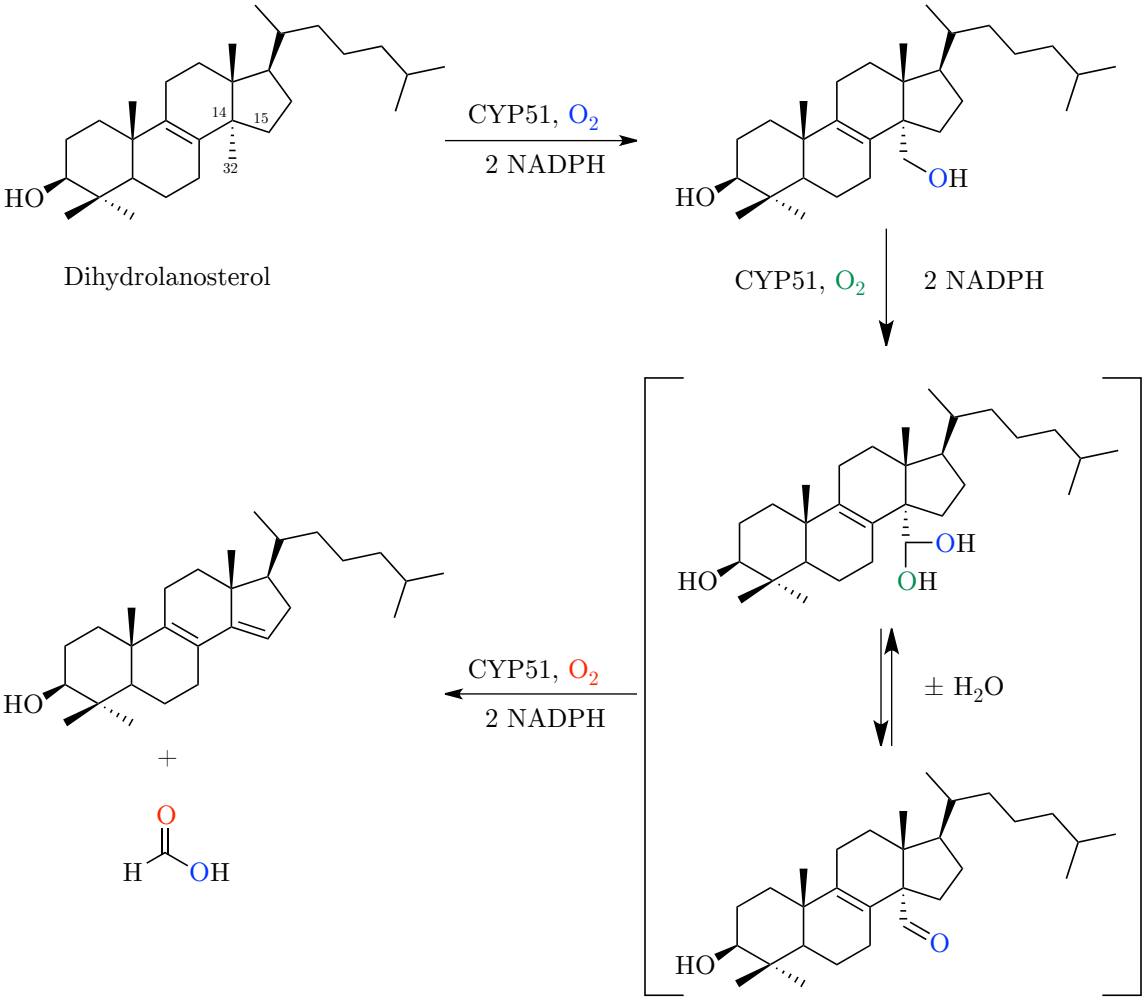
HO
14
15
32
Dihydrolanosterol
CYP51, O2
2 NADPH
OH
CYP51, O2
2 NADPH
OH
OH
± H2O
O
HO
CYP51, O2
2 NADPH
HO
+
O
H
OH

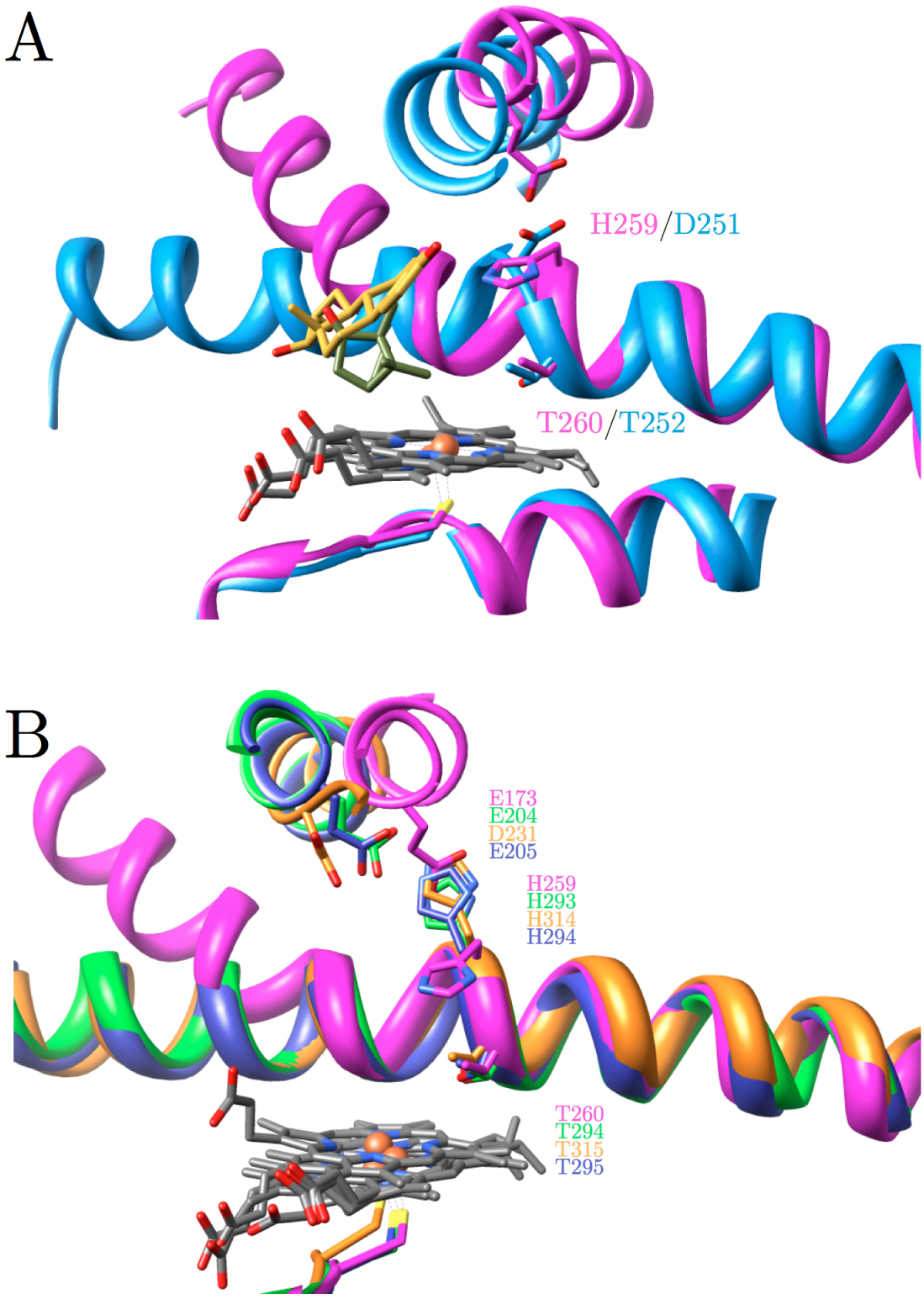

Figure 1.7: A) The aligned crystal structures of the active sites of CYP101 (blue PDB:1DZ8) and *Mycobacterium tuberculosis* CYP51 (magenta PDB:1X8V) B) Alignment of the active sites of CYP51 from *Leishmania infantum* (green PDB:3L4D), *Homo sapiens* (orange PDB:3JUV), *Trypanosoma cruzi* (blue PDB:3KHM) *Mycobacterium tuberculosis* (magenta PDB:1X8V)

with these drugs inhibiting the formation ergosterol, a necessary component in the maintenance of the structural integrity of the fungal cell membrane [88–90]. What was an important finding was that this was the first known prokaryotic CYP51. Mtb CYP51 lacks an N-terminal membrane anchor of its eukaryotic orthologs simplifying expression in bacterial expression systems. In 2000 Podust and coworkers published the first crystal structure of Mtb CYP51 [44], making it the first crystal structure of any C-C bond cleaving CYP. Using this crystal structure to align secondary structural elements of other CYP51s, it was seen that 41 amino acids were conserved between bacteria and animals [91]. Only three of these amino acids were conserved throughout the entire CYP superfamily. It is also noted that the SRS2 and SRS4 regions are highly conserved between species (Figure 1.7 **B**). The SRS4 should be noted for its unique acid-alcohol pair, which in contrast to CYP101 (and the rest of the CYP superfamily) does not have Asp or Glu in this position but rather His (Figure 1.7 **A** and **B**) [44, 92]. As previously mentioned the acid-alcohol pair is implicated in playing a critical role in oxygen activation and proton transfer. The difference in this proton relay system poses questions as to how CYP51 activates molecular oxygen and tuning the lifetimes of reactive oxygen intermediates.

1.4.2 Proton Relay and Oxygen Activation

The Hackett laboratory the studied proton shuttling and O_2 activation in Mtb CYP51 catalysis using explicit solvent molecular dynamics (MD) simulations and hybrid quantum mechanics/molecular mechanics (QM/MM) [93]. The hypothesis that the His259 and Thr260 could relay a proton from bulk solvent to the peroxoferric intermediate was tested by simulations of the histidinuim ion at the 259 position. Results of these simulations showed the formation of two networks which relay protons to the peroxo species. The first network, involving His-Thr dyad, was only capable of supporting

Cmpd 0 formation, while the second proton transfer network connected the distal O atom to Glu173 via four water molecules. In this configuration of the active site, QM/MM calculations revealed that the oxyferrous species has a triradicaloid electronic structure, resulting from protonation of Glu173. This triradicaloid structure has two electrons (either parallel or unparallel) localized on the Fe-O unit and the third on the protonated Glu173. Protonation of Glu173 resulted in polarization of electron density allowing for the tunability of the reactivity of the peroxo intermediate. In such a configuration the barrier for Cmpd 0 and Cmpd I formation is 2 kcal/mol and 12 kcal/mol respectively. Glu173 is located in the F-helix surrounded by polar residues and an easy access to bulk water making its transient protonation resonable.

The Hackett laboratory also went on to show using MD simulations that the carboxaldehyde intermediate of DHL may divert the hydrogen-bonded network from the O_2 intermediate, in the final catalytic step [94]. This diversion promotes the stability of the peroxo intermediate such that it is capable of attack on the C32 carbonyl. This in turn allows the peroxohemiacetal to form without an energy barrier to overcome. The formation of this the peroxohemiacetal was determined to be a branch point within the system (Scheme 1.7) with either protonation of this species or C-C cleavage initiating the release of formate. In the proton-independent path, the enzyme active site was seen to modulate the stability of the intermediates which could be used to explain how CYPs are capable of a number of mechanistic pathways in catalysis. Cmpd 0 and Cmpd I were found to be energetically unfeasible in this final catalytic step.

Scheme 1.7

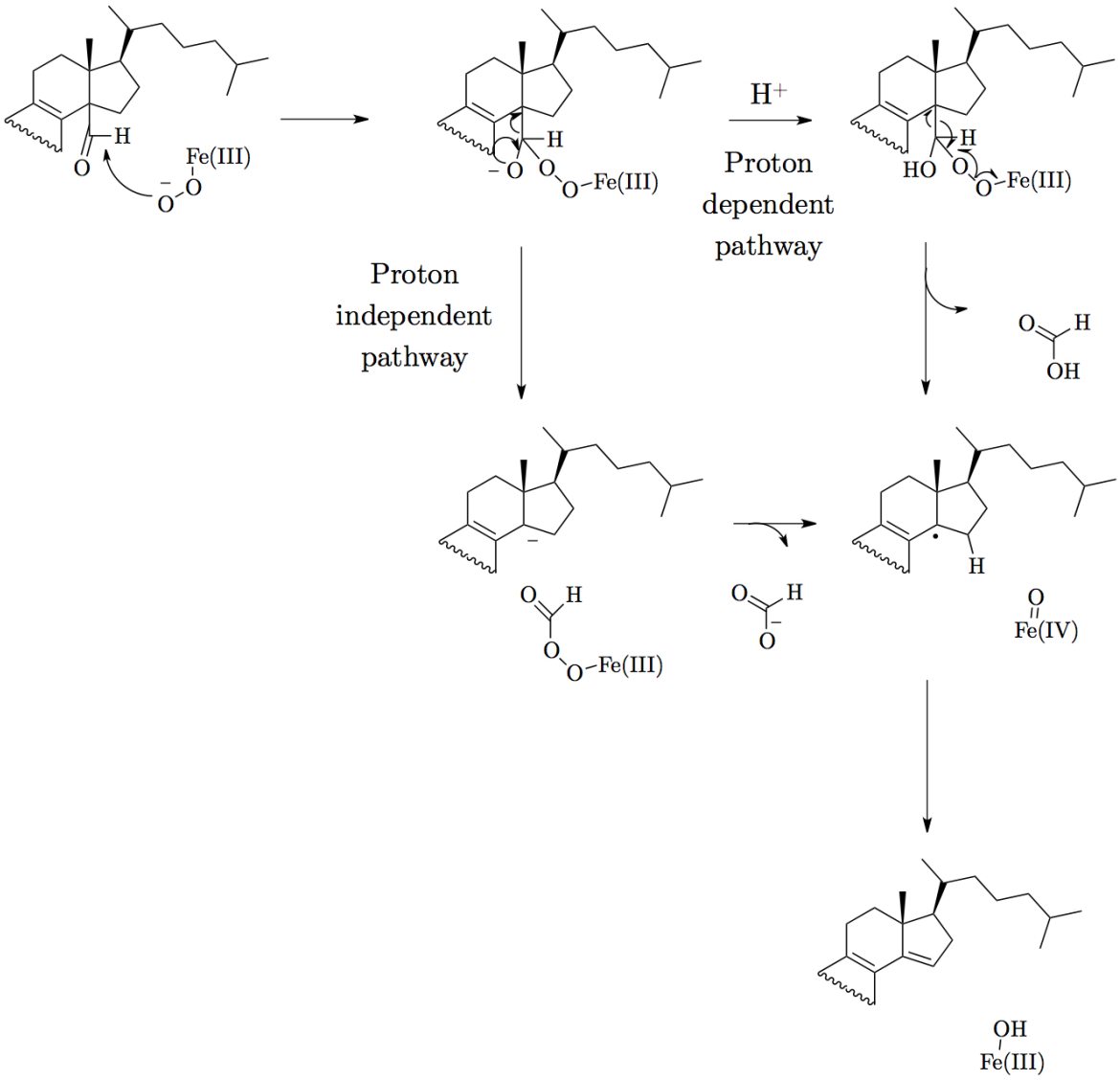
H
O
Fe(III)
O
O
H+
Proton
dependent
pathway
HO
Fe(III)
Proton
independent
pathway
O
H
OH
Fe(III)
Fe(IV)
OH
Fe(III)

1.5 **Significance**

1.5.1 Tuberculosis

M. tuberculosis is a tubercle bacilli bacterial pathogen, which causes Tuberculosis (TB). TB is a global health crisis, which is ever expanding, with 9 million new cases and 3 million deaths occurring each year [95, 96]. Approximately one third of the worlds population has been infected by Mtb, however only about 10% of these cases will have any clinical manifestations of disease. The cases, which remain asymptomatic, are due to the equilibrium achieved between the hosts immune system and the pathogen. Five percent of these asymptomatic cases will develop the active form of the disease spontaneously due to immune suppression [95].

Tuberculosis has only one vaccine, known as BCG (bacillus of Calmette and Gurin) and was prepared by repeated laboratory passage of an isolate of Mycobacterium bovis until it no longer caused disease in humans [97]. BCGs efficacy has been the subject of much controversy due to highly variable protection in adults to pulmonary tuberculosis. It was also apparent that protection varied with geographical distribution and may be explained by the exposure of people to environmental mycobacteria. It was concluded that the best responses to BCG were seen in people that had had no prior exposure to mycobacteria and less of an effect was noticed in people who had been previously exposed to mycobacteria, which had resulted in acquired immunity [98]. This theory is supported by the fact that protection by BCG vaccination in children is not that variable, as children may have been vaccinated prior to major exposure to environmental mycobacteria. When given to children who have not been infected, BCG confers protection against the consequences of primary infection such as pulmonary and meningitis tuberculosis [98]. It has also been speculated that certain BCG vaccines have become over attenuated due to passage in the laboratory and

this could have resulted in the deletions of segments of its genome. Potentially, the over attenuated BCG could have lost its ability to illicit a host response by either lacking key antigens or being unable to persist long enough in the host in order to illicit an immune response [97]. BCG however confers protection to primary infectious consequences such as spreading, but it does not prevent bacterial persistence and reactivation of tuberculosis.

An individual can only be infected with tuberculosis by inhalation of an aerosolised droplet containing *M. tuberculosis*. These droplets would be present in a person with active disease. The bacteria would be found in the terminal air spaces of the lung until they are engulfed by alveolar macrophages within which they replicate [98, 99]. *M. tuberculosis* uses multiple cell surface receptors in order to be phagocytosed by macrophages. Within the phagosomal vacuole *M. tuberculosis* modifies the activity of the vacuole in order to ensure its survival [100]. The colonization of the lung by M. tuberculosis is partitioned into two major phases, namely the acute phase and the chronic phase. The acute phase is characterised by the replication of the bacteria at the initial site of pulmonary infection, which leads to the formation of a small lesion, known as the Ghon Complex. The function of this Ghon complex is thought to allow for reinfection through drainage in the lymphatic and blood systems, which usually results in the infection of the apical regions of the lungs forming secondary lesions[101]. The hosts immune response however, usually controls the bacterial dissemination and replication . The immune response is cell mediated and results from the activation of macrophages by lymphokines released by lymphocytes in response to bacterial antigens. This is known as Cell mediated immunity [102]. The hosts immune response will ultimately lead to the formation of what are known as granulomas. The secondary lesions, which form after dissemination from the granulomas, are a direct result of the hosts immune response to the bacteria and are caseous (liquefied) granulomas due to

tissue necrosis. Necrosis occurs due to the proteolytic enzymes being released by the macrophages. Necrotic tissue has optimal pH (6.5) for *M. tuberculosis* growth however the lack of nutrients such as amino acids, a carbon source and oxygen is thought to cause non-replicating persistence or latency to occur [96]. M. tuberculosis can persist in this latent form for many years without replicating but it has the potential to resume growth and produce active tuberculosis [102].

The treament of Tuberculosis is dependent on eradication of latent tubercle bacilli as well as prevention of reactivation of the disease. Current drugs, although effective in treating latent *M.* tuberculosis infections, do not prevent reactivation at a later stage of an individuals life [103,104]. Azole antifungals have been shown to have antituberclear activities [91, 105–107] and even implicated in treating latent tuberculosis as well as decreasing the incidence of reactivation of the disease [108, 109]. These azole antituberclear drugs are inhibitors of CYPs and in particular CYP51.These potential new CYP inhibitors come at the cost of non-selective inhibition of human CYPs [110, 111].

CYPs as drug targets provide a perfect opportunity to develop drugs that would help to eradicate pathogens and disease because of their numerous pivotal homeostasis roles within pathogens and hosts. However, the fact that organisms rely so heavily on these essential enzymes, makes drug selectively targeting one CYP over another all the more important. Understanding of the catalytic mechanisms of the CYP of interest is of utmost importance in order to develop selective drugs. Studying molecular oxygen activation in CYP51 of *M.* tuberculosis could result in the elucidation of differences of catalytic mechanisms between it and other CYPs. These differences could be exploited in developing a highly selective irreversible inhibitors in the eradication of Tuberculosis.

Methodology

2.1 Cloning and Site Directed Mutagenesis

2.1.1 Site Directed Mutagenesis of *Mycobacterium tuberculosis CYP51*

The *CYP51* pET-17b plasmid, (Figure 2.1 B) was a gift from Larissa Podust of the University of California San Fransisco. This plasmid is the expression vector used to express the crystallized *M. tuberculosis* CYP51 (Mtb CYP51) [44, 105]. The *CYP51* gene (Rv0764c) from the *M. tuberculosis* strain H37RV was initially amplified by PCR with primers incorporating an upstream NdeI restriction site and a downstream primer which incorporated 4 His codons, a stop codon and a HindIII restriction site. This was amplified and cloned into the commercially available pET-17b plasmid (Novagen) by Bellamine and coworkers [112]. This vector was used for expression and characterization of Mtb CYP51 and later the crystal structure [113, 114]. This vector is characterized by its T7 promoter and ampicillin resistance.

Site directed mutagenesis comprised of a polymerase chain reaction (PCR) using primers with base pair mismatches (shown in bold and underlined) for the codons coding for His259 and Thr260. Primers used in these reactions were,

His259Ala:

5′ - GTTCGCCGGCCAT**GC**CACCAGCTCGGG - 3′ (sense)

5′ -CCCGAGCTGGTG**GC**ATGGCCGGCGAAC - 3′ (antisense)

Thr260Ala:

5′ - GCCGGCCATCAC**G**CCAGCTCGGGTAC - 3′ (sense)

5′ - GTACCCGAGCTGG**C**GTGATGGCCGGC - 3′ (antisense)

Thr260Val:

5′ - CGCCGGCCATCAC**GT**CAGCTCGGGTACG - 3′ (sense)

5′ - CGTACCCGAGCTG**AC**GTGATGGCCGGCG - 3′ (antisense)

The setup for each PCR reaction was as follows: on ice, a 50 μL reaction was set up using 0.5 ng of template *CYP51* pET-17b , 0.5 μM of each primer, 25 μL of 2X Phusion High Fidelity Mastermix (Thermo Scientific). Amplification conditions were initiated with a denaturation cycle of 180 s at 371 K followed by 30 cycles at 371 K for 10 s, 25 s at 341 K and 120 s at 345 K. A final extension was carried out for 600 s at 345 K. The template DNA was then degraded by incubation of the PCR mixture with the restriction endonuclease DpnI (New England Biolabs Inc.) (1 μL) for 1 hr at 310 K. DpnI recognizes the sequence G(m)ATC and as such will selectively target template DNA if it has been transcribed in an organism capable of DNA methylation [115]. Each reaction was lyophilized and resuspended in a final volume of 10 μL of diH_2O. Five microliters of each sample was analyzed by tris-acetate-EDTA gel electrophoresis using a 1 % agarose gel matrix with ethidium bromide (0.5 μL/mL) added to the gel (Figure 2.1 A, lane 1). Hyperladder I DNA standard (Bioline) was used to confirm correct plasmid size ($\sim$ 4600 bp; Figure 2.1 B) when visualized under ultra-violet light. This visualization served to confirm sufficient amplification of DNA had taken place.

One microliter of the resuspended DNA was used to transform previously prepared chemically competent DH5α *Escherichia coli* (*E. coli*). The 200 μL of cell stock was removed from 193 K and incubated on ice with the DNA for 20 min. At this time the cells were heat shocked by placing the cells at 277 K for 60 s, then placed on ice for an additional 60 s. The cells were supplemented with 800 μL of Super Optimal broth with Catabolite repression (SOC) media (which had been equilibrated to 310 K) and then incubated at 310 K shaking at 180 RPM for 45 min. The cells were plated onto

Lewis Broth (LB) agar plates supplemented with 200 μg/mL of ampicillin (amp) and incubated overnight at 310 K. Twenty colonies were picked and grown in 5 - 10 mL of LB (200 μg/mL amp) at 310 K while shaking at 180 RPM for 12 hr. Cells were spun down at 5000 RCF at 277 K for 10 min. The pelleted cells were lysed and the plasmid DNA was isolated using a plasmid miniprep kit (Qiagen). The plasmids were linearized by a 10 min digestion with Hind III (Fermentas) in the kit supplied buffer, and subjected to 1 % agarose gel to confirm length and verify concentrations (Figure 2.1 A, lane 2). All plasmids were subsequently sequenced using the T7 promoter and terminator universal primers at the Virginia Commonwealth University Nucleic Acids Research Facilities. These universal primers also served as internal controls for the integrity of the sequence of the T7 promoter and terminator site sequences of the pET-17b vector. This approach afforded sequencing of the *CYP51* inserts in their entirety. Plasmids with correct inserts were frozen at 253 K and stored for later use.

2.1.2 Cloning and Site Directed Mutagenesis of *Trypanosoma cruzi CYP51*

Previous work performed by Chen [116] had shown that expression of soluble *Trypanosoma cruzi* (Tc) CYP51 required truncation of the native protein and the incorporation of charged amino acid residues from the third to seventh amino acid of the protein. The highest quality and yield of expressed protein in an *E. coli* expression system was achieved when the first 21 amino acids of the native Tc CYP51 were replaced with the sequence Met-Ala-Lys-Lys-Lys-Lys-Lys [116]. Expression of soluble CYPs in bacterial expression systems has been problematic due to insolubility, poor yields and inactive proteins which lead to researchers attempting to understand the bacterial vectors as well as expression hosts. In 1990, Stewart published studies on an *E. coli* expression vector which had two *tac* promoter cassettes [117–119]. This pCW vector was under the control of the *tryp* and *lac* UV5 hybrid (*tac*) promoters

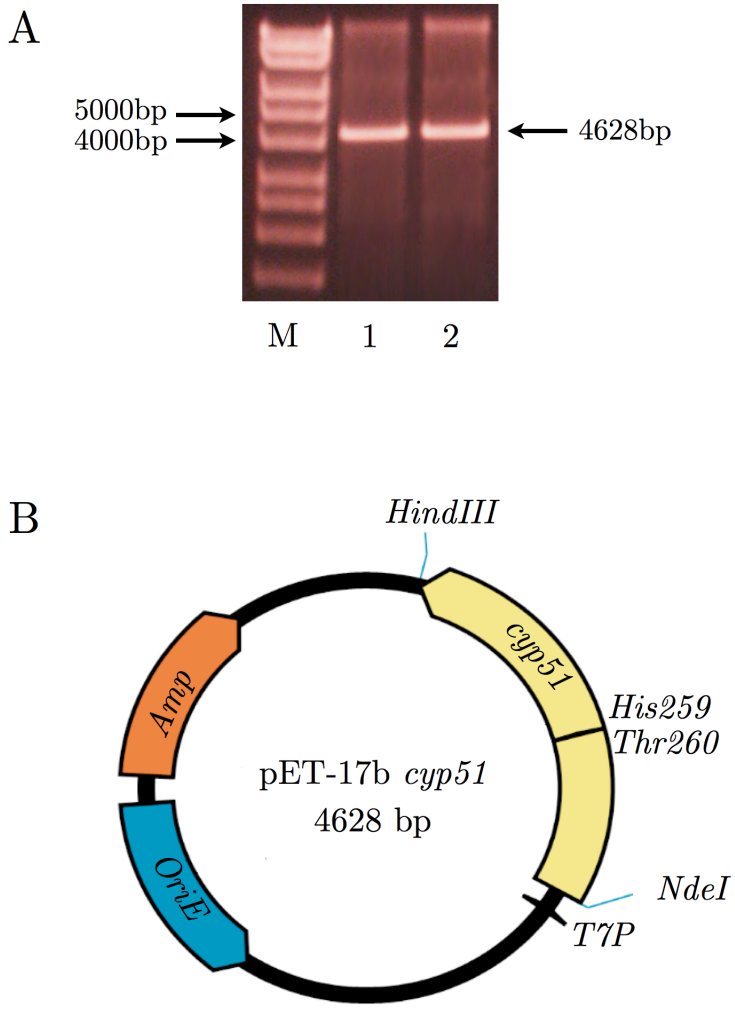

Figure 2.1: One percent agarose gel electrophoresis A) of the site directed mutagenesis PCR reaction (lane 1) and isolated plasmid DNA after transformation of DH5α *E. coli* which had been linearized with HindIII (lane 2). M is Hyperladder I. The graphical plasmid map of *CYP51* pET-17b B) indicating the two restriction sites used to insert the gene (NdeI and HindIII), the approximate location of the His259 Thr260 codons in the *CYP51* gene.

[120] and included a *lacI* gene, a repressor that serves to inhibit expression of the protein in the absence of an external inducer. In 1991 Barnes and co-workers [65] used this pCW vector (referred to as pCWOri(+) hereafter) to express a recombinant bovine microsomal 17α-hydroxylase cytochrome P450 and found as much as 16 mg/L of culture of spectrally detectable CYP was expressed. This expression vector makes use of an NdeI restriction enzyme site (CATATG) directly downstream of the *tac* promoters, and incorporates the ATG (Met codon) initiation sequence for protein expression.

Genomic DNA (gDNA) of the Esmaraldo strain of *Trypanosoma cruzi* (*T. cruzi*, Tc) was a gift from Gregory Buck at Virginia Commonwealth University. A PCR forward primer was designed to incorporate a "GC" clamp, a NdeI restriction endonuclease cut site with a Met ATG start sequence (Bold), the codons of the -Ala-Lys-Lys-Lys-Lys-Lys- sequence (underlined) and a identical sequence to the Tc *CYP51* gene downstream of Val21

5′ -

CGC**CATATG**GCTAAGAAGAAGAAGAAGAAGTCATTTAACACAACCCGTCCT

- 3′

The reverse primer similarly incorporated a "GC" clamp, a HindIII restriction endonuclease site (bold and underlined) and an antisense TGA stop codon (Bold), His_6-tag (underlined) and the last 7 codons prior to the stop codon of the native gene

5′ -

CGC**AAGCTTCA**ATGATGGTGATGATGATGCGAGGGCAATTTCTTCTTGCG

- 3′

A notable consideration utilizing NdeI as the upstream restriction endonuclease site was that the native Tc *CYP51* gene was found to have an internal NdeI restriction site approximately 1100 bp into the gene. In order to overcome this, an intermediate

cloning step into pGEM-T easy (Promega Corp.) would have to be performed followed by a silent mutation of the NdeI site.

Two separate PCR reactions, using different DNA polymerases, were performed in parallel in order to ensure that the amplified gene product would have a single 3′ - A overhang in order to be compatible with the 5′ - T overhangs of the pGEM-T easy linear vector. The two reactions were performed using either Phusion High Fidelity DNA polymerase (Thermo Scientific) or *Taq* DNA Polymerase (New England Biolabs Inc.). The *Taq* polymerase is used for cloning procedures requiring an 3′ - A overhang on the PCR product, however the enzymes error rate is high (285 x 10^{-6}) whereas the Phusion polymerase is a high fidelity enzyme making it 50 times less likely to incorporate a mismatched base, but produces a blunt ended PCR product. Each reaction was performed in order to ensure the correct outcome of the cloning procedure. *Taq* polymerase reactions were performed using 150 ng of *T. cruzi* gDNA, 5 μL 10X Standard Taq Reaction Buffer, 200 μM dNTPs, 0.1 μM of each primer, 1.25 units of *Taq* DNA polymerase and sterile ddH_2O water to a final volume of 50 μL. The temperature cycle for the reaction was as follows: a single denaturation step at 371 K for 120 s, followed by 35 cycles of denaturation at 371 K for 45 s, annealing at 332 K for 35 s, and extension at 345 K for 90 s. The final step in an extension step at at 345 K for 480 s. The setup for the Phusion polymerase PCR was as follows: on ice, 150 ng of template gDNA, 0.5 μM of each primer, 25 μL of 2X Phusion High Fidelity Mastermix (Thermo Scientific) and were made up to 50 μL with ddH_2O. Amplification conditions were an initial denaturation cycle of 371 K for 180 s, followed by 30 cycles of 371 K for 10 s, 332 K for 25 s and 345 K for 120 s. A final extension was carried out for 345 K for 600 s. After the entire PCR cycle was completed 1 unit of *Taq* DNA polymerase was added to the reaction and incubated at 345 K for 480 s. This step served to add a 3′ - A overhang to the already amplified, blunt PCR

product. Five microliters of each PCR reaction was analyzed by tris-acetate-EDTA gel electrophoresis using a 1 % agarose gel matrix with ethidium bromide (0.5 μL/mL). Hyperladder I DNA standard (Bioline) was used to confirm correct amplicon size Figure 2.2 A, lane 1).

This visualization served to confirm sufficient amplification of DNA had taken place. Contaminants in the remaining 45 μL of each reaction were removed using the Isolate PCR kit (Bioline Inc.) so as to not influence downstream applications of the amplified DNA, resulting in DNA of approximately 150 ng/μL suspended in ddH_2O.

By the equation:

$$\frac{ngV \times KbI}{KbV} \times I : V = ngI \tag{2.1}$$

where ng is defined as nanograms, V as vector, Kb as kilobases, I as insert and I:V as the insert to vector molar ratio, ligation reactions were prepared. Fifty nanograms of pGEM-T easy vector (3 Kb) was used in each ligation reaction with insert:vector ratios of 3:1, 1:1, 1:3 using 75 ng, 25 ng and 9 ng of PCR product (1.6 kB) respectively. Ligations reactions were carried out in 10 μL volumes consisting of 5 μL of 2X rapid ligation Buffer, previously calculated amounts of vector and insert, 3 Weiss units of T4 DNA ligase and ddH_2O. An amount of 0.01 Weiss units of T4 DNA Ligase is defined as the amount of enzyme required to catalyze the ligation of greater than 95 % of the Hind III fragments of 1 μg of Lambda DNA at 289 K in 20 minutes. The ligation reaction was incubated at 277 K for 14 hr, after which the T4 DNA ligase was heat inactivated at 338 K for 20 min. Three microliters of each reaction was transformed into DH5α *E. coli* as in section 2.1.1 and plated onto LB agar amp(100 μg/mL) plates which had been supplemented with 40 μL of 20 mg/mL solution of 5-bromo-4-chloro-3-indolyl-β-D-galactopyranoside (X-gal) (Sigma) in dimethyl sulfoxide (DMSO) and

40 μL of 0.1 M Isopropyl β-D-1-thiogalactopyranoside (IPTG) approximately 2 hr prior to use. The pGEM-T easy vector is supplied as a linear fragment of DNA with a fragment of the *lac*Z gene on both the 5′ and 3′ end. Should the linear vector be ligated into a closed circular plasmid, the gene would be complete and would be expressed in the presence of an inducer such as IPTG. The expressed protein, β-galactosidase, catalyzes the degradation of X-gal resulting in colonies which are blue in color. Successful cloning of the insert will result in an interrupted *lac*Z gene with colonies being incapable of degrading X-gal ultimately resulting in white colored colonies. This screening method, known as "blue-white colony screening", provides a rough visual distinguishing feature of which colonies may potentially have the correct insert ligated into the plasmid. White colonies were selected, grown in liquid cultures and their plasmids isolated and sequenced using the T7 promoter and SP6 universal primers as in section 2.1.1. Both the *Taq* polymerase and Phusion polymerase PCR reactions yielded the correct insert without any mutations.

The silent mutation of the internal NdeI restriction site (sequence: CATATG) which spanned the in-frame codons, TCA (encoding Ser357), TAT (encoding Tyr358) and GTT (encoding Val359), was performed using site directed mutagenesis as outlined in section 2.1.1. The codon which encodes Ser357 was an attractive candidate for the incorporation of a silent mutation due to the fact that a single base pair mutation (TCA to TCT) would result in the same amino acid coding while abolishing the NdeI site. The primers used were of the sequences

sense:

5′ - GAGGTCAAGGTTGGTTC**T**TATGTTGTTCCCAAAGG - 3′

antisense:

5′ - CCTTTGGGAACAACATA**A**GAACCAACCTTGACCTC - 3′

where the mutated base pair is bold and the remaining sequence of the now mutated

Nde I site is underlined. Amplification conditions was initiated with a denaturation cycle of 371 K for 180 s, followed by 30 cycles of 371 K for 10 s, 335 K for 25 s and 345 K for 120 s. A final extension was carried out for 345 K for 600 s. This was followed by DpnI digestion, purification and transformation of DH5α *E. coli*. After growth and isolation of the plasmid, sequencing was performed using the T7 promoter and SP6 universal primers in order to confirm the single base mutation. Plasmids containing the correct inserts were stored at 253 K until further use.

Two digestion reactions were performed in parallel using the Tc *CYP51* pGEM-T easy plasmid easy or the pCWOri(+) plasmid. In both experiments, 0.5 μg of plasmid DNA was added to 2 μL of 10X FastDigest Green Buffer (Fermentas), 1 unit of HindIII (Fermentas) and 1 unit of NdeI (Fermentas), and made up to a final volume of 20 μL with ddH_2O. The digestion was incubated at 310 K for 10 minutes after which the reaction was halted by direct loading of the mixture to a 1 % agarose gel matrix with ethidium bromide (0.5 μL/mL) and performing tris-acetate-EDTA gel electrophoresis. After sufficient migration of the bromophenol blue dye front of the FastDigest Green loading dye along the gel, the gels were visualized using UV light. The DNA bands corresponding to an approximate size of 1.5 Kb (in the digestion of Tc *CYP51* pGEM-T easy plasmid DNA) or 4.8 Kb [in the digestion of pCWOri(+)] was excised and cleaned using the Isolate Gel Kit (Bioline). Care was taken so as to limit the time of gel exposure to UV light during the visualization and band excision steps, as UV light is capable of damaging DNA which may result in mutations. Two microliters of gel purified DNA was once again subjected to electrophoresis and visualized, in order to estimate DNA concentrations by relating the intensity of the purified DNA bands to the known concentrations of the marker bands of Hyperladder I. Ligation reactions were performed using approximately 50 ng of purified digested pCWOri(+) and either 5 ng (1:3 insert:vector ratio), 15 ng (1:1) or 45 ng (3:1) of digested Tc *CYP51* as

calculated by equation 2.1. These DNA mixtures were incubated with 1 μL of 10X T4 DNA Ligase Reaction Buffer (New England Biolabs Inc.), 1 unit of T4 DNA Ligase (New England Biolabs Inc.) made up to a final volume of 10 μL with ddH_2O. One unit of T4 DNA ligase is defined as the amount of enzyme required to ligate 50% of HindIII fragments of λ DNA in a total reaction volume of 20 μL in 30 minutes at 289 K. Incubations were performed at room temperature for 16 hr at which time the reaction was halted by heat inactivation of the ligase enzyme at 338 K for 20 min. Five microliters of the ligation reaction was used to innoculate DH5α *E. coli* cells and plated onto LB agar amp(100 μg/ml) plates and incubated at room temperature for 20 hr. Colonies were grown as previously described and their plasmids isolated and sequenced in order to verify the correct inserts. Four internal primers (two sense and two antisense) were in the sequencing reactions. The sequence of the primers were:
sense:
5′ - CATTATGACTCCAGTGTTCGG - 3′
5′ - CTATTCGCCGTGATCCTCCACTC - 3′
antisense:
5′ - CATGGTGTGAGAGTAACGGTGAAC - 3′
5′ - GGATTGCAGGGACAAAGTTCTG - 3′
Plasmids of pCWOri(+) containing the correct Tc *CYP51* sequence were frozen at 253 K until further use.

2.2 **Expression and Purification**

2.2.1 Expression and Purification of *Mycobacterium tuberculosis* CYP51

Mycobacterium tuberculosis CYP51 (Mtb CYP51) and its mutants were overexpressed and isolated from HMS174(DE3) *E. coli* cells. Cells were transformed with the *CYP51*

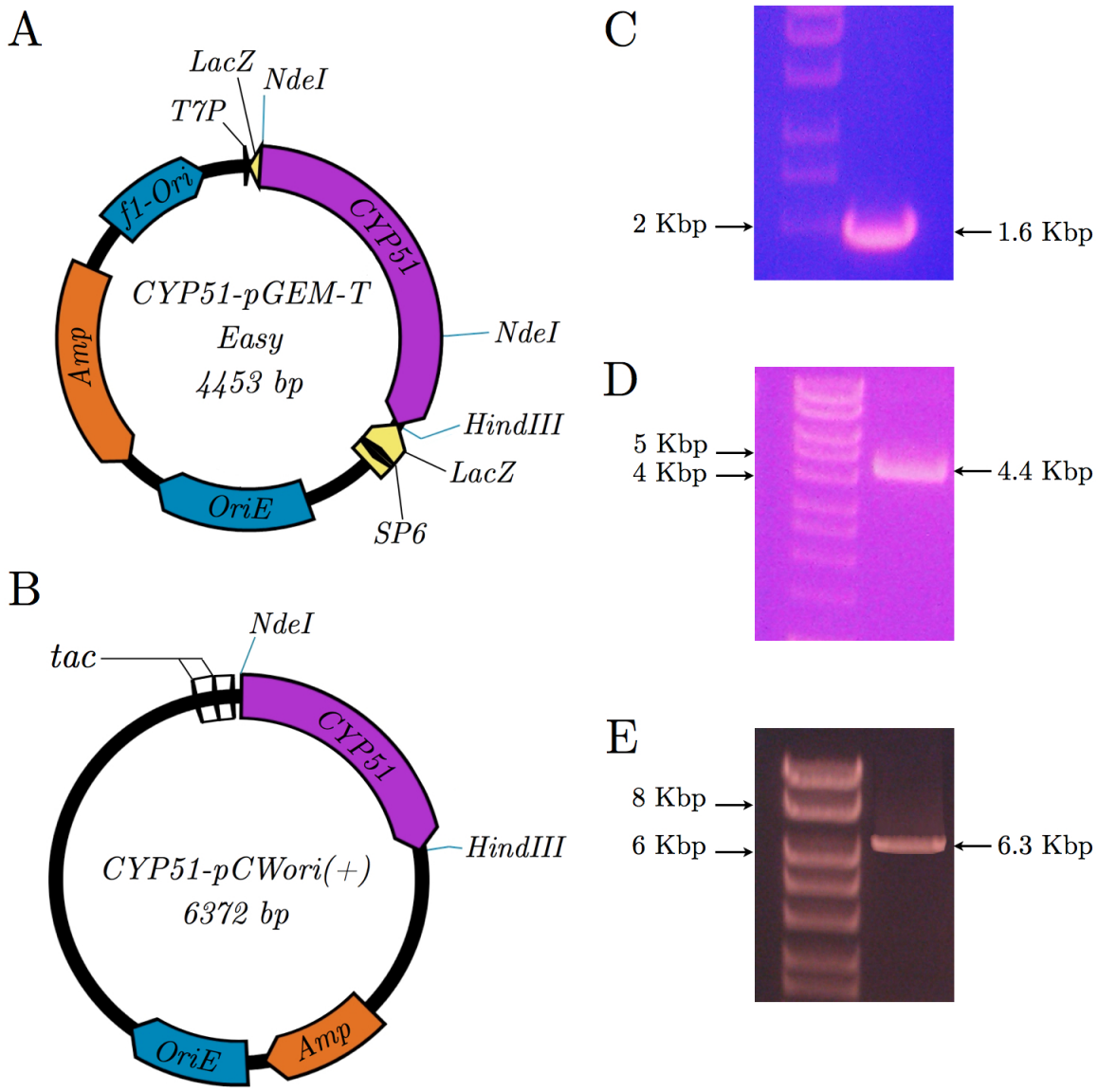

Figure 2.2: Vector maps of Tc *CYP51*-pGEM-T easy A) and *CYP51*-pCWori(+) B). One percent agarose gels indicating relative size of Tc *CYP51* PCR amplicon of approximately 1.6 Kbp C), linear Tc *CYP51*-pGEM-T easy D) (approximately 4.4 Kbp) and linear *CYP51*-pCWori(+) of approximately 6.3 Kbp E).

pET-17b expression vector by heat shocking chemically competent cells. One μg of isolated expression vector was incubated with 200 μL of chemically competent HMS174(DE3) cells on ice for 30 min. After the incubation, cells were placed into water at 315 K for precisely 60 s. Cells were then transferred back to ice for a further 60 s. Seven hundred μL of LB media (298 K) was added to the cells and placed in the shaking incubator at 310 K and 200 RPM for 45 min. The entire culture (900 μL) was plated onto LB-agar plates supplemented with ampicillin (200 μg/mL) and allowed to grow at 310 K for 16 hrs. A single colony was used to inoculate 100 mL of LB media with ampicillin (100 μL/mL) and grown overnight at 310 K and 200 RPM in the shaking incubator. Fifteen milliliters of this overnight culture was used to inoculate multiple 1 L batches of LB media containing 0.1 M KPhos (pH7.4) , ampicillin (100 μL/mL), and 5% glycerol (v/v) and grown at 310 K and 180 RPM. Once the OD_{600} had reached between 0.4 and 0.6, the temperature was decreased to 293 K (291 K for the Thr260Val mutant) and shaking at *strictly* 150 RPM. The OD_{600} was monitored until it reached 0.6 - 0.8 at which time the cultures were induced with 0.2 mM IPTG and 0.5 mM of the heme biosynthesis precursor, δ-Aminolevulinic acid (5-ALA), was added. After 20 hr of growth, cells were harvested by centrifugation at 277 K for 10 min at 5000 RCF and stored at 193 K for later use.

Cell pellets were defrosted on ice and 3 ml of lysis buffer [50 mM Tris-HCl (pH 8), 500 mM NaCl, 10 % glycerol, 1mM phenylmethylsulfonyl fluoride (PMSF)] to every gram of pellet was used to re-suspend the cells. The suspension was lysed and the cell debris was pelleted as in Section 2.2.3. The supernatant was loaded onto Qiagen Ni-NTA agarose resin that had been pre-equilibrated with lysis buffer. Once loaded, the column was washed with 1.5 - 2 L of lysis buffer and protein was eluted with lysis buffer with 50 mM Imidazole. All fractions containing P450 were concentrated in Amicon filtration units with molecular weight cutoff of 30 kDa. Concentrated protein

was loaded onto a Superdex-75 column and run with buffer at 0.2 mL/min [50 mM Tris-HCl (pH 8), 100 mM NaCl, 5 % glycerol]. Fractions with a A_{419}/A_{280} ratio of 1.8 was considered pure [11] and confirmed by SDS-PAGE (Figure 2.3. These fractions were pooled and stored at 193 K until further use.

2.2.2 Expression and purification of recombinant *Trypanosoma cruzi* CYP51

Initial expression and purification conditions were performed following the conditions published by Chen and coworkers in 2009 [121] and 2010 [116]. However, a combination of these protocols resulted in the best yield of functional CYP with regards to growth conditions, and modifications made to the protocols published in [116] were sufficient to achieve homogenous protein verified by SDS-PAGE. HMS174 (DE3) *E. coli* competent cell stocks were transformed with Tc *CYP51* pCWOri(+) using the previously described heat-shock method and plated onto LB Agar amp(100 μg/mL) plates. These transformations were incubated at 310 K for 16 hr after which a single colony was selected and used to inoculate 100 mL of LB broth supplemented with 200 μg/ml of Ampicillin. This seed culture was grown at 310 K for 12 hr shaking at 200 RPM. Fifteen milliliters of the seed culture were used to inoculate 1 L of Terrific Broth that had been supplemented with 1 mM thiamine and 150 μg/mL ampicillin and was grown at 310 K and 200 RPM agitation until the optical density at 590 nm reached an absorbance of 1.0. This initial growth of the culture took approximately 6 hr. At this time the agitation was decreased to 180 RPM, the temperature was decreased to 298 K and the cultures were induced with IPTG (final concentration of 0.2 mM) in the presence of 1 mM 5-ALA. After 40 hr cultures were centrifuged at 5000 RPM for 10 min, and the pellets were frozen at 193 K until further use.

A large scale expression (35 L) was performed using a BioFlo 510 Sterilize-In-Place 40 L Fermentor (New Brunswick Scientific) with conditions as previously

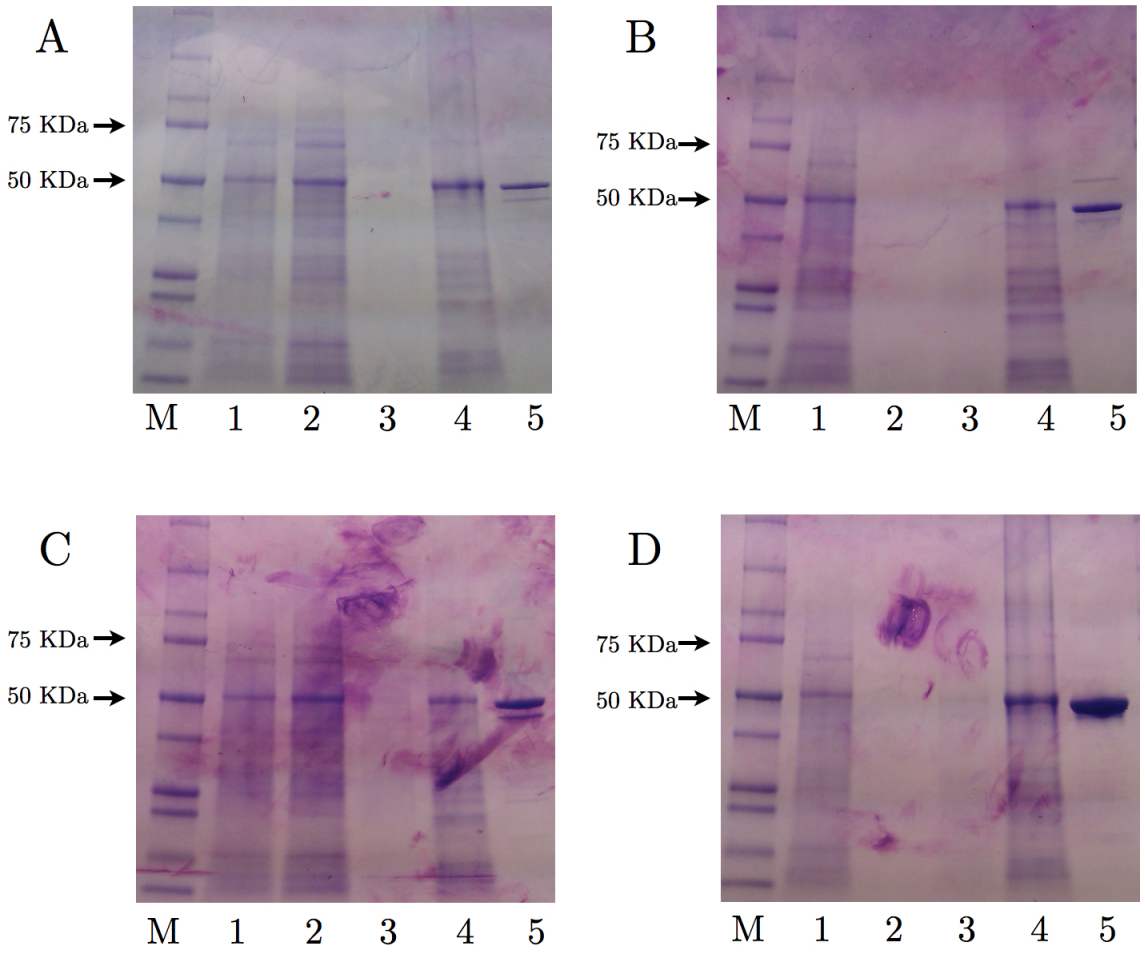

Figure 2.3: Tris-glycine SDS-PAGE gels of A) CYP51 wild type, B) CYP51 His259Ala, C) CYP51 Thr260Ala and (D) CYP51 Thr260Val. M - Protein standard, lane 1 - flow through of the Ni^{2+}-NTA column, lane 2 - 1st wash, lane 3 -2nd wash, lane 4 - elution from Ni^{2+}-NTA, lane 5 - Superdex 75 elution.

described. Scaling of the reaction was performed by increasing the initial seed culture from 100 mL to 1 L and the inoculation volume was increased from 15 mL to 1 L. Incubation times and temperatures remained unchanged. As it has been suggested that CYP51 expression is sensitive to excessive aeration [Larissa Podust (USFC), private communication], the scaling of agitation of cultures on a small scale setting (rotations of flask) to agitation by way of a propeller shaft in combination with sterile airflow into the BioFlo 510 vessel had to be estimated. Air pressure maintained throughout the growth at 10 lb/in^2 and agitation was initially set to 200 RPM before induction and decreased to 150 RPM after induction. Cells were pelleted as previously described.

Cell pellets were defrosted on ice and resuspended in 3 mL of lysis buffer [20 mM Tris-HCl (pH 8), 10 % glycerol, 1mM PMSF and 0.1 mM dithiothreitol (DTT)] to every gram of cell pellet. The cell suspension was lysed by two passes through a French pressure cell press (25 000 psi). The lysate was centrifuged at 10,000 RCF for 45 mins at 277 K. The supernatant was passed through a CM-cellulose (Whatman) matrix in a flow-through regime, as the protein did not bind to the matrix. The eluant was diluted with a 5 M NaCl solution to a final NaCl concentration of 500 mM NaCl. This was loaded directly onto a Ni-NTA gravity column. The matrix was washed with 1 L of wash buffer [20 mM Tris-HCl (pH 8), 10 % glycerol, 1mM PMSF, 500 mM NaCl and 50 mM imidazole] and protein was eluted with elution buffer [20 mM Tris-HCl (pH 8), 10 % glycerol, 1mM PMSF, 500 mM NaCl and 200 mM imidazole, 0.1 mM DTT]. The fractions with absorbance at A_{420} were pooled and subjected to two rounds of 6 hr dialysis at 277 K into [20 mM Tris-HCl (pH 8), 10 % glycerol and 0.1 mM DTT]. The NaCl-free protein dialysate was loaded onto a Fast Flow DEAE-sepharose (Sigma) ion exchange column and eluted over a gradient from 100 mM to 500 mM NaCl. This was analyzed for homogeneity by SDS-PAGE and protein integrity by

UV-vis spectroscopy as seen in Figure 2.4.

2.2.3 Expression of CYP101

Wild type cytochrome CYP101 was overexpressed and isolated from *E. coli* transformed with a vector containing the *Psuedomonas putida* strain ATCC 17453 P450cam gene [122, 123]. The *E. coli* BL21 strain as well as the methodology for growth, expression and purification of P450cam was a generous gift from Prof. John Dawson of University of South Carolina, Columbia. An LB-agar plate supplemented with ampicillin (200 μg/mL) was streaked with colonies from freezer stocks(stored at 193 K) and incubated at 310 K overnight. One hundred milliliters of ampicillin supplemented (100 μL/mL) LB broth was inoculated with two colonies from the overnight plates and grown in a shaking incubator for 6 hrs at 310 K and 200 RPM. After this growth, 4 1 L batches of LB media supplemented with camphor (80 mg/L) and ampicillin (200 mg/L), were inoculated with 2 mL of overnight culture. These cultures were grown at 310 K and 180 RPM in the shaking incubator for 18 hr. Cells were pelleted by centrifugation at 277 K for 10 min at 5000 RCF and broth was discarded. Pellets were either used immediately or frozen at 193 K until further use.

Three milliliters of lysis buffer [50 mM potassium phosphate (KPhos) pH 7.4, 1 mM camphor, 1mM PMSF] to every gram of pellet was used to re-suspend the cells. Cell lysis was performed by subjecting the suspension to two passes through a French pressure cell press (25 000 psi). The lysate was centrifuged at 277 K at 10,000 RCF for 45 mins in order to remove cell debris. The supernatant was loaded onto a pre-equilibrated DEAE-sepharose fast flow ion-exchange column and washed with 1 L of lysis buffer. P450cam was eluted with a KCl gradient (50 mM to 250mM) over 2 L of buffer at a flow rate of 1 mL/min and P450 containing fractions were pooled and concentrated in Amicon filtration units with a molecular weight cut off

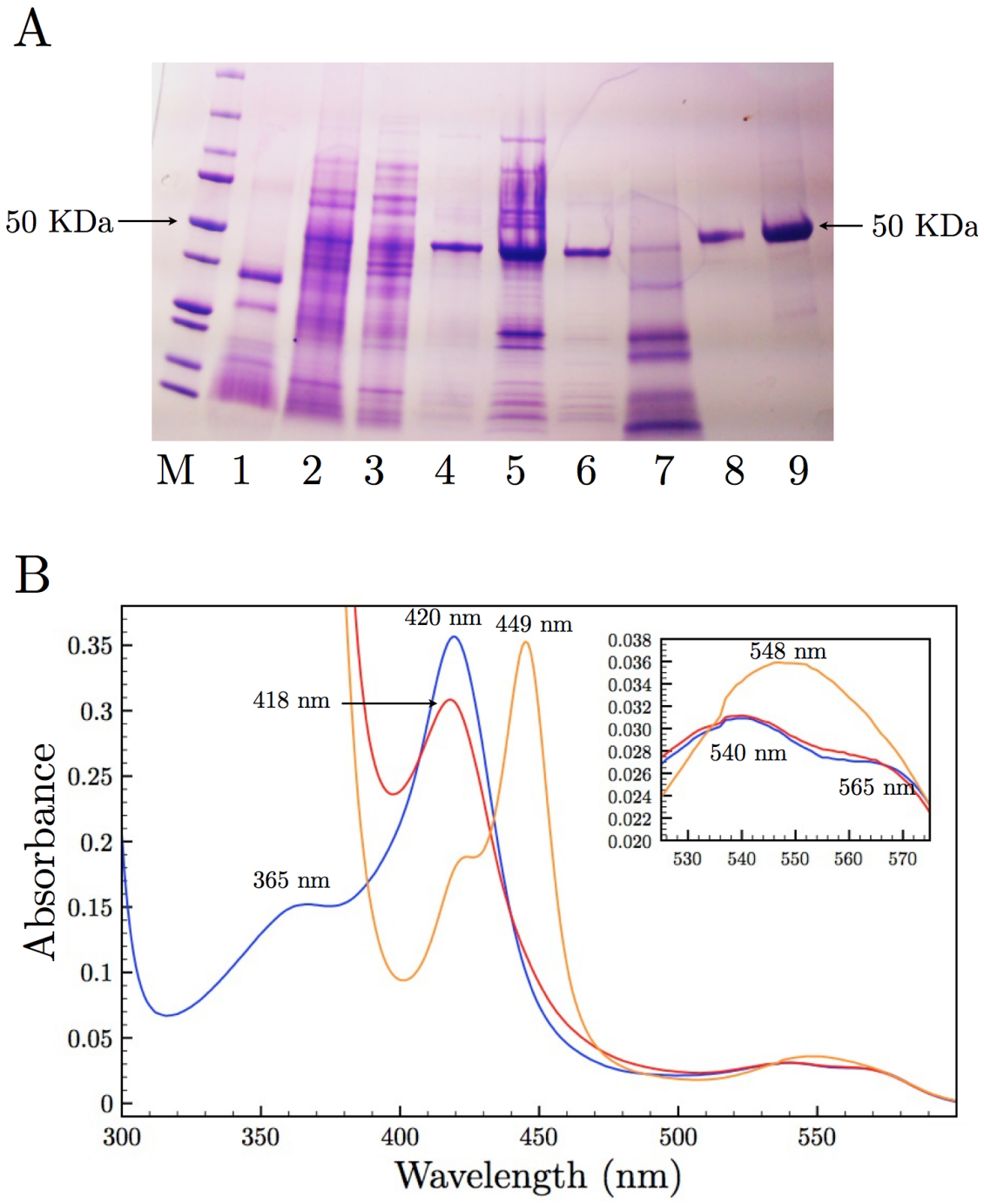

Figure 2.4: A) Tris-glycine SDS-PAGE gel of *T. cruzi* CYP51. M - Protein standard, lane 1 - Flow through of the Ni^{2+}-NTA column, lane 2 - 1st wash, lane 3 -2nd wash, lane 4 - elution from Ni^{2+}-NTA, lane 5 - 10x concentrated elution from Ni^{2+}-NTA, 6 - after dialysis, 7 - Flow through of DEAE column, lane 8 - elution from DEAE column, lane 9 - 10x concentrated elution from DEAE column. B) Absolute UV-vis spectra of *T. cruzi* CYP51, ferric (blue), ferrous (red), and carbon monoxyferrous (orange).

of 30 kDa. P450cam was loaded onto a Superdex-75 column pre-equilibrated with buffer containing 50 mM KPhos (pH 7.4), 50 mM KCl, and 1 mM camphor and run at 0.2 mL/min. Fractions were monitored for purity by their A_{391}/A_{280} ratio, with fractions of equal purity being pooled and either subjected to further rounds of size exclusion chromatography (fractions with A_{391}/A_{280} ratio <1.4) or concentrated in Amicon filter units and stored at 193 K (A_{391}/A_{280} ratio >1.4) for later use.

2.3 **Protein Characterization**

2.3.1 Ferric (Fe^{3+}), Ferrous (Fe^{2+}) and Fe^{2+}-CO/Fe^{2+} difference spectra

Characterization of P450s is primarily performed using UV-visible spectroscopy. A dual-beam scanning spectrophotometer with a sample and reference light cells is critical when performing difference spectra. Each protein that has been purified must be assessed for its ability to be reduced, and whether the reduced protein is capable of binding carbon monoxide (CO) ultimately shifting the Soret from $\sim$ 420 nm to $\sim$ 450 nm. Two reduced volume poly(methyl methacrylate) (PMMA) disposable cuvettes were filled with 1 mL of buffer and were placed into the reference and sample light chambers and a scan from 300 nm to 700 nm was taken, the spectra of which was assigned as the baseline. In order to acquire an absolute spectra of the ferric protein 2 mL of ferric P450 (5 - 10 μM) was placed in the sample chamber and scanned over the same wavelengths relative to the buffer. This protein was removed and a few crystals of the reductant, sodium dithionite, were added to the protein and once again was scanned relative to buffer in order to establish the absolute ferrous species' spectral properties. In order to perform a CO or P450 difference spectra, the reduced protein was split into two cuvettes and and were loaded into both the sample and reference cells. A scan was performed and the spectra was assigned as a baseline. CO is then

bubbled into the protein sample in the sample chamber, for 30 - 60 s and a scan relative to the reduced protein is performed. The ability of the protein to bind CO and produce a Soret shift is indicative to its functionality [1, 124].The P450 concentration was then calculated from the absorption change at 450 nm relative to the absorbance change at 490 nm using the Beers Law equation and the extinction coefficient $\epsilon_{450-490}$ = 91 $mM^{-1} \cdot cm^{-1}$ [2].

2.3.2 Pyridine Hemochromogen

In the case of CYP51, The CO-bound complex rapidly decays (in the order of seconds) making P450 quantification difficult. It has been suggested that a suitable measure for amount of heme containing protein is to measure the amount of heme that complexes with pyridine in a basic environment [11]. This was performed based on the methodology from [124]. Purified protein was made up to 2 mL total volume and final concentration of 0.2 M NaOH and 20 % pyridine. This was split into two PMMA cuvettes and both samples were placed into the dual beam spectrophotometer . A baseline spectrum was recorded between 600 and 500 nm. A few crystals of sodium dithionite were added to the sample cuvette and another spectrum was recorded. Using the Beers Law equation and the extinction coefficient $\epsilon_{557-575}$ = 32.4 $mM^{-1} \cdot cm^{-1}$, the concentration of heme can be measured [124].

2.3.3 24,25 Dihydrolanosterol Synthesis and Solubilization

Lanosterol was hydrogenated by Thuy Nguyen to 24,25-Dihydrolanosterol (DHL). The synthesis was as follows: Lanosterol (Steraloids Inc., Newport, RI, USA) containing 55-65 % of this sterol was purified by column chromatography (silica gel, ethyl acetate:hexane 1:4). In a Parr hydrogenator jar, a solution of lanosterol (2 mmol, 0.85 g) in dichloromethane (40 ml) was added 5 % Pd/C [20 % (w/w), 0.17 g] and

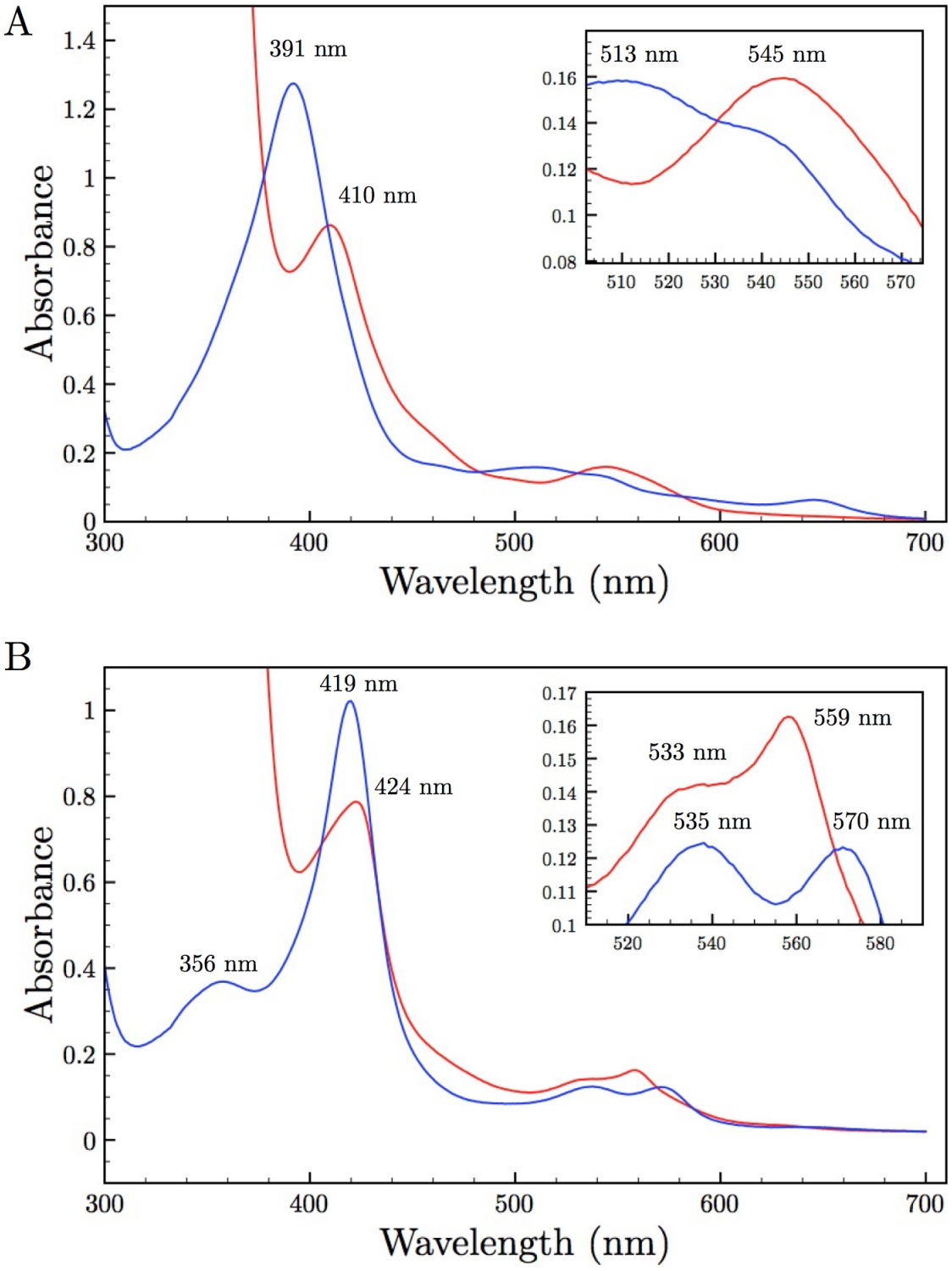

Figure 2.5: Spectra of Ferric (blue) and ferrous (red) of CYP101 A) and CYP51 wild type B).

hydrogenated at room temperature at 50 psi for 24 hr. The mixture was filtered through celite, and the filter cake was washed with dichloromethane (3 x 5 ml). The filtrate was concentrated in vacuo to afford dihydrolanosterol as a white solid in quantitative yield. ^{1}H NMR (400 MHz, $CDCl_3$) δ 3.2 (m, 1H), 2.1-0.9 (m, 45 H), 0.8 (s, 3H), 0.7 (s, 3H). ^{13}C NMR (100 MHz, $CDCl_3$) δ 134.5, 134.5, 79.1, 50.7, 50.6, 50.0, 44.6, 39.7, 39.0, 37.2, 36.6, 35.8, 31.2, 31.0, 29.8, 28.4, 28.2, 28.1, 28.0, 26.7, 24.4, 24.2, 23.0, 22.7, 21.2, 19.3, 18.9, 18.4, 15.9, 15.6.

This molecule is insoluble in almost all biologically compatible solvents, and was dissolved in 100 mM Kphos (7.5) buffered saline, 45 % (2 - Hydroxypropyl) - β - cyclodextrin (HPβCD) solution. Four and a half grams of HPβCD was added incrementally to 8 mL of a stirring, refluxing solution of KPhos buffered saline. After each addition of HPβCD the solution was allowed to stir until all the HPβCD had dissolved before more was added. After all 4.5 grams of HPβCD had been added, the solution was made up to 9.5 mL and the heat of the solution was lowered below refluxing of the solution. DHL was then added (2.143 mg) while the warm solution was stirring. The temperature and stirring was maintained until all DHL had dissolved ($\sim$ 2 hr). The solution was made up to 10 mL with diH_2O making the final concentration of DHL 500 μM. The solution was aliquoted, lyophilized and stored at 253 K. The lyophilized product was made up in appropriate volumes with diH_2O before use.

2.3.4 Ligand Binding Difference Spectra

Ligand binding studies were performed using 1 μM protein in a dual-beam spectrophotometer. Two milliliters of protein in 50 mM Tris-HCl (pH 8), 100 mM NaCl, buffer was split into two cuvettes and placed into the sample and reference cells of the spectrophotometer. As temperature can affect binding of substrates the proteins and ligands were allowed to equilibrate at room temperature for 20 minutes before

spectra were recorded. An initial spectrum is recorded between 450 and 350 nm with protein in both the sample and reference cells of the spectrophotometer and assigned as baseline. One microliter of ligand solution was added to the sample cuvette and 1 μL of solvent (in which the compound was dissolved) was added to the reference cuvette and both were mixed thoroughly by pipetting. To the same cuvettes increments of ligand/solvent are added and spectra are recorded until no increase or decrease in spectral features are observed. Total volume of the drug/solvent added must not be more than 2 % of the initial volume of the protein. This ensures that protein concentration is not altered to the extent that absorbance values will be perturbed (Beer's law) as difference spectra such as ligand binding produce very small spectral changes that are required to be observed. From the spectra the inverse of δA (the difference in absorbance between the peak and the trough of the spectrum) is plotted against the inverse of ligand concentration. Using the equation:

$$\frac{1}{\delta A} = \left(\frac{K_s}{\delta A_{max}}\right)\left(\frac{1}{[L]}\right) + \frac{1}{\delta A_{max}} \tag{2.2}$$

the K_s for the ligand can be calculated, where δA is the absorbance difference between the peak and trough of the spectra, δA_{max} is the final absorbance difference between the peak and trough of the spectra and L is ligand concentration. Figures 3.4 and 3.5 in Chapter 3 show the binding data and calculated K_s for the wild type, His259Ala and Thr260Val proteins with DHL. Figures 2.6 and 2.7 in this chapter show the binding data and calculated K_s for the wild type, His259Ala Thr260Ala and Thr260Val proteins using the clotrimazole.

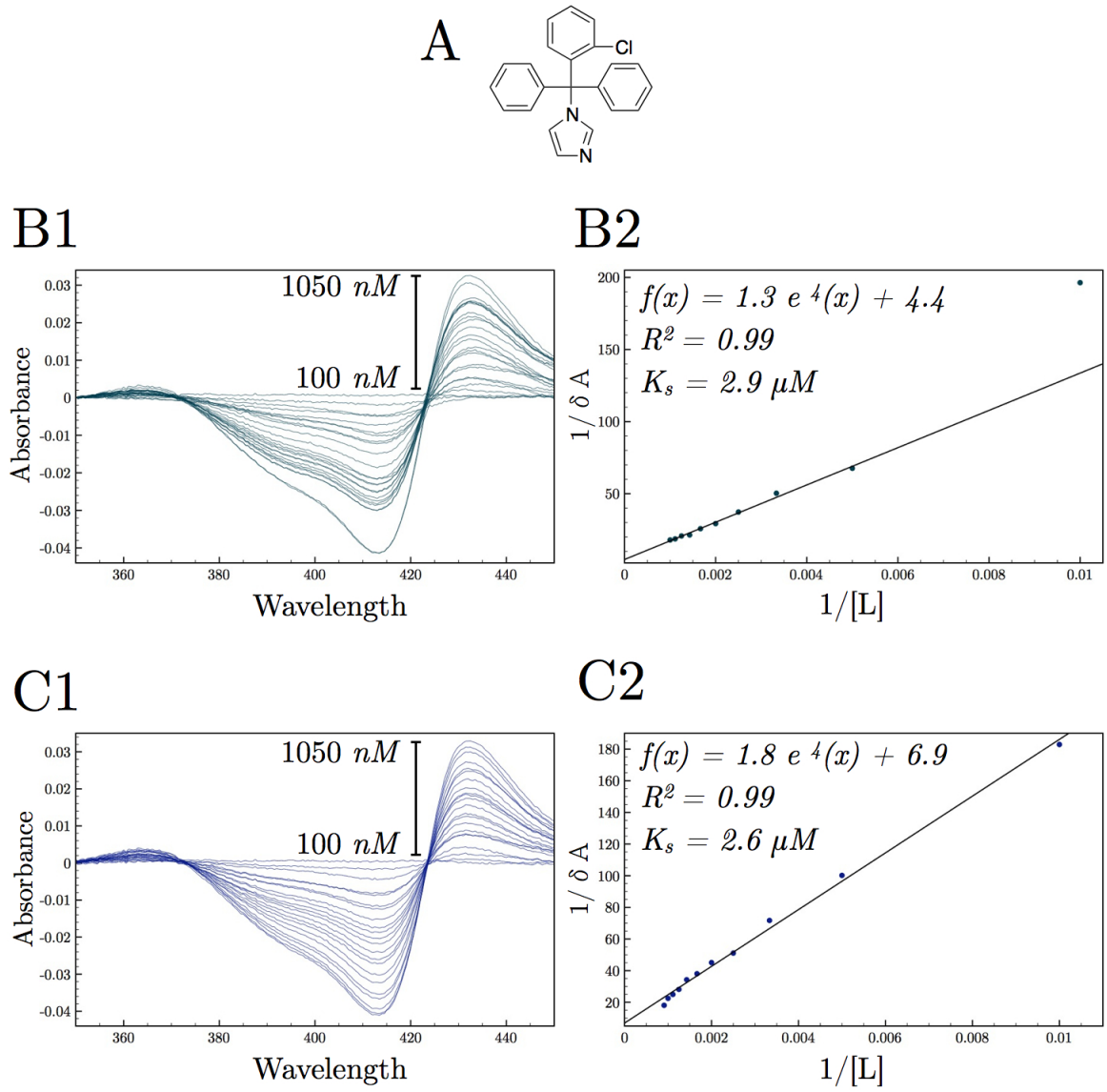

Figure 2.6: A) Clotrimazole B1)Clotrimazole binding difference spectra of CYP51 wild type. B2) Calculated K_s of clotrimazole for CYP51 wild type. C1)Clotrimazole binding difference spectra of CYP51 His259Ala C2) Calculated K_s of clotrimazole for CYP51 His259Ala by plotting $\frac{1}{\delta A} = \left(\frac{K_s}{\delta A_{max}}\right)\left(\frac{1}{[L]}\right) + \frac{1}{\delta A_{max}}$, where δA is the absorbance difference between the peak and trough of the spectra, δA_{max} is the final absorbance difference between the peak and trough of the spectra and L is ligand concentration.

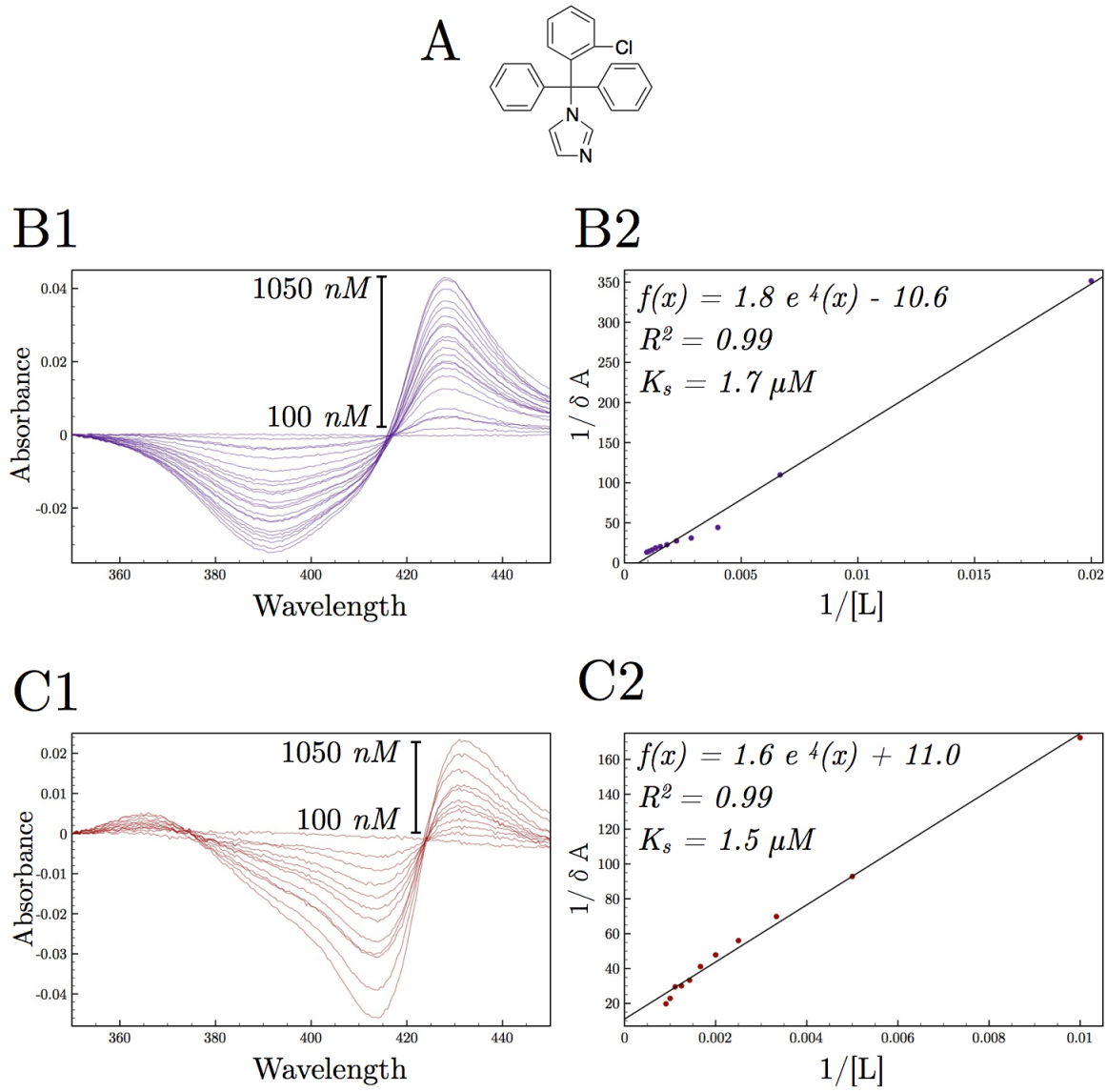

Figure 2.7: A) Clotrimazole B1)Clotrimazole binding difference spectra of CYP51 Thr260Ala. B2) Calculated K_s of clotrimazole for CYP51 Thr260Ala. C1)Clotrimazole binding difference spectra of CYP51 Thr260Val C2) Calculated K_s of clotrimazole for CYP51 Thr260Val by plotting $\frac{1}{\delta A} = \left(\frac{K_s}{\delta A_{max}}\right)\left(\frac{1}{[L]}\right) + \frac{1}{\delta A_{max}}$, where δA is the absorbance difference between the peak and trough of the spectra, δA_{max} is the final absorbance difference between the peak and trough of the spectra and L is ligand concentration.

2.3.5 Magnetic Circular Dichroism

Magnetic Circular Dichroism (MCD) spectra was recorded on an Olis DSM 1000 circular dichrograph (CD) (Olis) using purified CYP51 and His259Ala, Thr260Ala and Thr260Val mutants. UV-vis spectra of one milliliter of protein (of concentrations between 1-10 μM [20mM Tris-HCl buffer (pH 8), 100 mM NaCl and 5% glycerol]) in a quartz cuvette (pathlength 1 cm) were recorded in order to establish the protein concentration in each sample using the A_{419} extinction coefficient of 134 $mM^{-1}.cm^{-1}$. The ferric protein was then placed into a 1.4 T magnetic field in the assigned north to south orientation. Three spectra were recorded from 300 to 700 nm using a 1200 lines/mm grating and a slit width of 0.6 mm. These three spectra were averaged by the Olis Global Works CD software to produce the assigned north spectrum. The polarity of the magnetic field was reversed to south to north orientation and three spectra were recorded, averaged and assigned as the south spectrum. The Olis Global Works CD software was used to subtract the south spectrum from the north spectrum rendering the MCD spectrum of the protein. HPβCD-DHL was then added to the protein to final concentration of 50 μM and the MCD spectrum was recorded. The values recorded by the CD over the 300 - 700 nm range were in the units of millidegrees. These units were converted to $mdeg.M^{-1}.cm^{-1}.T^{-1}$, using previously calculated protein concentrations, the magnetic field of 1.4 T and a pathlength of 1 cm.

2.4 **Cryogenic Spectroscopy**

2.4.1 "Freeze–Pump–Thaw" Buffer Degassing

When conducting experiments requiring observation of reactive oxygen intermediates of CYPs it is necessary to remove all dissolved gases from the buffers being used in the experiments. In the case of the buffers being used in the cryogenic experiments,

dissolved gases such as oxygen and carbon monoxide which are known ligands of the CYPs need to be removed. This was done using the "freeze–pump–thaw" method. This is a three step process which is typically performed with organic solvents employed in organic synthesis of air sensitive compounds. The freezing of the solvents effectively abolishes any evaporation during the application of vacuum. Once most of the gases have been evacuated from the headspace, the vessel is closed to the pump and the surrounding atmosphere, maintaining vacuum within it and the solvent is allowed to defrost. During this step, dissolved gases will come out of solution and fill the evacuated headspace. This cycle is repeated until all dissolved gases are removed.

Airfree Schlenk tubes were filled to half of their total volume with buffers glycerol (required for the formation of an optically pure glass at cryogenic temperatures) and were connected to a gas/vacuum manifold. In the case of CYP51 buffers were either 0.1 M KPhos buffer pH 8 for cryoradiolytic studies or 0.2 M Tris pH 8 for oxyferrous formation, while the buffer for CYP101 was 0.1 M KPhos buffer, pH 8.0, containing 1 mM camphor. The Schlenk tubes were submerged in liquid N_2 so that the surface of the buffer within the tube was level with the surface of liquid N_2. Submersion of the tubes lower than the level of liquid N_2 could result in the liquefaction of gases on the surface of the frozen buffer. Thirty minutes freeze time is required to sufficiently freeze a sample of 100 mL. After this time, the tubes were opened to the vacuum line and the tubes were evacuated until the headspace pressure was between 50 – 100 mTorr (5 min). Tubes were then removed from liquid N_2 and submerged fully in warm water ($\sim$318 K) until no ice was present. This cycle was repeated until the pressure readings were identical before and after opening the Schlenk tube to the vacuum line (4 – 5 cycles). Once sufficient degasification had been performed, the gas manifold was purged with N_2 and the Schlenk tubes were carefully opened to the gas line in order to layer an inert atmosphere over the buffer and the glass stoppers were replaced with

rubber septa, parafilmed, and the tubes were closed off to the gas line. Buffers and glycerol were used within two days of degasification.

It is important to note that the Schlenk tubes will shatter if the buffers are not sufficiently frozen before vacuum is applied, the tubes are warmed up in air or cold water, and the sample is not totally defrosted before freezing in the subsequent cycle.

2.4.2 Preparation of Oxyferrous Cytochrome P450

Previously purified proteins and their mutants (Section 2.2) were defrosted on ice and concentrated to 1 – 10 μM in a total volume of 1.5 mL. In order to minimize dissolved oxygen protein solutions were purged under N_2 gas for at least 20 minutes while on ice. The protein samples were moved to a N_2-filled glovebox where the remainder of sample manipulations were performed. Proteins were reduced with "a few crystals" of sodium dithionite. Any remaining dissolved oxygen will react with sodium dithionite [125]. Oxygen levels present in protein samples that have not been purged with N_2 will result in elevated levels of sulfate and sulfite when sodium dithionite is added. These elevated levels of sulfates and sulfites will precipitate the protein. The proteins were incubated with sodium dithionite for 15 min on ice and removed from the glovebox in a sealed cuvette and monitored spectroscopically between 350 and 700 nm in order to confirm full reduction of the protein by the appropriate shift in the Soret and charge transfer bands. Removal of excess sodium dithionite is performed using a 5 mL G-25 Hi-Trap desalting column which had been equilibrated with 6 column volumes of appropriate degassed buffer at $\sim$ 5 mL/min. One and a half milliliters of protein was loaded onto the desalting column at a rate of 1 mL/min and the flowthrough was discarded. The protein was eluted with 2 mL of buffer at a rate of 1 ml/min. Plastibrand 1.5 mL polymethylmethacrylate disposable cuvettes were filled with 0.75 mL of degassed glycerol and 0.25 mL of reduced, sodium dithionite free protein or

degassed buffer (blank) was added and was mixed thoroughly by gentle pipetting. The cuvettes were sealed and parafilmed and incubated on ice for 1 hr. Addition of oxygen was performed by bubbling oxygen gas into the cold glycerol/protein mixture for 3 minutes after which the cuvettes were resealed and placed in liquid N_2 vapors for at least 45 min. Cuvettes were then submerged in liquid N_2 and remained at this temperature (77 K) for the remainder of the study. This method of freezing (incubation in vapors then submersion in liquid N_2) allows for slow and controlled freezing of the sample in order to maintain the integrity of glycerol glass required for optical spectroscopy. Insufficient mixing of the samples would lead to"pockets" within the glycerol/protein buffer matrix which are not in a 3:1 glycerol/buffer ratio. These pockets will undergo phase transitions above 180 K leading to sample cracking and which renders the prepared samples opaque and unusable. It is assumed that glycerol does not perturb the catalytic cycle of CYP51 as previous studies use concentrations as high as 20 % (v:v) [11, 44, 105, 126].

2.4.3 Sample Preparation for Phosphorus-32 Radiolytic Studies

A 100 mM potassium phosphate (pH 8) 90% (v:v) glycerol solution was oxygenated by bubbling oxygen gas into the solution at ambient temperature for 25 min. To this solution, 200 μL of ^{32}P-enriched orthophosphoric acid (50 mCi/mL) purchased from Perkin-Elmer (MA, USA) was added and was supplemented with 25 μL of bovine liver catalase, from Sigma-Alderich ($\sim$ 1500 units) and incubated at 277 K for 1 hr. This incubation is required for the complete elimination of H_2O_2 that was generated by the radiolytic decay of H_2O by the isotope during its transportation [127, 128]. Cooling of the oxygenated glycerol helps to minimize the autooxidation that may occur during mixing of the reduced protein and the glycerol. Reduction of the protein and removal of excess of sodium dithionite was performed as in 2.4.2. Samples were

drawn into a 1 mL syringe and placed on ice within the N_2 filled glovebox. The syringes were removed from the glovebox and 300 μL of protein was injected into the oxgenated glycerol buffer/^{32}P-enriched orthophosphoric acid/catalase solution. This was thoroughly mixed for less than 3 minutes to minimize autooxidation of the oxyferrous species. The samples were frozen as in Section 2.4.2 and left at 77 K for four to six weeks.

2.4.4 UV-Visible Spectroscopy of Catalytic Intermediates

In order to record spectra at cryogenic temperatures and controlled annealing conditions, samples were housed in Janis STVP-100 Cryostat (Figure 2.8) with fused-silica optical windows. Ten to twenty hours prior to use, the cryostat was mounted into position within an Olis Cary-14 Spectrophotometer Conversion with a custom chamber capable of housing the cryostat. The vacuum jacket of the cryostat was evacuated using a Hi Cube Turbo Pump (Pfeiffer Vacuum). Once the cryostat jacket pressure was between 1 and 3 e^{-6} mbar the cryostat was purged with either N_2 or He gas for 10 min depending on what liquid cryogen was used. In each case, liquid N_2 or liquid He, the cryogen was transferred into the cryostat using the "push and pull" method for initial cool down. An over pressure is placed on the cryogen dewar with gas and a pump is attached to the sample tube pumping port of the cryostat, and while cryogen is "pushed" into the cryostat by the gas over-pressure, it is also being "pulled" out by the pump. This transfer of cryogen was maintained until the silicon diode temperature sensors on the cryostat vaporizer was at the temperature of the respective cryogen liquid (lN_2 - 77 K, lHe - 4 K). At this point the sample tube pumping port was closed and pressure within the cryostat was increased until the over-pressure relief valve opened. The sample tube pumping port was then opened to atmosphere and the cryostat was allowed to equilibrate at this temperature until the sample holder

reached the same temperature. Samples were loaded into the custom made spring loaded sample holder (Figure 2.8) while submerged under liquid N_2. The sample holder was rapidly transferred to the cryostat with sample being exposed to air for less than 2 s. All UV-vis spectroscopy at cryogenic temperatures was performed using an Olis Cary-14 Spectrophotometer Conversion with a custom chamber capable of housing a Janis STVP-100 cryostat. Temperature output of the Janis cryostat was performed using a Lakeshore 332 Temperature controller. The Olis spectrophotometer was controlled using the Olis Global Works software package.

The cryoradiolytic samples of Mtb CYP51 and its mutants were to be incubated at 77 K and the temperature gradually increased in increments of 10 K while recording spectra, in order to evaluate the formation and decay of distinct spectroscopic species. To evaluate the background of the glycerol buffer and ^{32}P-ortho-phosphoric acid over the temperature range, a protein free sample was subjected to UV-vis spectroscopy from 10 K to 120 K in order to determine a temperature specific baseline. The spectra of the standard can be seen in Figure 2.9A. These temperature specific baselines would reduce the noise component of the spectra when SVD analysis was performed. In order to indirectly observe the decay of ^{32}P-ortho-phosphoric acid, a protein sample was evaluated over 4 hr at 10 K. During this time, the formation of solvated electrons can be seen as a broad peak from ∼500 nm to ∼700 nm as shown in Figure 2.9B and is consistent with what has been observed in other studies [129]. The protein Soret is present however the Q-bands are obscured by the broad solvated electron peak. The solvated electrons were removed by photobleaching with a cutoff filter of $\lambda > 450$ nm [127, 130, 131] as shown in 2.9B.

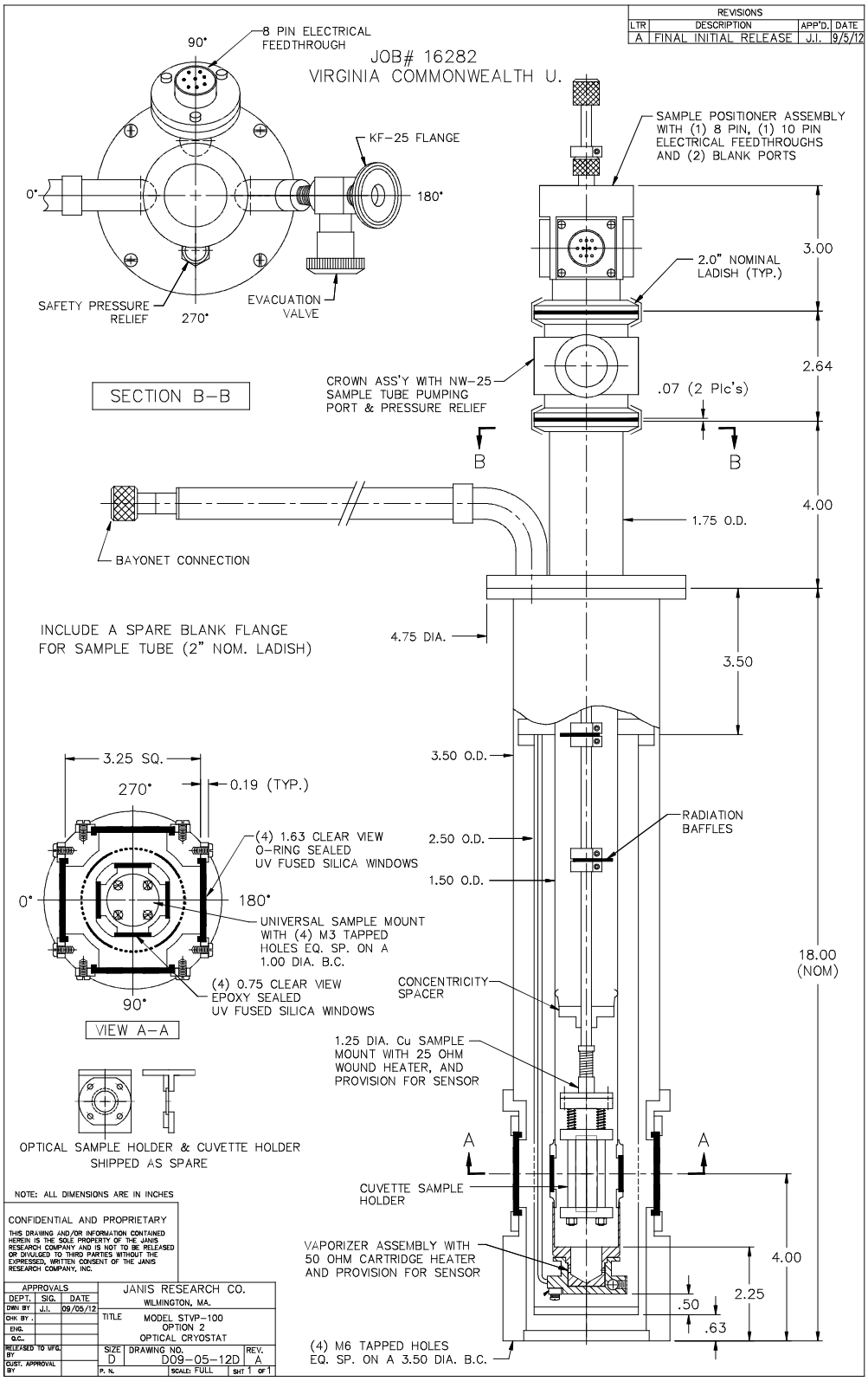

Figure 2.8: Schematic of the Janis STVP-100 Cryostat.

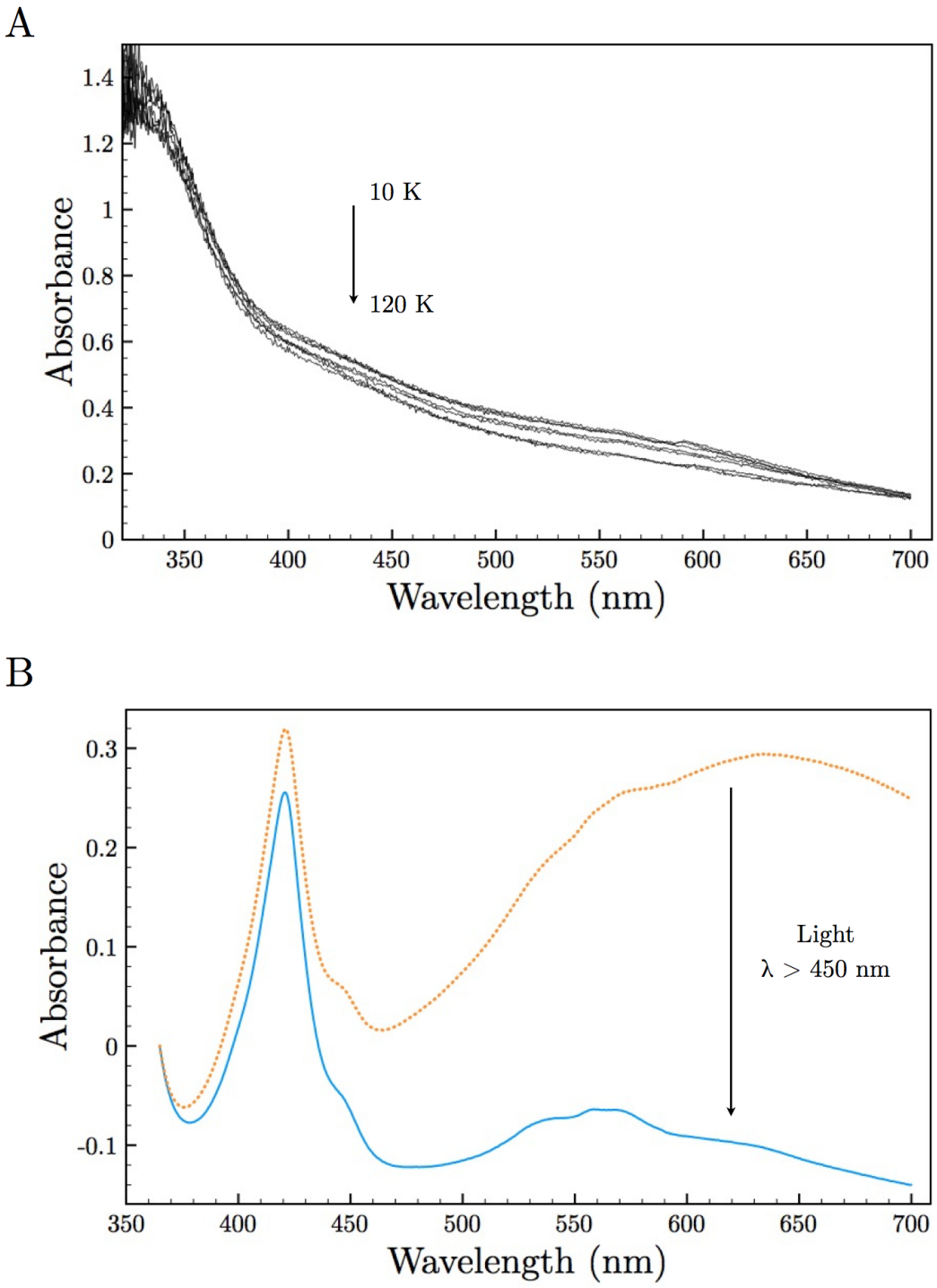

Figure 2.9: A) UV-vis spectra of protein-free glycerol buffer standards with ^{32}P-ortho-phosphoric acid over 10 - 120 K . B) UV-vis spectrum of protein with solvated electrons (dotted orange) and the same sample photobleached for 30 mins (blue).

2.5 **Stopped Flow UV-visible Spectroscopy**

2.5.1 Buffer Preparation

Fifty millimolar Tris-HCl (pH 8) buffer was degassed as in Section 2.4.1 and was bubbled with oxygen for approximately 30 min. The dissolved oxygen was found to be approximately 900 μM using a dissolved oxygen water quality test kit available from LaMotte. The principles of the test are based upon an azide modification of the Winkler method for determining dissolved oxygen [132, 133]. Essentially this method is performed as a titration resulting in a visible colorimetric change of the solution. The first step of the oxygen determination is the dropwise addition of $MnSO_4$ followed by the dropwise addition of KOH to the buffer being tested resulting in a $Mn(OH)_2$ precipitate:

$$MnSO_4 + 2KOH \rightarrow Mn(OH)_2 + K_2SO_4 \tag{2.3}$$

This precipitate is oxidized by dissolved oxygen present, forming a brown precipitate [$Mn(OH)_3$] by the reaction:

$$Mn(OH)_2 + O_2 + 2H_2O \rightarrow 4Mn(OH)_3 \tag{2.4}$$

Sulfuric acid is added converting the hydroxide to a sulfate which is then soluble:

$$2Mn(OH)_3 + 3H_2SO_4 \rightarrow Mn_2(SO_4)_3 + 6H_2O \tag{2.5}$$

At this stage known quantities of buffer and reagents are used in order to accurate quantify the amount of oxygen present. Twenty milliliters of the previously manipulated buffer is measured to which 250 μL of starch indicator solution (with KI) is

added in a dropwise manner resulting in a blue color.

$$Mn_2(SO_4)_3 + 2KI \rightarrow 2MnSO_4 + K_2SO_4 + I_2 \tag{2.6}$$

sodium dithionite is then added in a measured dropwise manner, and is the final titration step that results in the solution turning to a colorless solution. With the known amount of added sodium dithionite, the dissolved oxygen can be calculated in parts per million and converted to molarity.

$$2Na_2S_2O_3 + I_2 \rightarrow Na_2S_2O_6 + 2NaI. \tag{2.7}$$

2.5.2 Decay rates of Oxyferrous CYP51

CYP51 wild type, mutants, P450cam and Ligand solutions were defrosted on ice and purged under an atmosphere of N_2 for 20 min. After purging the samples and ligands, each was sealed and transferred to an N_2-filled glovebox. Each protein sample was reduced with a few crystals of sodium dithionite and allowed to at room temperature. A 5 mL G-25 desalting column was equilibrated with 5 volumes of degassed buffer at a flow rate of 5 mL/min and 1.5 mL of reduced protein was loaded. The excess sodium dithionite is removed as 1.5 mL of protein is eluted from the column at 1 mL/min. GE Lifesciences instructs to collect 2 mL of eluate, however it was found that 2 mL of eluate will still contain excess sodium dithionite, whereas 1.5 mL does not. The protein is then diluted to 3 mL with degassed buffer and split in two and DHL-HPβCD was added to one (final concentration 50 μM). The reduced protein (with and without ligand) was taken up in a 10 mL syringe and placed in sealable Ziploc ® bag purged with N_2 and sealed. Three milliliters of degassed buffer that had been oxygenated (2.5.1) was taken up in 2 10 mL syringes (ligand was added to a final concentration

of 50 μM in one of the syringes). Each syringe was allowed to equilibrate to room temperature for 15 minutes. All stopped flow measurements were performed using an Applied Photophysics SX-18MV stopped flow UV-visible spectrophotometer with a photodiode array detector and the associated Acorn PC with X-Scan software (Applied Photophysics) allowed for multiple wavelength absorption spectra to be acquired. The dead time of the machine is approximately 2 ms. After flushing with degassed buffer, the stopped flow apparatus was loaded with 1.5 mL of oxygenated buffer and 1.5 mL of protein. The machine was baselined with oxygenated buffer. Each syringe was set to drive 175 μL (total mixing volume of 350 μL) and 400 scans/second were performed for 2 seconds. Data sets were analysed using Pro-K software (Applied Photophysics) perfoming Singular-Value-Decomposition (SVD) and global fit in order to reconstruct single data sets and the rates of formation or decay of particular species.

The Role of the Acid-Alcohol Pair in *Mycobacterium tuberculosis* CYP51 Oxyferrous Formation and Stability

3.1 Introduction

In order to fully understand the catalysis of a particular cytochrome P450, it is important to characterize each intermediate in the catalytic cycle (Scheme 1.1). Characterization of some intermediates pose difficulties due to their transient lifetimes. The oxyferrous state of CYP101 has been well characterized using a number of spectroscopic techniques including UV-vis [134], magnetic circular dichroism (MCD) [135] Mössbauer [136] and resonance Raman [13, 14]. This oxygen intermediate is considered to be the last "easily" characterizable intermediate of the CYP catalytic cycle. As much of this work has been performed with CYP101, CYPs capable of catalyzing reactions that diverge from classical CYP hydroxylation such as the C-C bond cleaving enzymes may not adhere to the same catalytic intermediates. The characterization of the oxyferrous intermediate, its formation as well as its decay, in a particular enzyme is important as it represents the first step in the process of oxygen activation. Oxygen activation in CYP51 catalysis is of particular interest owing to the fact the enzyme is capable of tuning its reactivity solely on the basis of its activation and stabilization of oxygen intermediates.

The oxyferrous species is common to all CYP reactions, regardless of their end point and is the critical intermediate that will undergo one electron reduction to form a peroxo-anion adduct. This adduct represents a branch point in the catalysis

of C-C cleaving CYPs. It can either be protonated to ultimately generate Cmpd I or participate directly as a nucleophile. The commitment to one of these pathways depends on how the active site environment tunes proton delivery to the peroxoanion intermediate. The axial thiolate ligand of the CYPs as well as reduction of this oxyferrous species will result in oxygen-oxygen bond scission active heme-oxidant capable of substrate oxidation [1].

The characterization of the oxyferrous species of CYPs has led to elaborate studies in which this intermediate is reduced [15, 127]. This one electron reduction of the oxyferrous intermediate generates intermediates which do not accumulate to an extent that they may be detected on an appreciable timescale and hence have to be trapped in matrices at cryogenic temperatures. Due to the transient lifetimes of oxygen intermediates, their experimental observation can be performed using one of two approaches. These are techniques capable of detecting intermediates on a short timescale or methods requiring low temepratures to stabilize otherwise short lived intermediates.

In this study rapid-scanning stopped-flow UV-vis spectroscopy is used in order to measure the rates of formation and decay of the oxyferrous intermediate in wild type Mtb CYP51 and its mutants. In order to understand and characterize oxygen intermediates within Mtb CYP51 and its mutants, it was critical to investigate the kinetics of oxygen binding and release. These studies demonstrate the role of the His-Thr dyad in binding of oxygen and stability of oxyferrous CYP51.

3.2 Results and Discussion

3.2.1 UV-vis and Magnetic Circular Dichroism

A description of the methods for expression and preliminary characterization of Mtb CYP51 and the His259Ala, Thr260Ala and Thr260Val mutants are described in Chapter 2. Ferric and ferrous absolute UV-vis spectra of the wild type protein (Figures 3.1B) were consistent with previously reported spectra [11,112] of this protein. The UV-vis spectrum of the ferric wild type protein spectrum has a Soret at 419 nm with charge-transfer bands (Q-bands) at 535 nm (β band) and 571 nm (α band) as well as a smaller peak at 363 nm. The absolute ferrous spectrum of the wild type protein shows a red-shifted Soret to 424 nm with two smaller peaks at 530 nm and 559 nm. Each mutant shared the same features as the wild type CYP51 in their ferric and ferrous spectra (Figures 3.2 B). The carbon monoxyferrous complex was consistently unstable in all proteins. A representive spectrum illustrating a decrease of the Soret at 449 nm, with concomitant increase of a peak at 420 nm over time shown in Figure 3.3 which occurs over a minute or so. This CO-adduct collapse has been shown to occur at a slower rate (4x) in the prescence of estriol [11], however this was not observed in the presence of 50 μM of DHL although this was not further investigated. As no major differences in these spectra were observed, it was assumed that the mutations did not drastically change the resting state, oxidation states and CO binding of the proteins.

As the endogenous substrate of Mtb CYP51 is unknown, it was decided to proceed with the mammalian CYP51 substrate dihydrolanosterol (DHL) as a ligand for further studies. DHL binding to Mtb CYP51 produces a"Type 1" binding spectra which is characteristic of a peak at ~390 nm and a trough at ~420 nm. Figures 3.4 and 3.5 show the DHL binding data and calculated K_s for the wild type, His259Ala and

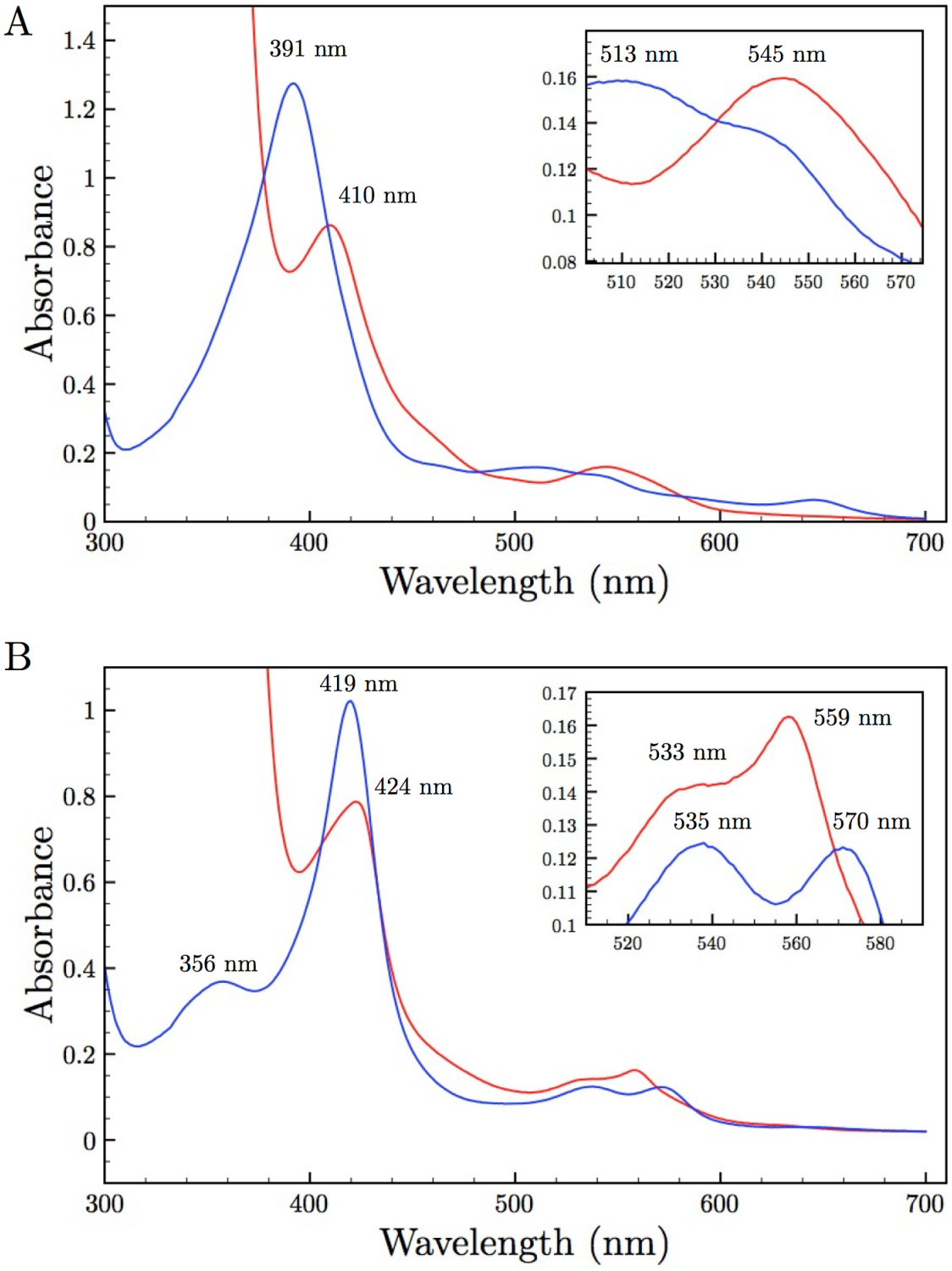

Figure 3.1: Spectra of Ferric (blue) and ferrous (red) of CYP101 A) and CYP51 wild type B).

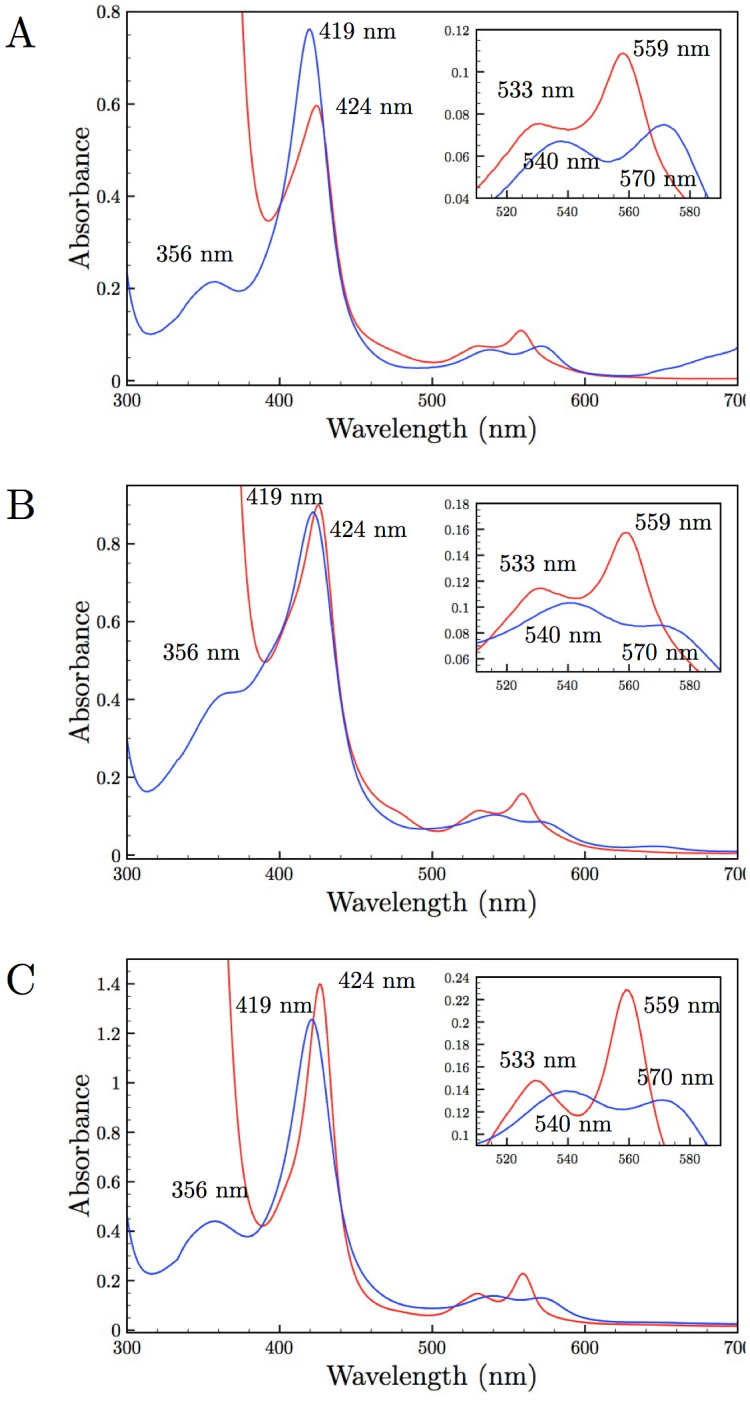

Figure 3.2: Spectra of Ferric (blue) and ferrous (red) Mtb CYP51 His259Ala A), CYP51 Thr260Ala B), CYP51 Thr260Val C)

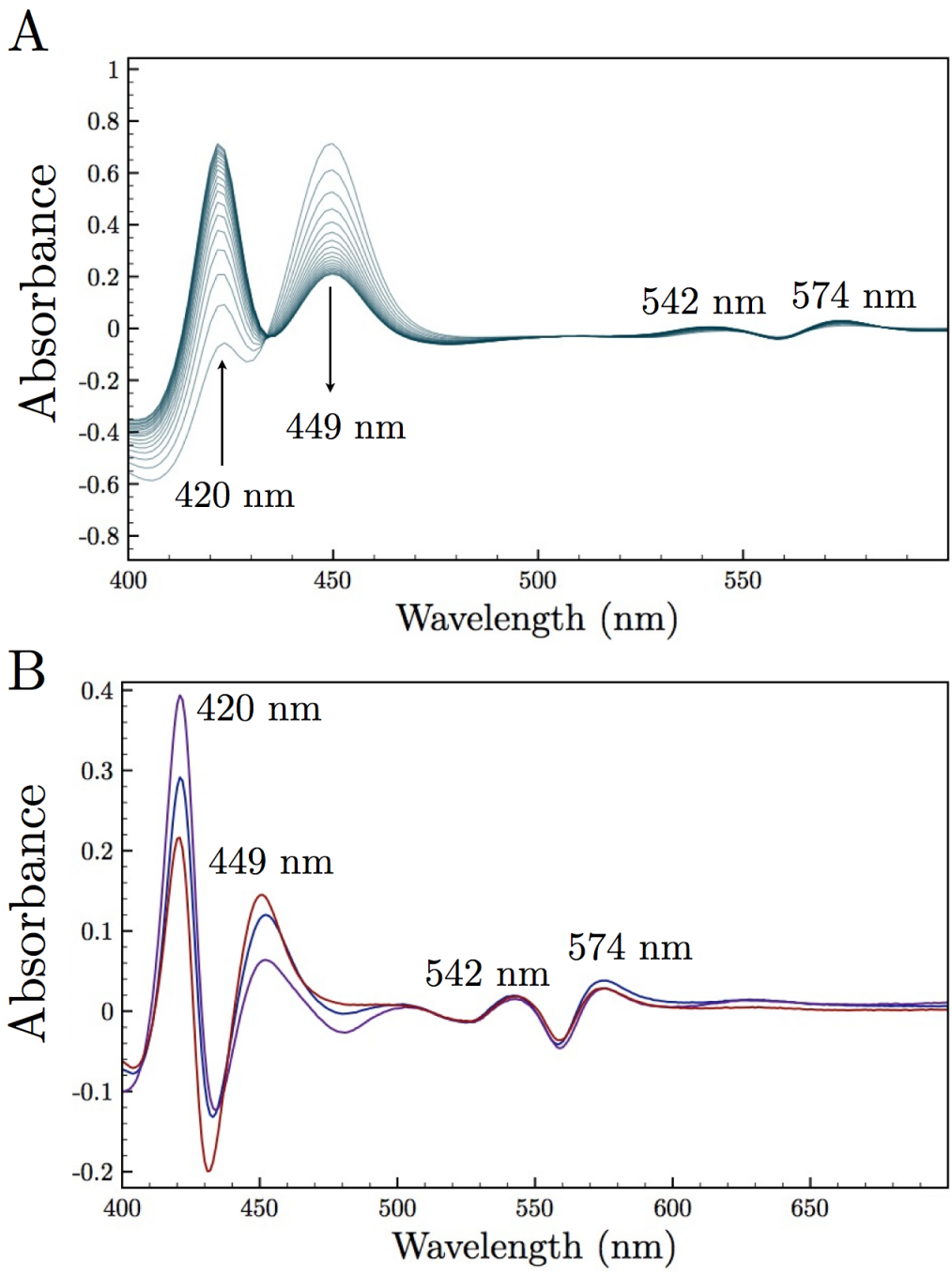

Figure 3.3: A) A time scan of Mtb CYP51 wild type Fe^{2+}-CO/Fe^{2+} difference spectra. (B) CYP51 His259Ala (blue) CYP51 Thr260Ala (purple) and CYP51 Thr260Val (red) Fe^{2+}-CO/Fe^{2+} difference spectra.

Thr260Val proteins. The calculated K_s of DHL binding to the wild type protein was 0.2 μM which is slightly lower than the 1 ($\pm$ 0.5) μM reported by Bellamine [112]. Both His259Ala and Thr260Val showed a higher K_s for DHL during binding studies with 0.43 and 1.2 μM respectively. Both of these mutants also showed a much greater absorbance in their ligand binding difference spectra with the A_{390} (indicative of HS) being $\sim$5 and $\sim$20 times greater than wild type in the His259Ala and Thr260Val mutants respectively. This may be due to these mutations increasing the hydrophobicity of the active site making it more likely for DHL to bind and displace the co-ordinated H_2O. In the case of Thr260Val mutant this could also be due to the fact that this mutation would remove a hydrogen bonding site capable of stabilizing the heme co-ordinated H_2O molecule. However the Thr260Ala mutant shows no significant spin shift on the addition of DHL, even when concentrations as high as 5 μM of ligand was added (data not shown). This suggests that either DHL does not bind, or when the DHL binds to the active site it does not displace the heme co-ordinated H_2O molecule shifting the spin state from low to high spin.

3.2.2 Magnetic Circular Dichroism

In order to understand the population of spin states of the heme prosthetic group in each protein in the presence and absence of DHL, MCD spectra were recorded. If performed in the UV-vis region of heme (300 - 700 nm) the MCD spectra is capable of revealing the spin state of the ferric CYP. Initial spectra were recorded with CYP101 in the presence and and absence of camphor. These spectra are illustrated in Figure 3.6 and spectra features are recorded in Table 3.1 and represent the low spin (Figure 3.6 A) and high spin (Figure 3.6 B) states of CYP101. These spectra can be used as a comparison in determining the spin state populations in CYP51 wild type and mutants. The spectra of CYP51 wild type illustrated in Figure 3.7 A and Table 3.1 showing

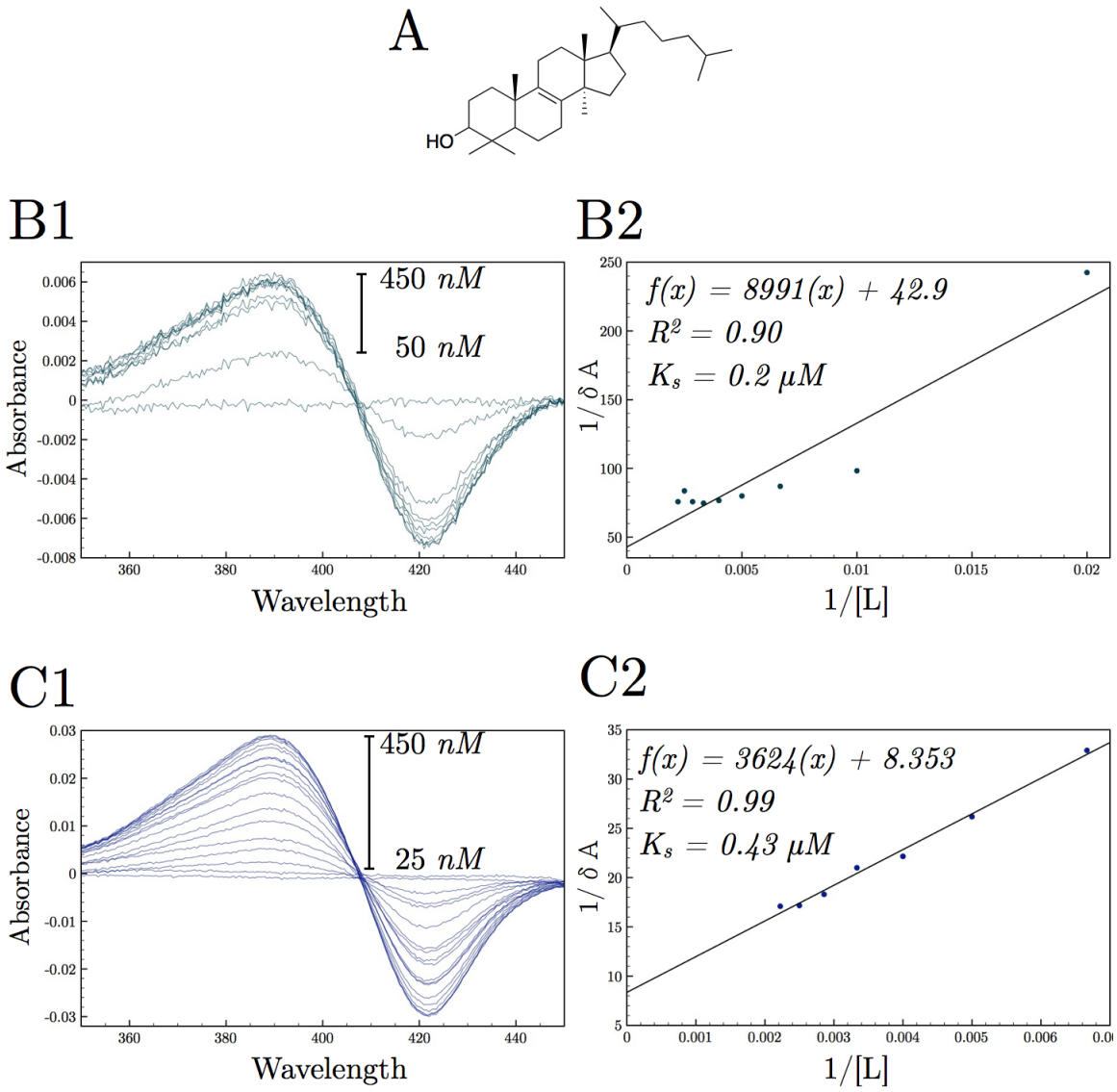

Figure 3.4: A) Dihydrolanosterol B1)Dihydrolanosterol binding difference spectra of CYP51 wild type. B2) Calculated K_s of DHL for CYP51 wild type. C1)Dihydrolanosterol binding difference spectra of CYP51 His259Ala C2) Calculated K_s of DHL for CYP51 His259Ala by plotting $\frac{1}{\delta A} = \left(\frac{K_s}{\delta A_{max}}\right)\left(\frac{1}{[L]}\right) + \frac{1}{\delta A_{max}}$, where δA is the absorbance difference between the peak and trough of the spectra, δA_{max} is the final absorbance difference between the peak and trough of the spectra and L is ligand concentration.

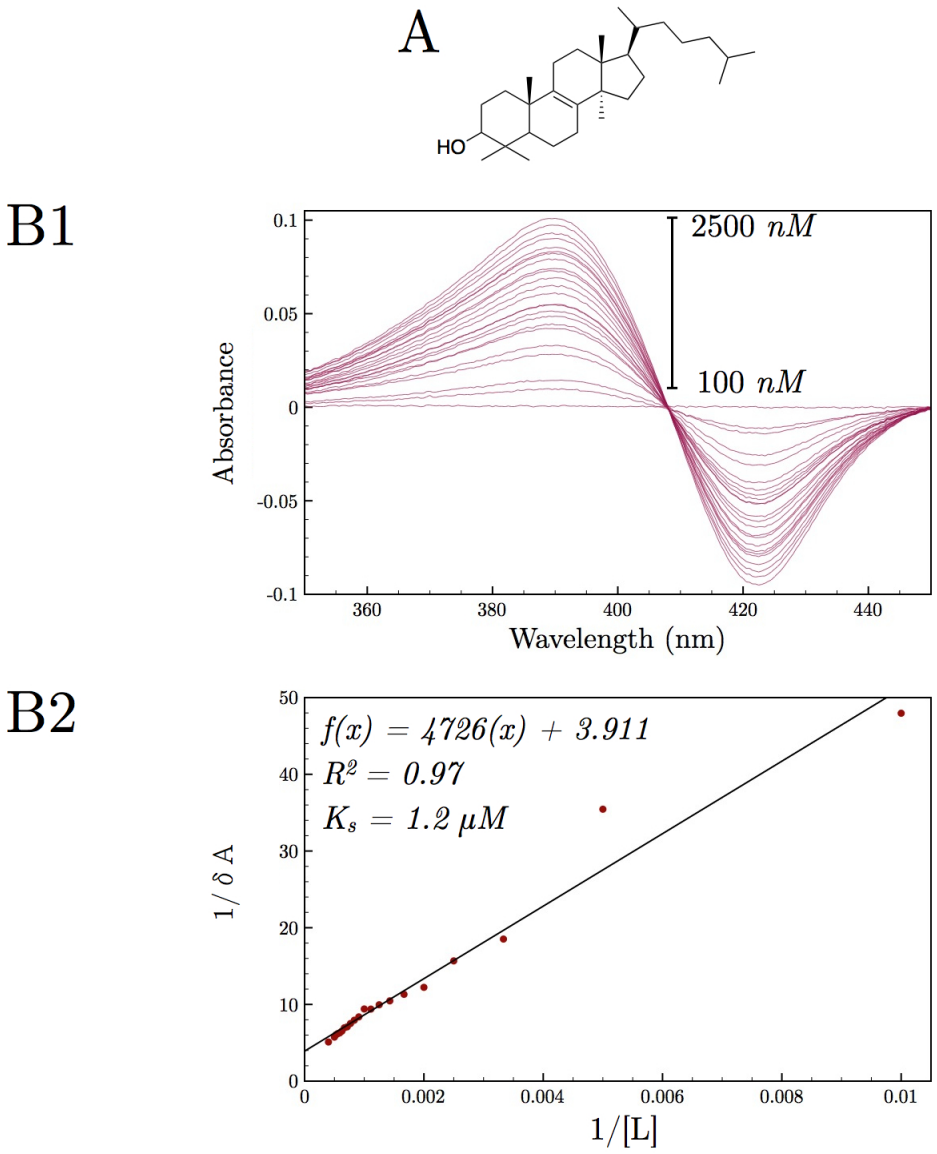

Figure 3.5: A) Dihydrolanosterol B1)Dihydrolanosterol binding difference spectra of CYP51 Thr260Val. B2) Calculated K_s by plotting $\frac{1}{\delta A} = \left(\frac{K_s}{\delta A_{max}}\right)\left(\frac{1}{[L]}\right) + \frac{1}{\delta A_{max}}$, where δ A is the absorbance difference between the peak and trough of the spectra, δA_{max} is the final absorbance difference between the peak and trough of the spectra and L is ligand concentration.

peaks at 358 nm, 411 nm and the crossover at 420 nm. Additional bands are found at 428 nm, 522 nm, 562 nm, 579 nm. These peaks when compared to that of CYP101 and P450LM-2 are consistent with a hexacoordinated low spin state of the enzyme [137–140]. On the addition of saturating concentrations of substrate, the spectrum of wild type protein did not significantly change, confirming the results of UV-vis ligand titration studies. The His259Ala mutant in the absence of substrate showed nearly identical peaks as that of the low spin wild type protein (Figure 3.7 B). In saturating concentrations of substrate, evidence of a slight trough at 396 nm is present. Although the amplitude of this trough is not great and other spectral features are missing, it is evident of a small population of the protein being in the pentacoordinated high spin state as seen in CYP101[141], P450terp [137] and chloroperoxidases [142]. The MCD spectra of both the Thr260Ala (Figure 3.8 A) and Thr260Val (Figure 3.8 B) mutants are slightly red shifted relative to that of the wild type protein as is shown in Table 3.1. Although the shift of these peaks is not indicative of spin state, they provide insight into the active site environment. On the addition of substrate to the Thr260Ala mutant, no distinct spectral changes are seen in the MCD spectrum. This confirms UV-vis ligand binding studies and strengthens the argument that the Thr260Ala mutant does not bind DHL. The MCD spectrum of Thr260Val however shows the most dramatic change of all the proteins used in the study. The troughs appearing at 396 nm, 553 nm and 655 nm (slight) are all indicative of a pentacoordinated high spin protein [137, 141, 142]. Although some of the low spin spectral features are present, a large proportion (60 %) of the protein is in the high spin state as confirmed by UV-vis ligand titration data.

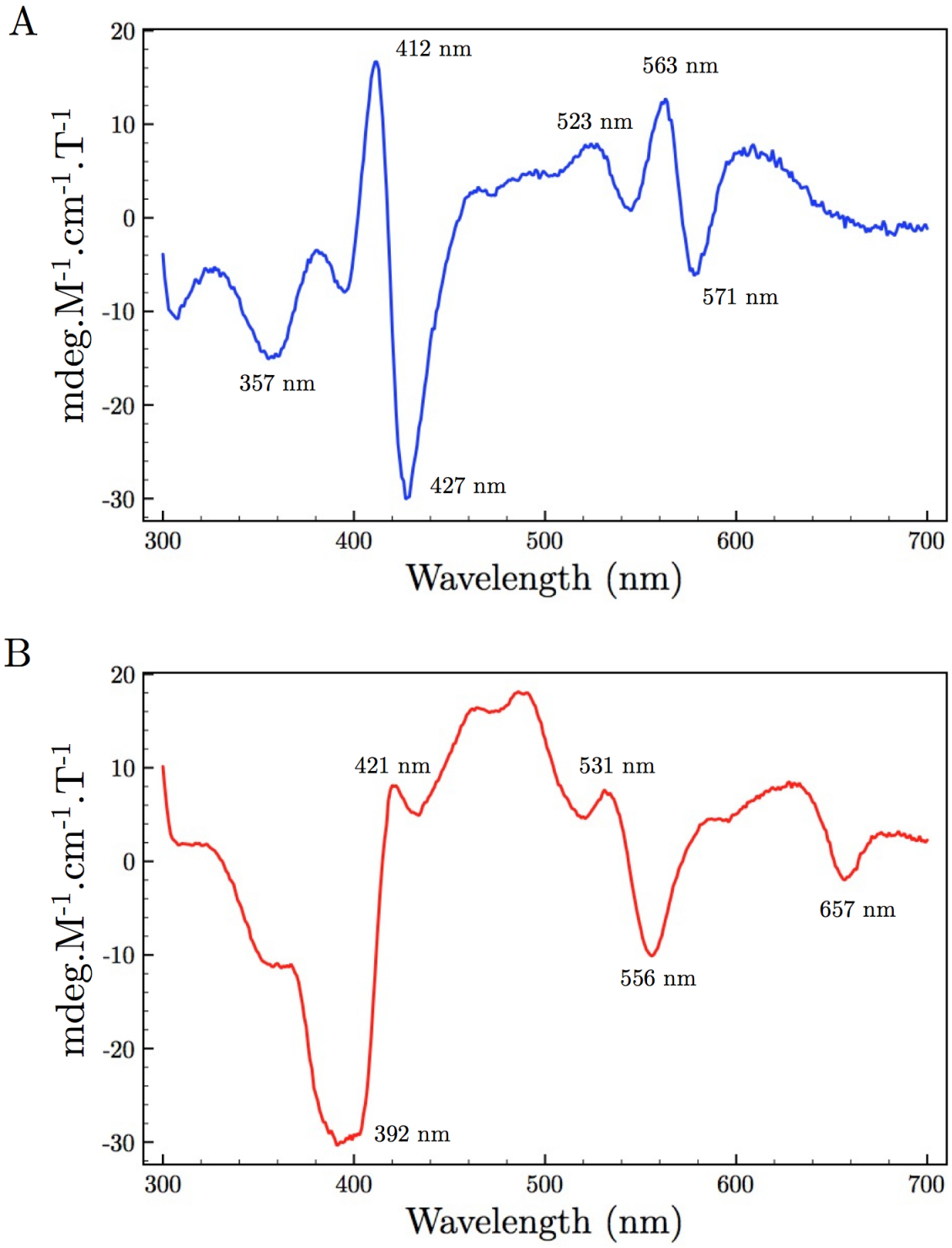

Figure 3.6: MCD Spectra of A) ligand free low-spin CYP101 and B) High spin CYP101 in the presence of camphor (100 mM)

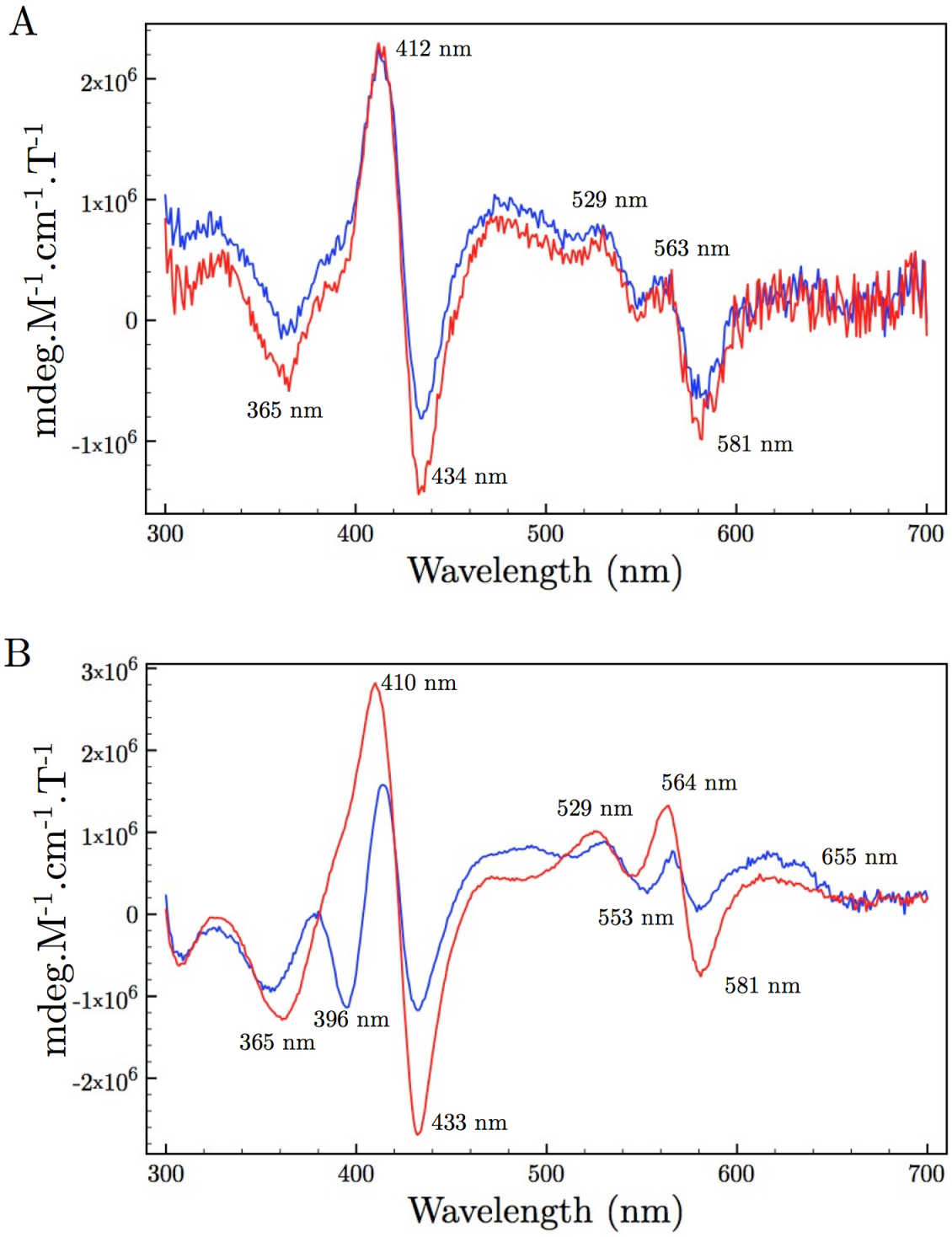

Figure 3.7: MCD Spectra of A) Mtb CYP51 wild type and B) His259Ala mutant in the absence (red) and presence of DHL (50 μM)

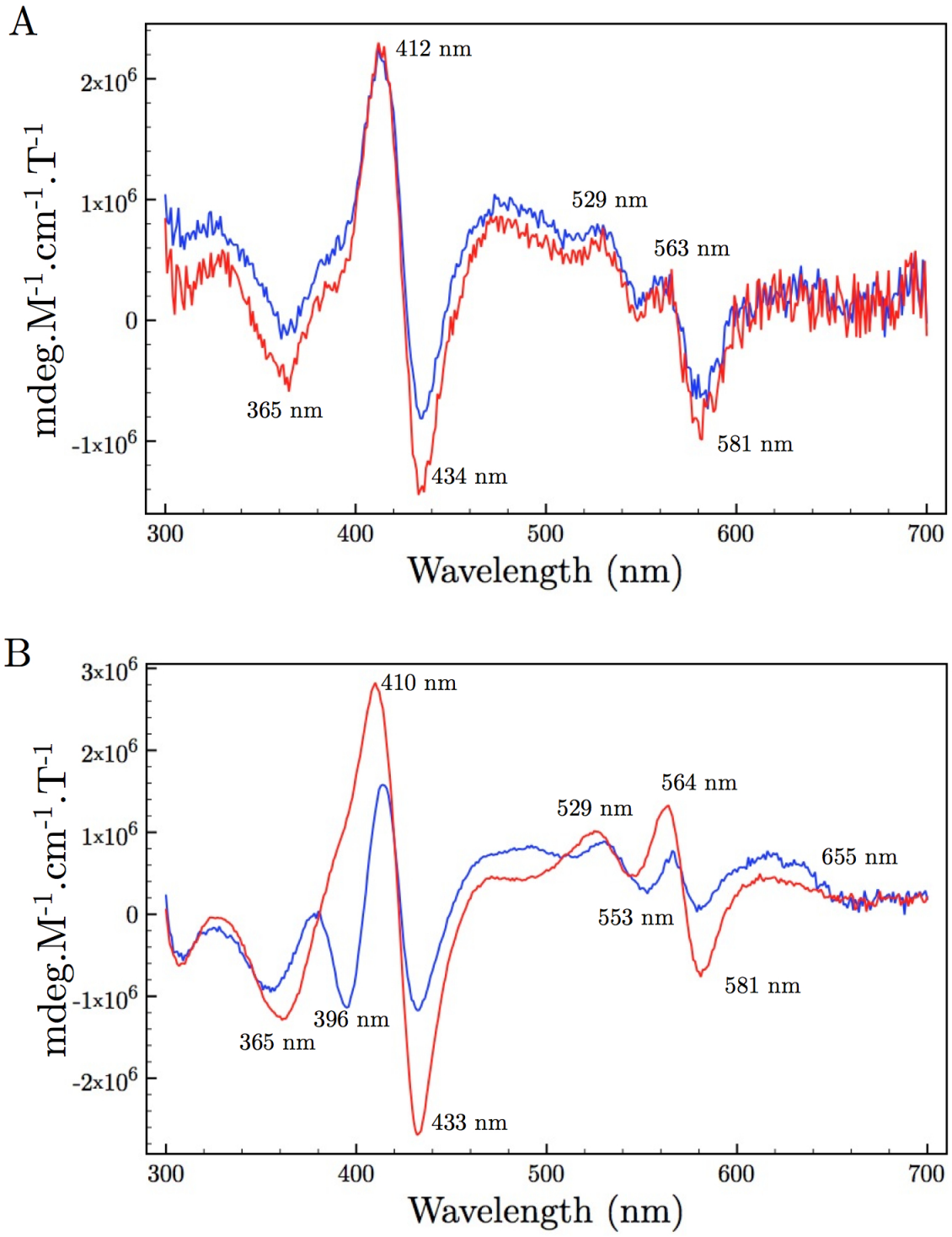

Figure 3.8: MCD Spectra of A) Thr260Ala and B) Thr260Val mutant in the absence (red) and presence of DHL (50 μM)

Table 3.1: Soret MCD Spectral Features of CYP101 and Mtb CYP51 proteins

Protein	**Spectral bands, nm**							
CYP101	356	412	418(0)	428	464	523	563	579
CYP101 + Cam	394	-	414(0)	420	-	532	555	656
WT CYP51	358	411	420.5(0)	428	465	522	562	579
WT CYP51 + DHL	358	411	420.5(0)	428	465	522	562	579
His259Ala	358	411	421(0)	430	465	524	562	579
His259Ala + DHL	356	411	422(0)	429	464	524	562	579
Thr260Ala	365	412	425(0)	434	473	529	563	581
Thr260Ala + DHL	365	412	425(0)	434	473	529	563	581
Thr260Val	362	410	422(0)	433	471	525	564	581
Thr260Val + DHL	354	414	423(0)	432	478	531	566	581

3.2.3 Oxygen Binding Kinetics

In order to understand the role of the acid-alcohol pair of Mtb CYP51 plays in O_2 binding and stability, double mixing stopped flow was performed. Ferrous CYP51 in anaerobic buffer was rapidly mixed with oxygenated buffer and 800 spectra were recorded over ∼2 seconds. This was sufficient time to observe the oxyferrous intermediate form and decay to the ferric form by the equation:

$$Fe^{2+} + \mathrm{O}_2 \xrightarrow{k_1} Fe^{2+}\mathrm{O}_2 \xrightarrow{k_2} Fe^{3+} + {\mathrm{O}_2}^{-\cdot} \tag{3.1}$$

Where k_1 is the pseudo-first order rate constant of oxygen binding to form the oxyferrous intermediate and k_2 is the rate constant for the autoxidation of oxyferrous to ferric protein and the release of the superoxide anion. Initial experiments were

performed with CYP101 in the presence of camphor as shown in Figure 3.9. The formation of oxyferrous is observed with a Soret at 421 nm which was consistent with literature [134, 143]. This peak at 421 nm decreased time dependently with the increase of a peak at 391 nm indicative of CYP101 in the ferric HS state. In order to decompose the raw time course data into basis spectra of individual components, SVD analysis was performed using the Pro-K software (Applied Photophysics). SVD analysis generated up to 8 principal components, however as only three distinct spectral species were expected (by equation 3.1), the three most relevant spectral components were selected for further analysis. These principal components were then used to perform a global fit, and reconstitute calculated spectra. This was performed by fitting the spectral components to a 3 component model i.e. A $\rightarrow$ B $\rightarrow$ C. Using this information as well as the starting concentration of the protein, three basis spectra and their concentration profiles are illustrated in Figures 3.9 B and C respectively. Experimentally, 800 spectra were recorded over 236 s. As oxyferrous formation in CYP101 is so rapid, the first scan of the mixing experiment was unable to record pure ferrous CYP101. During SVD analysis and global fit, the ferrous species was of too low a concentration to calculate a spectrum and hence is not shown in Figures 3.9 B.

The calculated k_1 for this reaction was 2.2 $\mu M^{-1}.s^{-1}$ which is comparable to literature values of 1.7 $\mu M^{-1}.s^{-1}$ [144, 145]. The autoxidation rate (k_2) was calculated to be 0.006 s^{-1} at 298 K. This is consistent with literature values for CYP101 of 0.004 s^{-1} measured at 293 K [146] and 0.0043 s^{-1} measured at 296 K [143]. The reproduction of the published rate constants validated this approach in our hands.

Figure 3.10A shows the time profile of the mixing of ligand free ferrous Mtb CYP51 wild type with oxygenated buffer. The first and last scan over a two second timescale show spectral features features consistent with ferrous and ferric CYP51 wild type respectively. As no distinct oxyferrous species was observed over this timescan, SVD

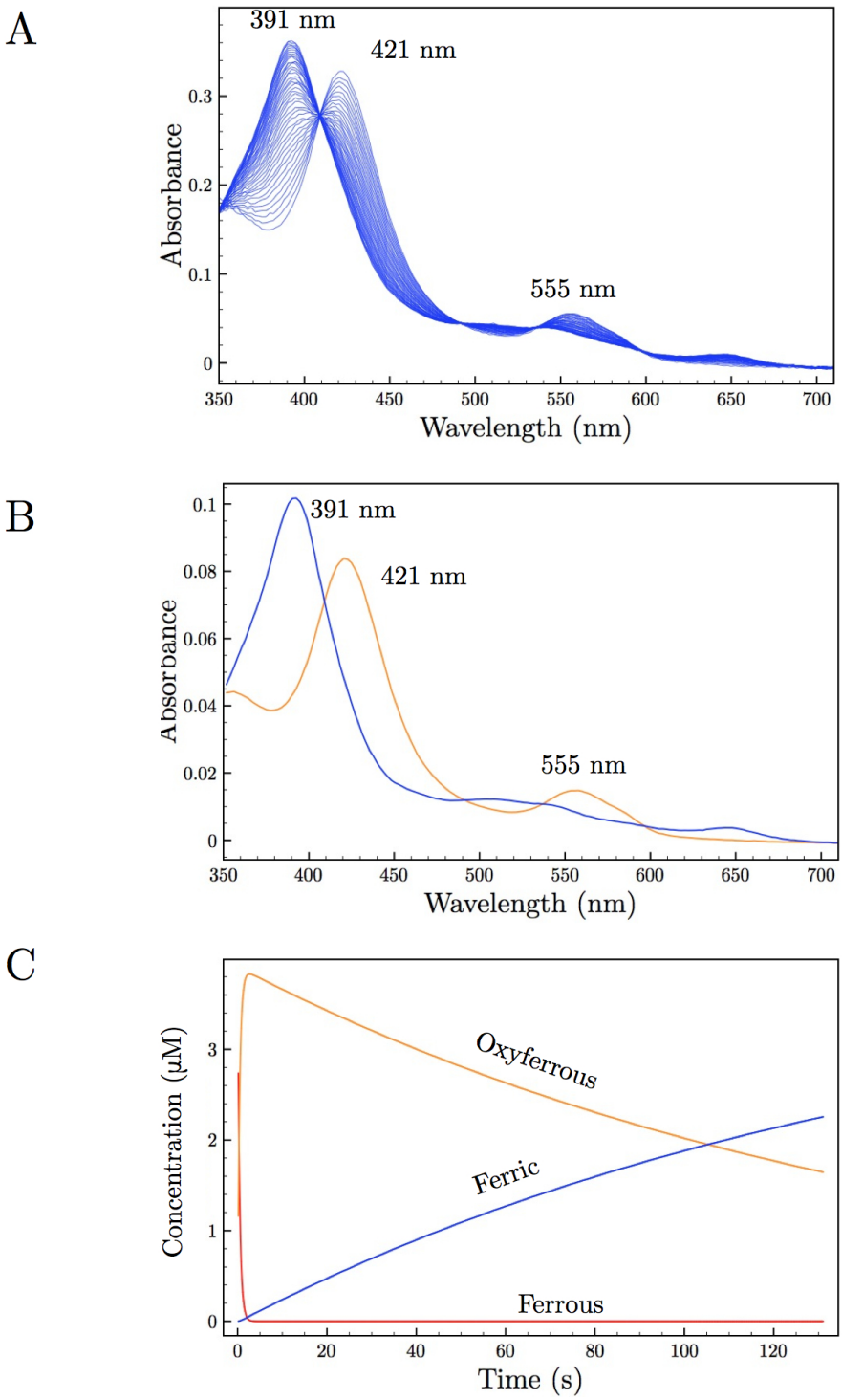

Figure 3.9: A)Stopped flow spectra over 236 seconds of CYP101 at 298 K. B) Invdividual components from the calculated spectra of global fit of SVD analysis where the blue spectrum is the ferric high spin and orange is the oxyferrous state of CYP101. C) The concentration profiles of each of the calculated spectra over time.

Table 3.2: Rate Constants of Oxyferrous Formation and Oxidation in CYP51 proteins

	- DHL		**+ DHL (50 μM)**	
Protein	k_1	k_2	k_1	k_2
WT CYP51	63.1(±3.6)	2.1(±0.1)	15.3(±0.9)	2.6(±0.1)
His259Ala	35.7(±3.8)	2.0(±0.1)	67.85(±1.3)	1.8(±0.1)
Thr260Ala	30.9(±4.6)	3.4(±0.5)	31.6(±3.4)	2.9(±0.1)
Thr260Val	16.2(±2.6)	2.5(±0.4)	32.0(±5.6)	7.3(±1.3)

Where k_1 (units $\mu M^{-1}.s^{-1}$) is the rate constant for binding of oxygen to the ferrous species and k_2 (units s^{-1}) is the autoxidation of the oxyferrous species to the ferric protein. Bracketed values represent the standard deviations of three repeated mixing experiments of the same conditions.

analysis was performed as previously described. Using this information as well as the starting concentration of the protein, three spectral species are illustrated in Figure 3.10 B. The calculated spectra of the oxyferrous species was slightly blue shifted in its Soret (422 nm) when compared to the ferrous Soret (424 nm). The charge transfer bands of the oxyferrous species overlapped that of the peaks seen in the spectrum of the ferrous species. This spectrum of the oxyferrous species was confirmed by cryogenic oxyferrous formation (Chapter 4). All the rate constants for the wild type and each mutant protein in the absence and presence of substrate are shown in Table 3.2. The rate constant k_1 for oxygen binding to the ferrous enzyme was 63.1 $\mu M^{-1}.s^{-1}$ and k_2 for the autoxidation of the oxyferrous species was 2.2 s^{-1} (Table 3.2).

The rate constants for oxygen binding (k_1) to the ferrous wild type protein is decreased by approximately four fold in the presence of saturating concentrations of DHL as shown in Table 3.2. The rate of autoxidation or k_2 however is not changed in the presence of ligand. In the case of the His259Ala mutant, k_1 is just over half the rate of the wild type enzyme and the rate of autoxidation is unaffected by this

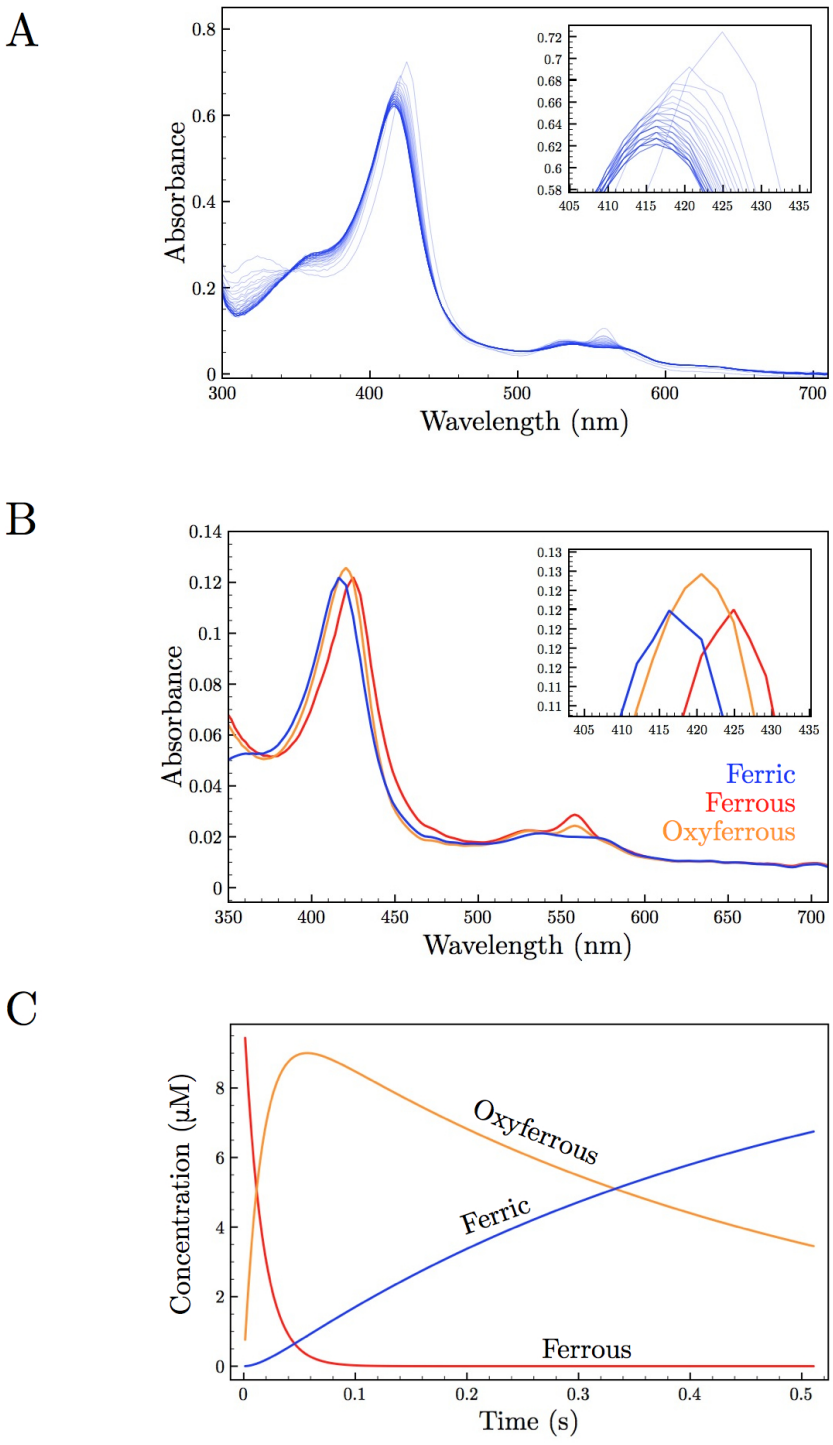

Figure 3.10: A)Stopped flow spectra over 2 seconds of CYP51 wildtype at 298 K. B) Invdividual components from the calculated spectra of global fit of SVD analysis where the blue spectrum is the ferric low spin, the red is ferrous and orange is the oxyferrous state of CYP51 wild type. C) The concentration profiles of each of the calculated spectra over time .

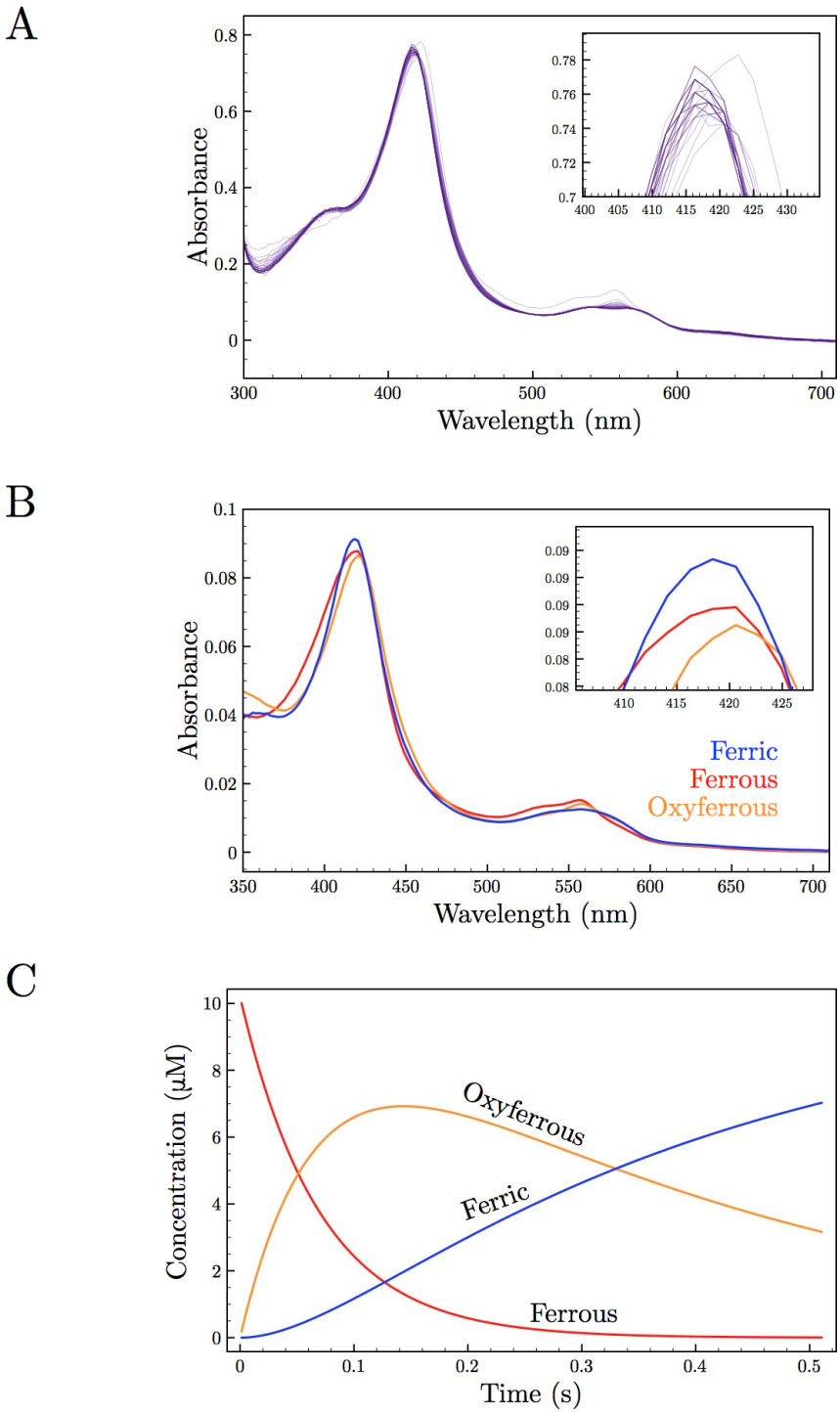

Figure 3.11: A)Stopped flow spectra over 2 seconds of CYP51 wildtype in the presence of 50 μM DHL at 298 K. B) Invdividual components from the calculated spectra of global fit of SVD analysis where the blue spectrum is the ferric low spin, the red is ferrous and orange is the oxyferrous state of CYP51 wild type. C) The concentration profiles of each of the calculated spectra over time .

mutation. However in the presence of DHL the His259Ala mutant shows a k_1 of 67.85 $\mu M^{-1}.s^{-1}$ which is approximately four fold higher than the rate constant of the wild type protein with ligand. The rate of autoxidation in this mutant is also not affected by DHL being present. The Thr260Val mutant shows a decreased rate constant of oxygen binding almost 4 times slower than that of the wild type and half that of the His259Ala mutant, but without significant difference in the autoxidation rate constant. Substrate bound Thr260Val showed a two fold increase in k_1 to 32.0 $\mu M^{-1}.s^{-1}$ but showed a 3 fold increase in the rate constant of autoxidation. The Thr260Ala mutant's rate constants were similar to that of the His259Ala mutant. As there is evidence that the Thr260Ala mutant does not bind DHL, it would be expected that the rate constants for this mutant would not change in the presence of substrate, which was the case.

Comparing the wild type protein in the presence of DHL to CYP101 in the presence of camphor (1 mM), wild type CYP51 has an oxygen binding rate constant of 15.3 $\mu M^{-1}.s^{-1}$ at 298 K, and CYP101 has an oxygen binding rate constant of 1.7 $\mu M^{-1}.s^{-1}$ [144, 145]. The difference between ligand free and ligand bound forms of the wild type protein may be due to the ligand partially shielding the active site. In the absence of ligand Mtb CYP51 shows a much quicker autoxidation rate in comparison to CYP101 (0.014 s^{-1}) [146]. Mtb CYP51 has a much slower rate constant for this substrate-free autoxidation however, when compared to CYP3A4 (100 s^{-1}) [23]. What is consistent between CYP101 and CYP3A4 is that in the presence of ligand, the rate constant for autoxidation, is increased by 3 - 8 fold. This is however not the case when when comparing the autoxidation rate constants of wild type CYP51 protein in the substrate bound and substrate free forms.

The His259 in Mtb CYP51 is similar to to Asp251 in CYP101 as it plays the role of the acid, in the conserved acid-alcohol pair. The fact that the ferrous form of the

His259Ala mutant shows a slower rate in oxygen binding implies that it would have a slower turnover of product if this is the rate determining step. The Asp251Asn mutant of CYP101 was shown to decrease the turnover rate of NADH however the mutant still retained the ability to hydroxylate substrate [57, 147]. This decreased turnover of NADH was attributed to the retarded rate of ferrous formation of the Asp251Asn mutant, and not oxygen binding to the ferrous form. The rate of oxygen binding however is decreased in this mutant of CYP101 by almost half [57] in the presence of camphor. This is in contrast to the His259Ala mutant which shows an accelerated rate constant by almost four times when compared to wild type in the presence of DHL. Under the same conditions there is slight decrease in autoxidation rate (1.8 s^{-1}) in the His259Ala mutant compared to wild type (2.6 s^{-1}).

The Thr260Ala mutant shows comparable oxygen binging rate constants to the His259Ala mutant in the absence of ligand with a slight increase in autoxidation rate (3.4 s^{-1} for Thr260Ala) relative to wild type (2.1 s^{-1}) and His259Ala (2.0 s^{-1}) mutants. This is comparable to the Thr252Ala mutation of CYP101 however the rate of autoxidation in this mutant was almost an order of magnitude greater in the mutant [148]. It is thought that the Thr252 in CYP101 forms a hydrogen bond to the bound oxygen and stabilizes this state [46, 149]. The data with regards to Thr260Ala of CYP51 supports that this mutant does not bind to DHL.

The Thr260Val mutant shows a four fold decrease in oxygen binding rate relative to wiltype in the absence of substrate, however there is no major difference in the autoxidation rates. In the presence of ligand however, the Thr260Val mutant behaves as expected with regards to autoxidation rates relative to the wild type protein when compared to the Thr252Ala and Thr252Val mutants in of CYP101. That is, this mutation would have an increased rate of autooxidation. The Thr260Val mutant's rate of autoxidation was almost three fold higher than that of the wild type (7.3 s^{-1} vs 2.6

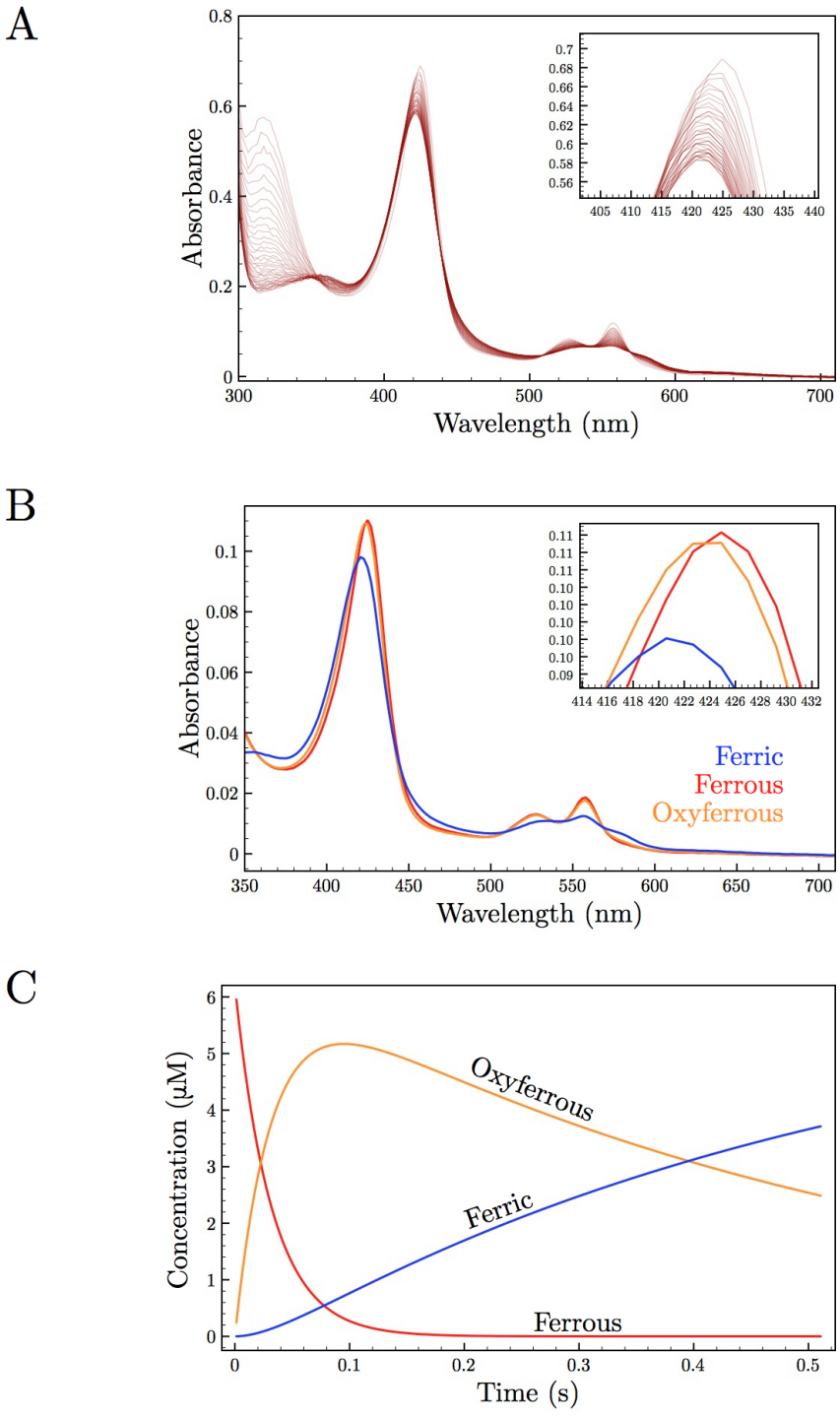

Figure 3.12: A)Stopped flow spectra over 2 seconds of CYP51 His259Ala at 298 K. B) Invdividual components from the calculated spectra of global fit of SVD analysis where the blue spectrum is the ferric low spin, the red is ferrous and orange is the oxyferrous state of CYP51 His259Ala. C) The concentration profiles of each of the calculated spectra over time .

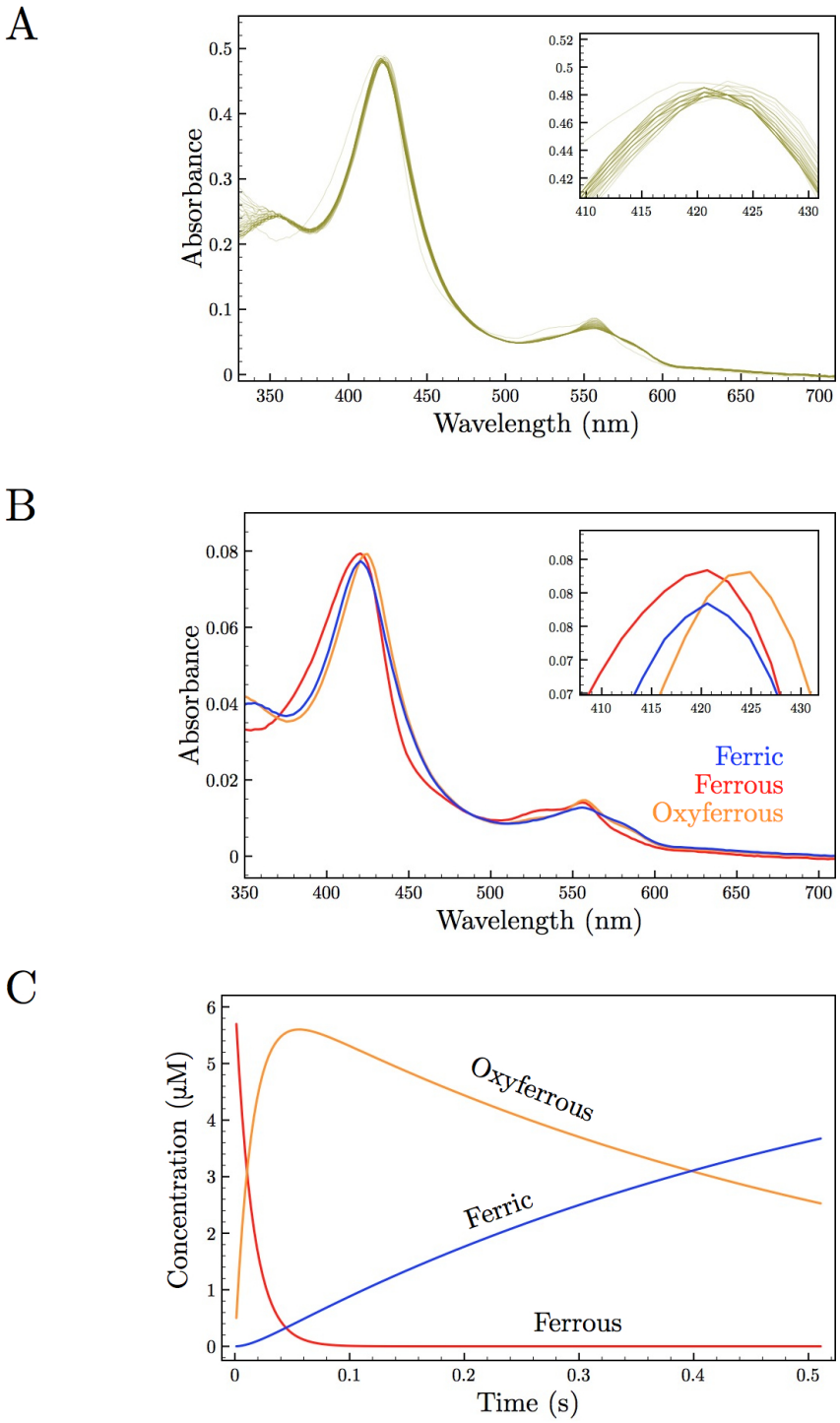

Figure 3.13: A)Stopped flow spectra over 2 seconds of CYP51 His259Ala in the presence of 50 μM DHL at 298 K. B) Invdividual components from the calculated spectra of global fit of SVD analysis where the blue spectrum is the ferric low spin, the red is ferrous and orange is the oxyferrous state of CYP51 His259Ala. C) The concentration profiles of each of the calculated spectra over time .

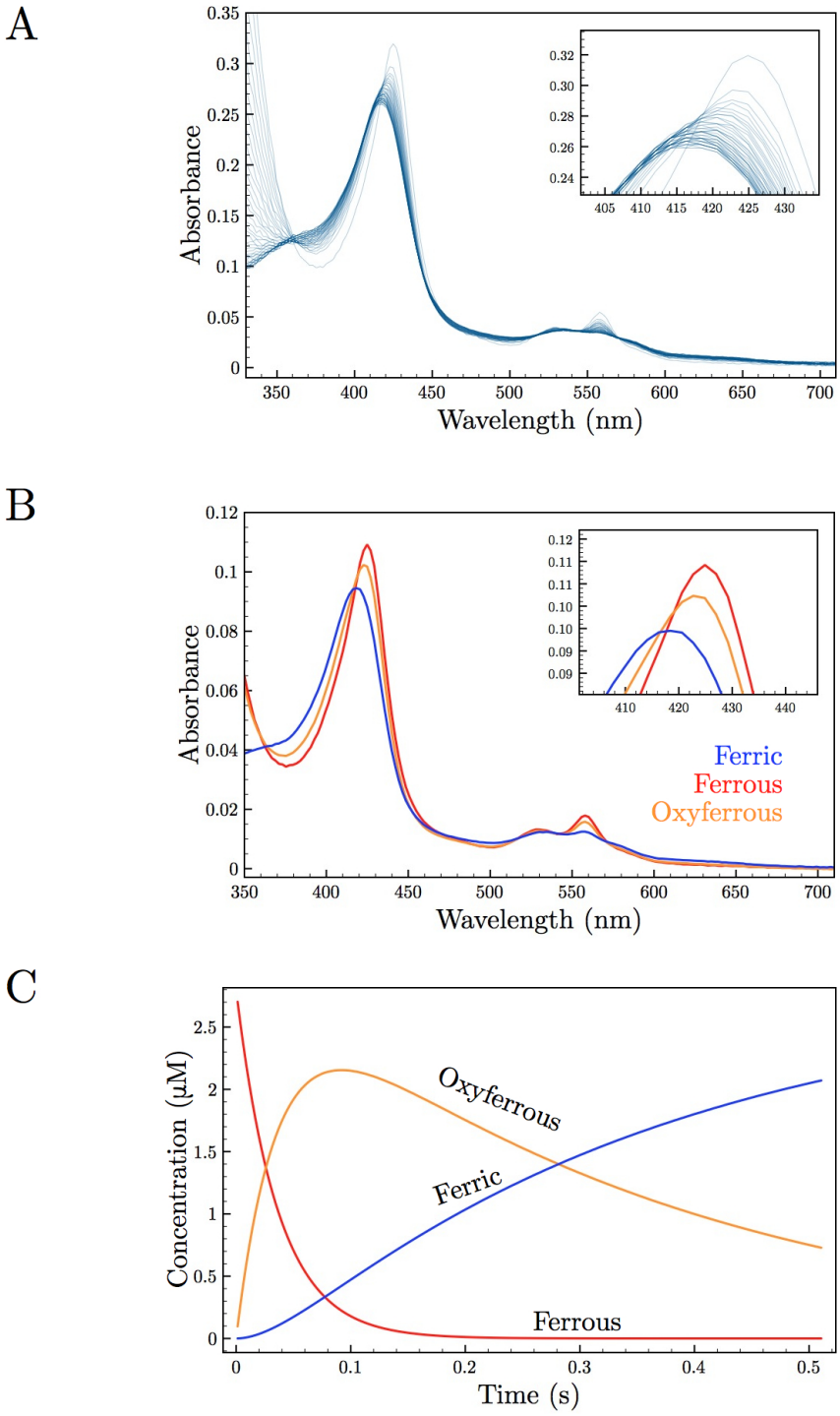

Figure 3.14: A)Stopped flow spectra over 2 seconds of CYP51 Thr260Ala at 298 K. B) Invdividual components from the calculated spectra of global fit of SVD analysis where the blue spectrum is the ferric low spin, the red is ferrous and orange is the oxyferrous state of CYP51 Thr260Ala. C) The concentration profiles of each of the calculated spectra over time

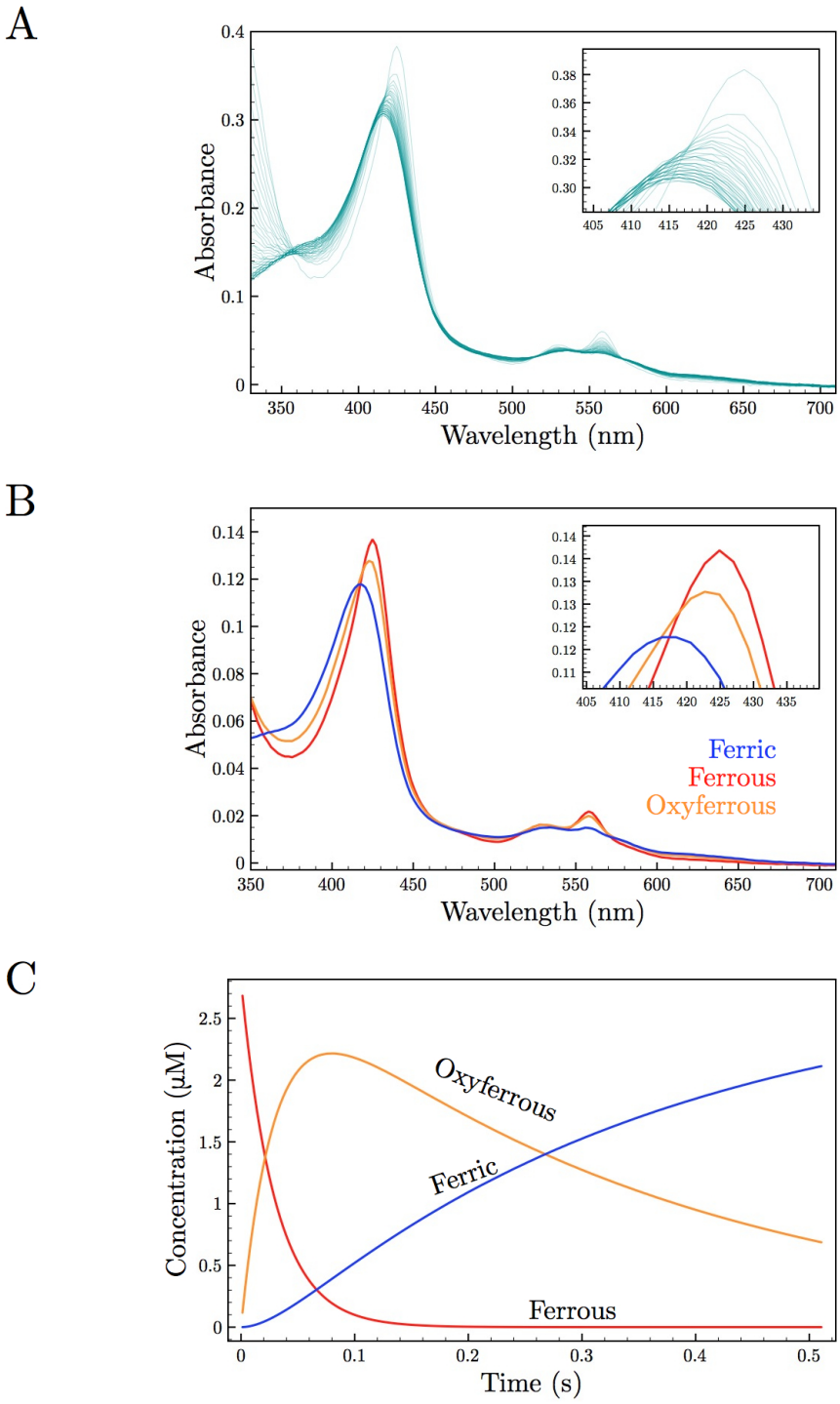

Figure 3.15: A)Stopped flow spectra over 2 seconds of CYP51 Thr260Ala in the presence of 50 μM DHL at 298 K. B) Invdividual components from the calculated spectra of global fit of SVD analysis where the blue spectrum is the ferric low spin, the red is ferrous and orange is the oxyferrous state of CYP51 Thr260Ala. C) The concentration profiles of each of the calculated spectra over time .

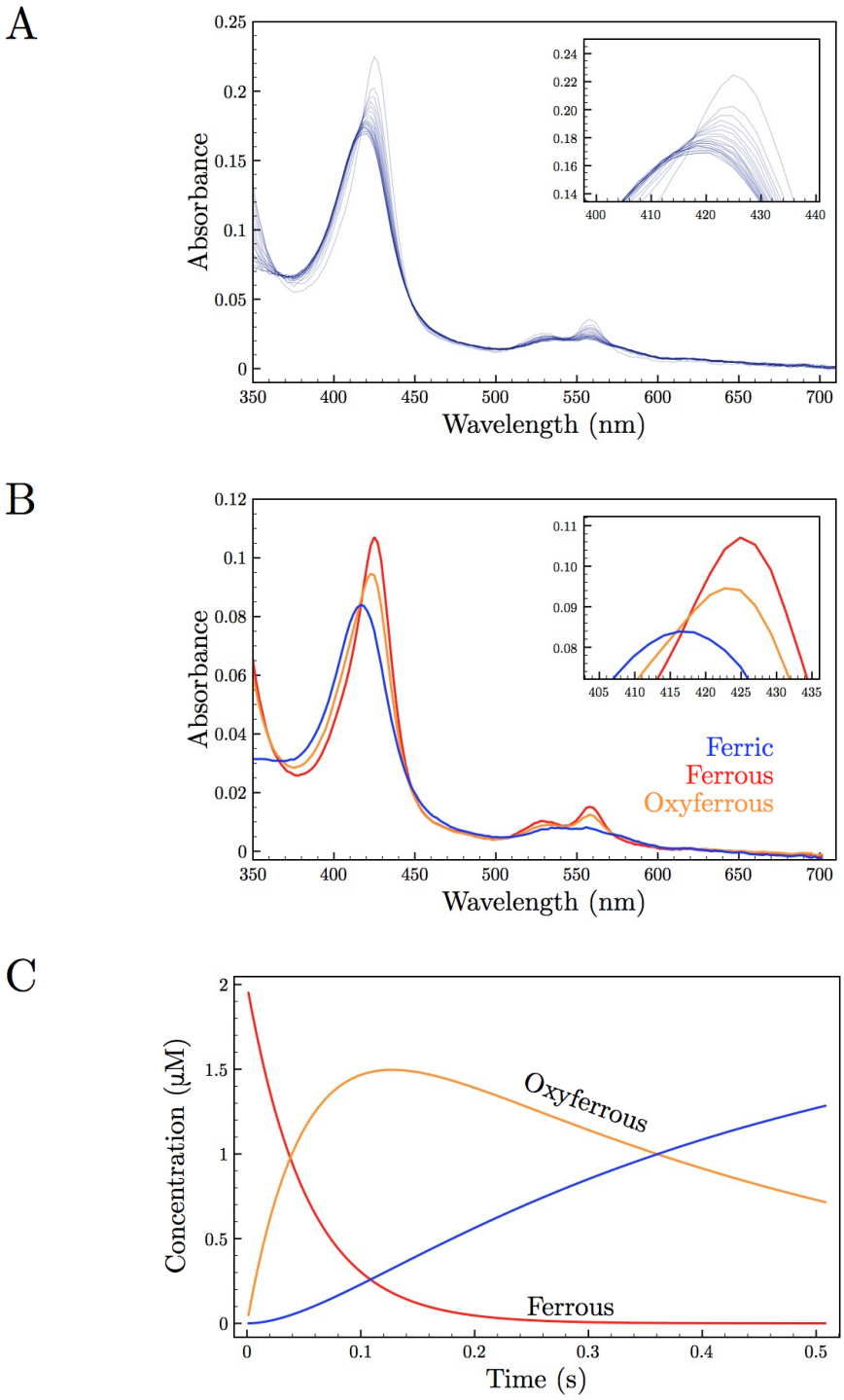

Figure 3.16: A)Stopped flow spectra over 2 seconds of CYP51 Thr260Val at 298 K. B) Invdividual components from the calculated spectra of global fit of SVD analysis where the blue spectrum is the ferric low spin, the red is ferrous and orange is the oxyferrous state of CYP51 Thr260Val. C) The concentration profiles of each of the calculated spectra over time

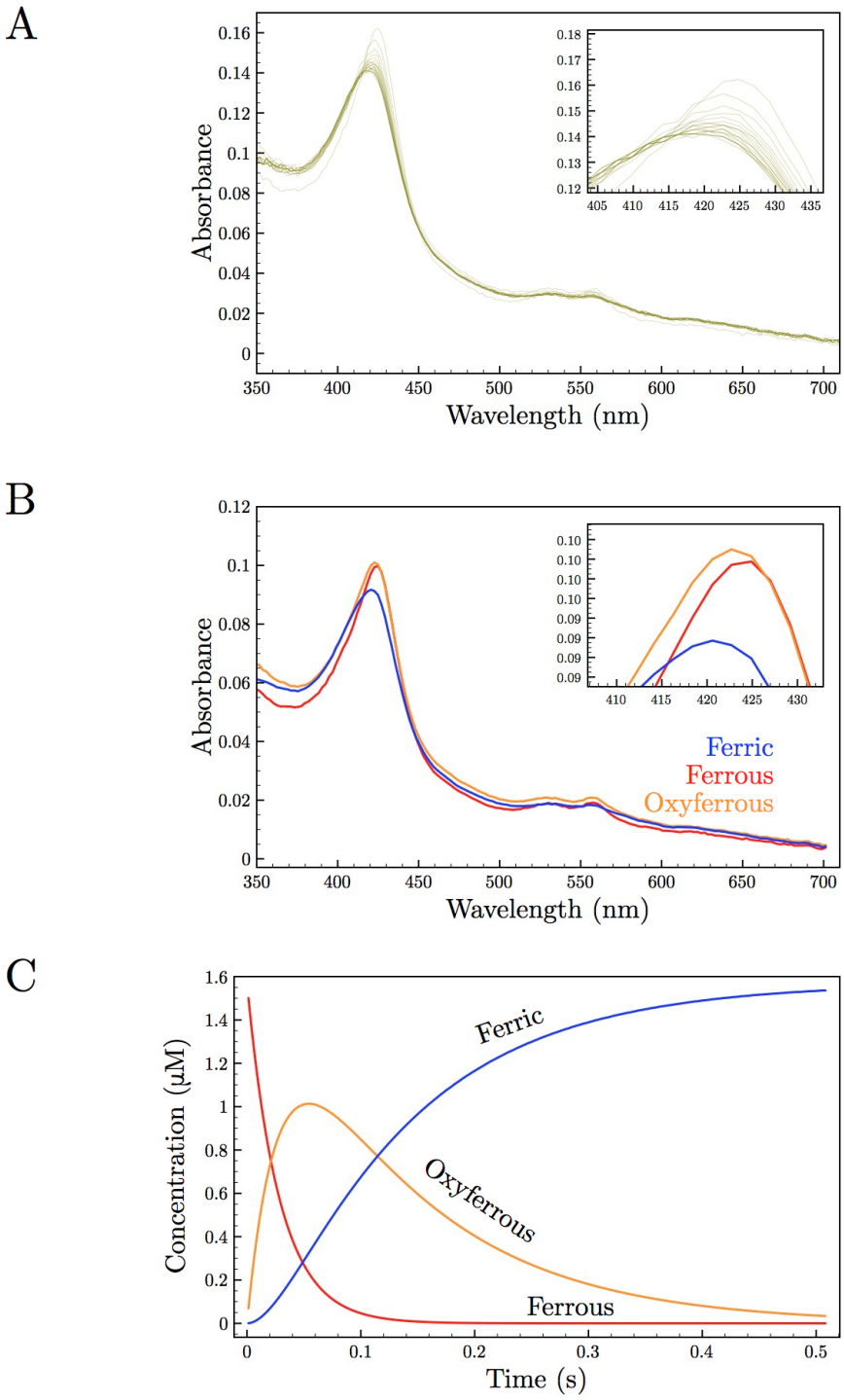

Figure 3.17: A)Stopped flow spectra over 2 seconds of CYP51 Thr260Val in the presence of 50 μM DHL at 298 K. B) Invdividual components from the calculated spectra of global fit of SVD analysis where the blue spectrum is the ferric low spin, the red is ferrous and orange is the oxyferrous state of CYP51 Thr260Val. C) The concentration profiles of each of the calculated spectra over time .

s^{-1}) and those of the Thr252Ala and Thr252Val mutants of CYP101 were almost 10 times higher than that of the wild type [46]. This implies that in the presence of DHL, the oxyferrous form of Mtb CYP51 might be stabilized through an interaction between Thr260 and the iron-bound dioxygen. Potentially Thr260 is positioned so that it may interact with the iron-bound peroxide in the peroxo intermediate of the wild-type enzyme. Potentially the presence of substrate is sufficient to disrupt the hydrogen bonding water network so that in the absence of the Thr260 hydroxyl group, the oxyferrous rapidly autoxidizes. In the absence of ligand, O_2 may not have a hydrogen bond from the Val residue, however the remaining volume of the active site may be filled with water for hydrogen bonding. Addition of DHL may displace this water and abolish any potential hydrogen bond interactions, effectively destabilizing the oxyferrous complex.

In situ Generation of Early Oxygen Intermediates in *Mycobacterium Tuberculosis* CYP51

4.1 Introduction

The oxyferrous intermediate of Mtb CYP51 had previously been observed and characterized by stopped flow UV-vis spectroscopy, in Chapter 3 at 298 K. This previous work established an important experimental platform in order to study more reactive intermediates intermediates of the CYP catalytic cycle. *In vivo*, the reduction of the oxyferrous species results from the transfer of an electron from a ferredoxin. In most CYPs, this reduced oxyferrous species does not accumulate in ambient temperatures. Cryogenic trapping is one tool that can be utilized to isolate, directly observe and characterize these transient species. Cryogenic trapping of catalytic intermediates requires a protein to be trapped in a matrix in a manner akin to isolating organic molecules in frozen noble gases [150, 151] at very low temperatures (between 4 K - 77 K). Cryogenic matrix isolation studies of enzymes are not new, as spectroscopic techniques such as electron paramagnetic resonance (EPR) and Mössbauer make use of cryogenic temperatures.

Optical spectroscopy such as UV-vis requires the trapping of an enzyme in a transparent matrix in the wavelength range used in the experiment. Many solvents have been exploited in order to attain an optically transparent "glass" at low temperatures, ranging from methylcyclopentane, to ethanol and boric acid [152]. The requirements of the solvent used in these studies are, they must be non-denaturing and cause very

little if any, perturbation to the protein. Ethylene glycol, trehalose and glycerol have also been used for low cryogenic trapping of proteins [153]. Glycerol solutions in a ratio of >65% (w/w) were shown to be adequate to inhibit a process of water crystallization which causes a phase separation ultimately destroying the sample's optical transparency [154].

The process of cryogenically trapping CYP catalytic intermediates relies on the process of stabilizing these intermediates for an appreciable timescale at temperatures low enough for there to be insufficient energy to overcome the energetic barrier of the intermediates decay. Generating these intermediates, in particular the one electron reduced oxyferrous species, requires a cryoreduction technique. Essentially, the oxyferrous intermediate must be formed at ambient temperatures (277 K) in order to be experimentally feasible, after which this intermediate must be frozen (77 K) at which point a cryoradiolytic technique can be used in order to reduce this intermediate. Cryoradiolytic techniques can employ a number of methods in order to reduce the trapped oxyferrous species. These include irradiating samples with high-energy photons such as a X-rays, gamma rays from ^{60}Co [15, 130, 155], or ^{32}P [127, 155, 156]. The latter can be added to the sample as which can be conveniently added to the sample in the form of ^{32}P-ortho-phosphoric acid to afford *in situ* radiolysis.

The cryoradiolytic technique generates intermediates *in situ* while the protein is trapped within a frozen matrix. Other techniques such as rapid scanning UV-vis stopped flow are able to observe more stable catalytic intermediates as well. However they require elaborate machinery, that will allow for mixing of multiple buffers (oxygenated versus deoxygenated) and proteins (CYP and ferredoxin) in order reconstitute the catalytic cycle. It is because of these reasons as well as its relative ease in generating and stabilizing these intermediates that makes cryoradiolysis an indispensable technique. Isolating the reduced oxygen intermediates is critical in the

understanding of which catalytic intermediates may be stabilized by CYP51 during its catalysis and under which conditions these intermediates are present if we are to fully understand the mechanism by which CYP51 promotes C-C cleavage.

After this cryoradiolytic reduction, the newly formed intermediates will be stable at 77 K. Spectroscopic characterization of these intermediates can then take place. In this study, proteins were reduced in an oxygen free environment to form the ferrous species. After excess reductant was removed, the ferrous protein was mixed with oxygenated glycerol and ^{32}P-ortho-phosphoric acid in order to form the oxyferrous intermediate. These samples were frozen at 77 K and left untouched for four weeks at at this temperature. This four week incubation of the oxyferrous protein with ^{32}P-ortho-phosphoric acid was sufficient to allow *in situ* radiolysis to occur. After this incubation, the samples were subjected to UV-vis spectroscopy and temperature annealing experiments were performed. Temperature annealing is the raising of the temperature in increments and at each temperature, spectra are recorded. The catalytic intermediates and their stability are dependent on temperature, hence as temperature is raised, intermediates will decay and new intermediates will form. This decay and formation of new intermediates can be monitored spectrscopically.

With the previously characterized oxyferrous intermediate of Mtb CYP51 and its mutants described in Chapter 3 further studies at cryogenic temperatures were performed to capture and characterize reduced dioxygen intermediates in wild type and mutant CYP51.

4.2 **Results and Discussion**

4.2.1 UV-visible spectroscopy of Oxyferrous Intermediates at Cryogenic Temperatures

Exploiting the handful of literature describing radiolytic reduction of CYP101, we aimed to reproduce these observations to evaluate our experimental approach. CYP101 served as a convenient standard for which to compare our cryogenic studies for several reasons. First, oxyferrous CYP101 can be prepared in high yield and is stable at 277 K. Second, there are easily recognizable differences in the Soret bands of CYP101 species. Three experimental reactions were set up, to evaluate varying conditionsin collecting UV-vis spectra at low temperature. The ferric, ferrous and oxyferrous states, would allow for observation of any perturbations that could occur as a result of low temperatures as well as the increased concentrations of glycerol, when compared to those performed at ambient temperatures. As shown in Figure 4.1 A, the three distinct spectral signatures are apparent for ferric, ferrous and oxyferrous. The ferric spectra is identical to that of CYP101 in the high spin state at ambient temperatures, with a Soret at 393 nm and a weak band at 645 nm. As with the ferrous spectra, a Soret at 410 nm and a shoulder at 543 nm were as expected [127, 157, 158]. The oxyferrous species showed a Soret at 417 nm a weak band at 351 nm and a peak at 553 nm which as previously reported are all spectral features of CYP101 in the oxyferrous state [127, 157, 158]. The spectral characteristics of these states of CYP101 were indicative of the fact that minor if any perturbations occurred under the conditions of high concentrations of glycerol, and temperatures below 77 K. The stability of the CYPs at 77 K is critical for the generation of reduced oxyferrous species. It is known that certain proteins may undergo cold denaturation [159,160]and these studies served to confirm the absence of this denaturation The incubation of protein with ^{32}P-ortho-phosphoric acid would have to be performed at 77 K for four weeks at a

time for there to be sufficient isotope decay in order for cryoradiolysis to occur.

As with CYP101, the ferric, ferrous and oxyferrous states of Mtb CYP51 and its mutants were prepared, each in the presence and absence of 50 μM DHL. Results of each spectra recorded (Figures 4.2, 4.3, 4.4 and 4.5) were consistent with previously recorded spectra at ambient temperature as well as the basis spectra of the oxyferrous spectra from Chapter 3. With only slight shifts in ($<$ 2 nm) peaks being seen, which when taking into consideration the wavelength intervals of the stopped flow instrument was 2 nm is within the resolution of the instrument.

4.2.2 Reduced Oxyferrous Intermediates and Temperature Annealing

Following our success in capturing oxyferrous CYP101, we adapted the *in situ* cryoradiolysis technique using 10 mCi of ^{32}P-ortho-phosphoric acid to reduce oxyferrous CYP101. Incubation of these samples took place for up two 6 weeks but no less than four weeks at 77 K. Previous work performed by Denisov using a ^{60}Co had shown that 4-5 Mrad was sufficient to reduce the oxyferrous of species of CYP101 [130]. The addition of 10 mCi of ^{32}P-ortho-phosphoric acid would be equivalent to 3.5 Mrad during its first half-life (342 hr or $\sim$2 weeks). This incubation was sufficient to yield a species with Soret at approximately 440 nm at 77 K as shown in Figure 4.1 B. This 440 nm Soret is characteristic of the hydroperoxo species as confirmed by Denisov and coworkers [127, 130].

The intermediates generated by cryoradiolytic reduction of wild type Mtb CYP51 after four weeks of incubation shows a split Soret at approximately 421 nm and 442 nm seen in Figure 4.6 C, with α-band at 565 nm and 531 nm. When comparing this to CYP101, the newly formed peak at 442 nm is distinctly red shifted from that of the oxyferrous complex in both proteins. The peak at 442 nm in Mtb CYP51 wild type is speculated to be either the ferric-peroxo or ferric-hydroperoxo species as seen in the

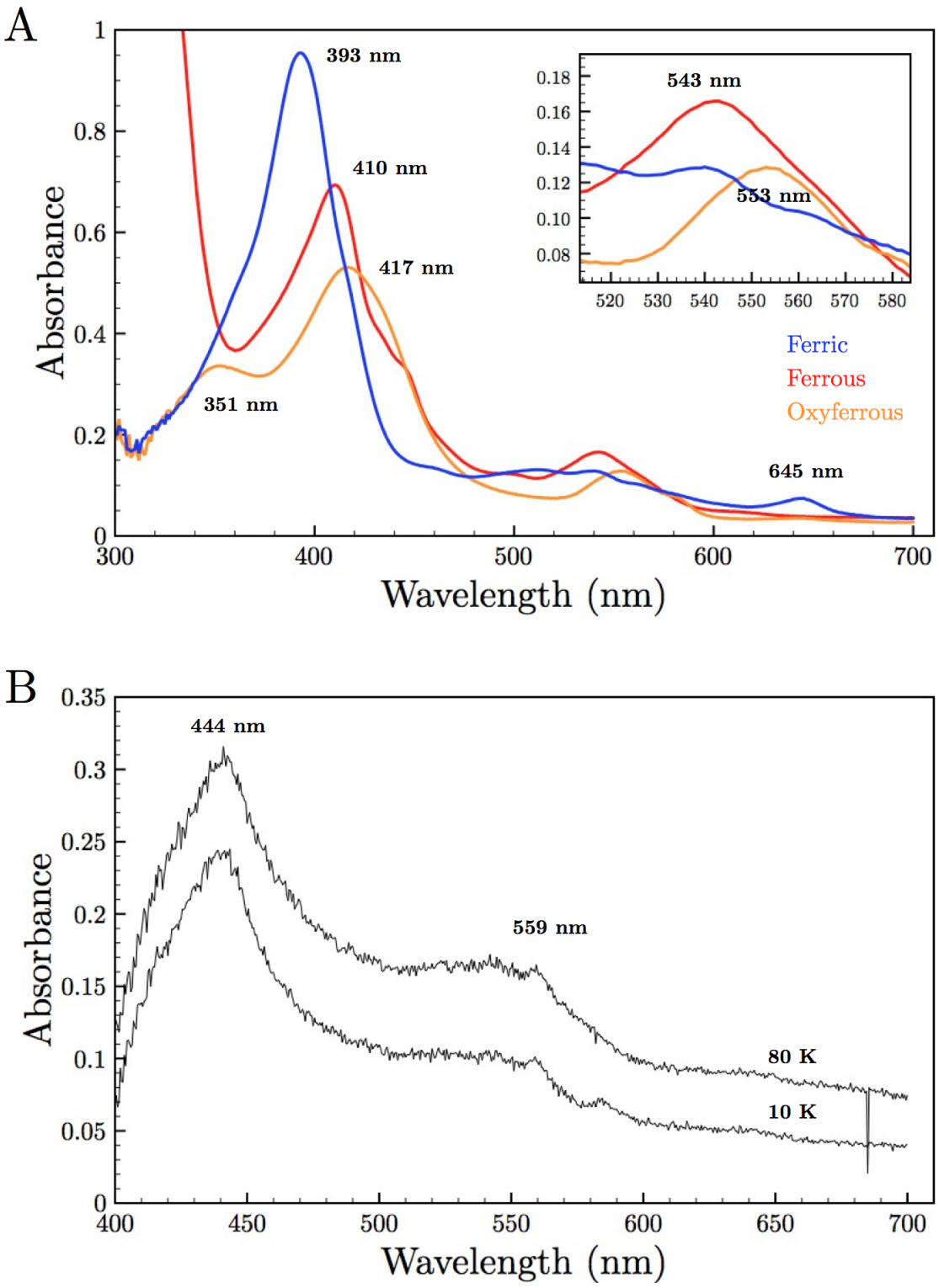

Figure 4.1: A)UV-vis spectra of Ferric, Ferrous and Oxyferrous CYP101 at 77 K. B) UV-vis spectra of CYP101 at 77 K after four weeks of incubation with ^{32}P-orthophosphoric acid at 77 K

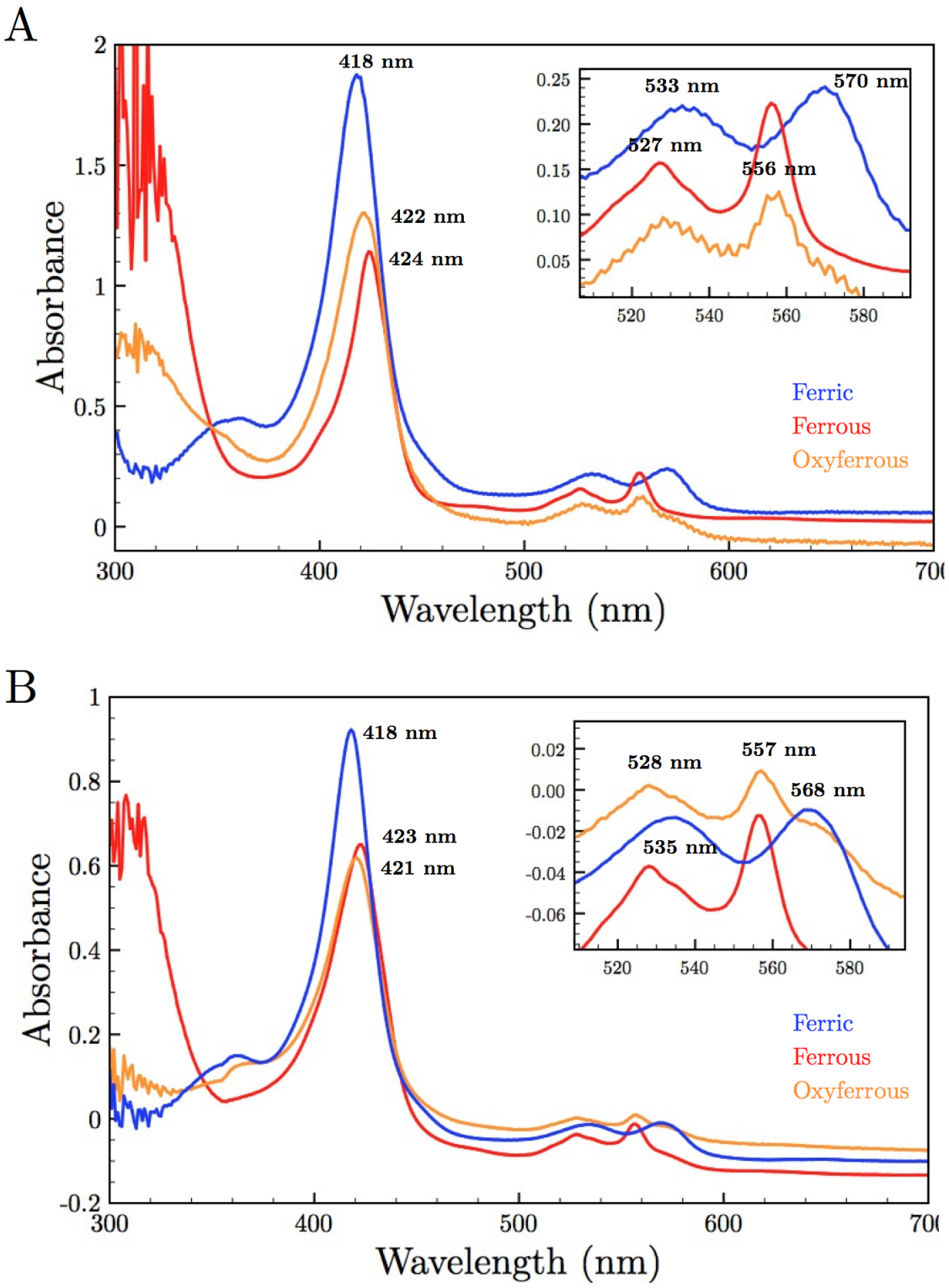

Figure 4.2: A)UV-vis spectra of Ferric, Ferrous and Oxyferrous CYP51 wild type at 77 K. B) UV-vis spectra of Ferric, Ferrous and Oxyferrous CYP51 wild type at 77 K in the presence of 50 μM DHL

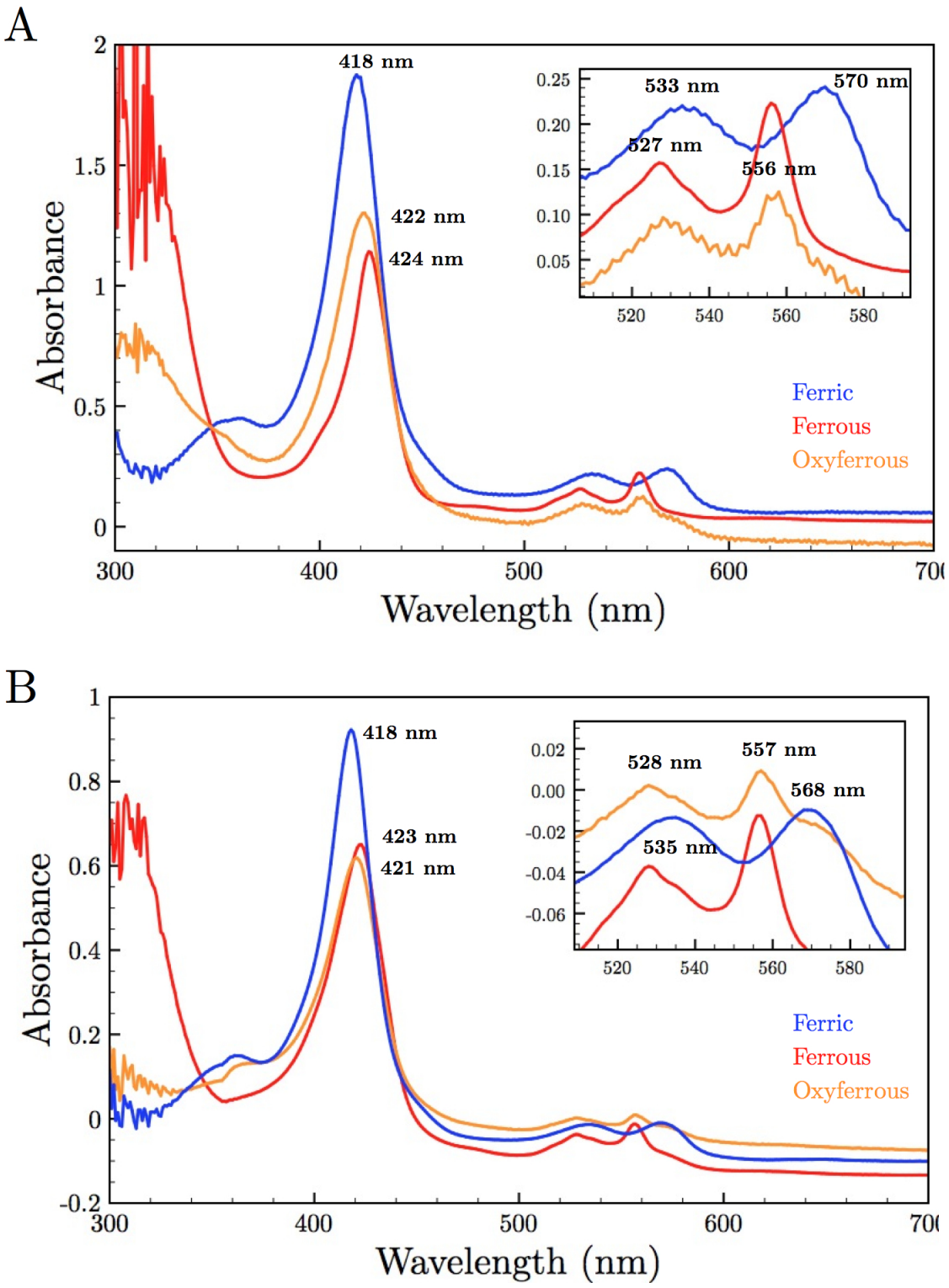

Figure 4.3: A)UV-vis spectra of Ferric, Ferrous and Oxyferrous CYP51 His259Ala at 77 K. B) UV-vis spectra of Ferric, Ferrous and Oxyferrous CYP51 His259Ala at 77 K in the presence of 50 μM DHL

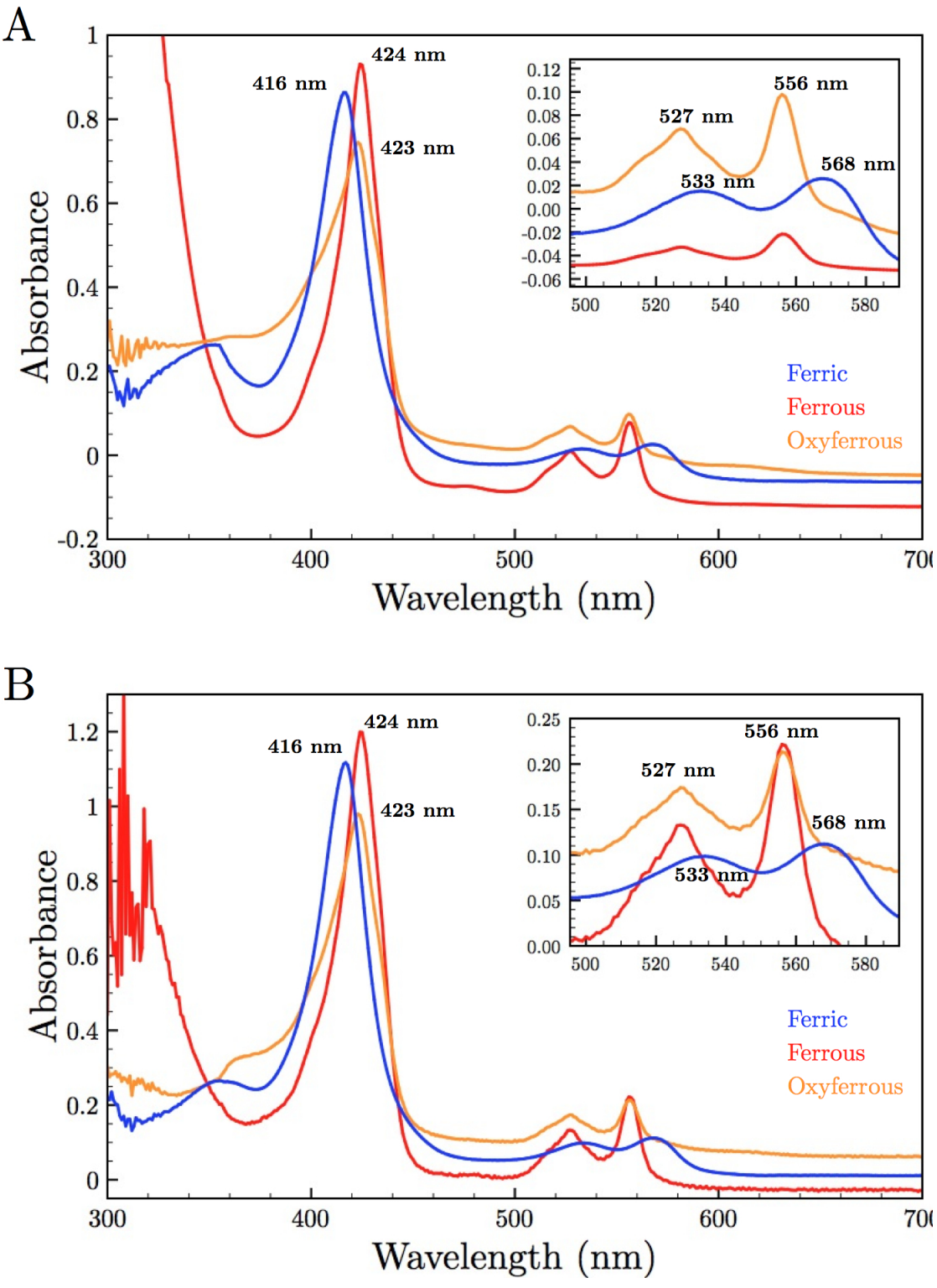

Figure 4.4: A)UV-vis spectra of Ferric, Ferrous and Oxyferrous CYP51 Thr260Ala at 77 K. B) UV-vis spectra of Ferric, Ferrous and Oxyferrous CYP51 Thr260Ala at 77 K in the presence of 50 μM DHL

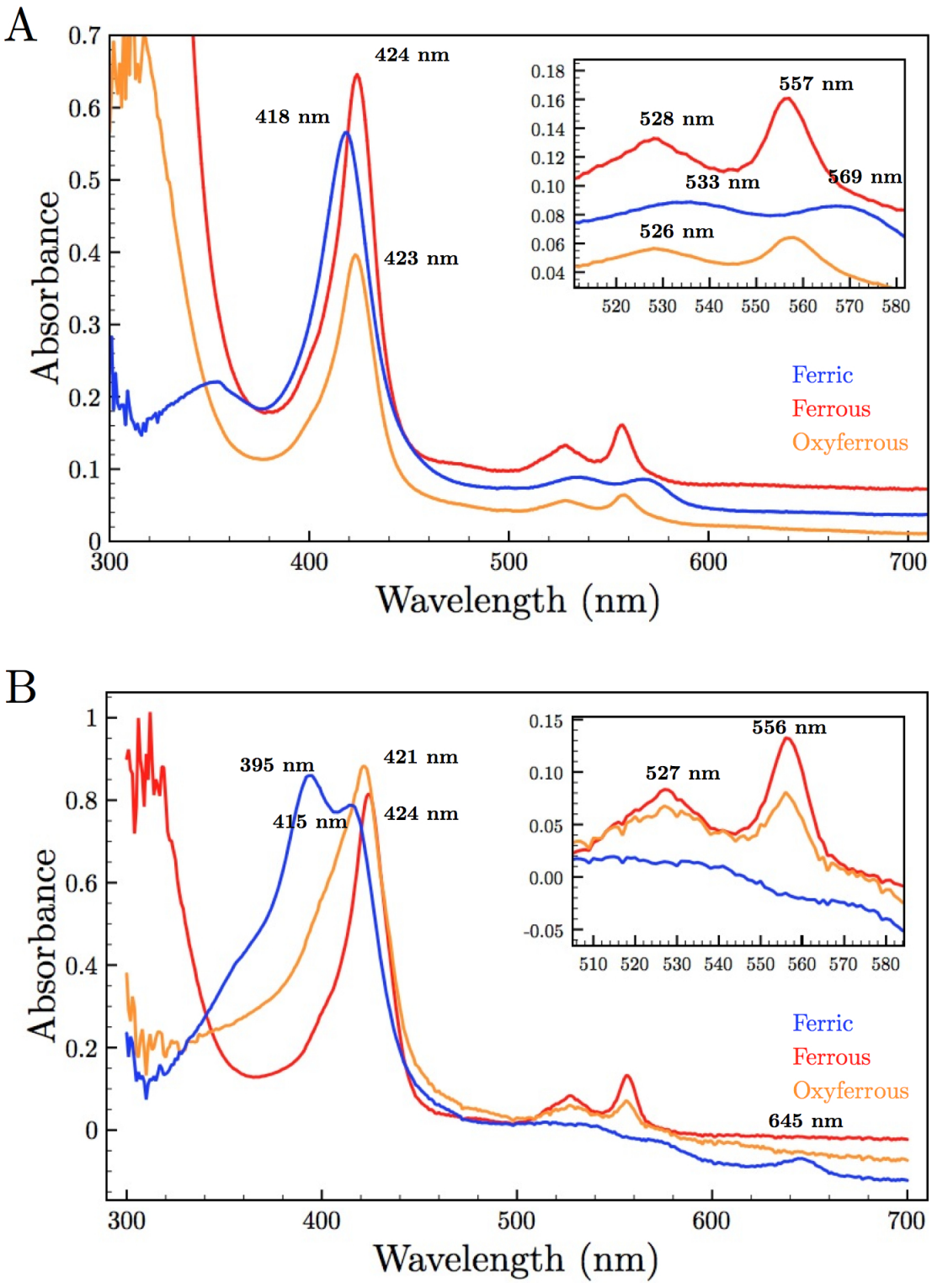

Figure 4.5: A)UV-vis spectra of Ferric, Ferrous and Oxyferrous CYP51 Thr260Val at 77 K. B) UV-vis spectra of Ferric, Ferrous and Oxyferrous CYP51 Thr260Val at 77 K in the presence of 50 μM DHL

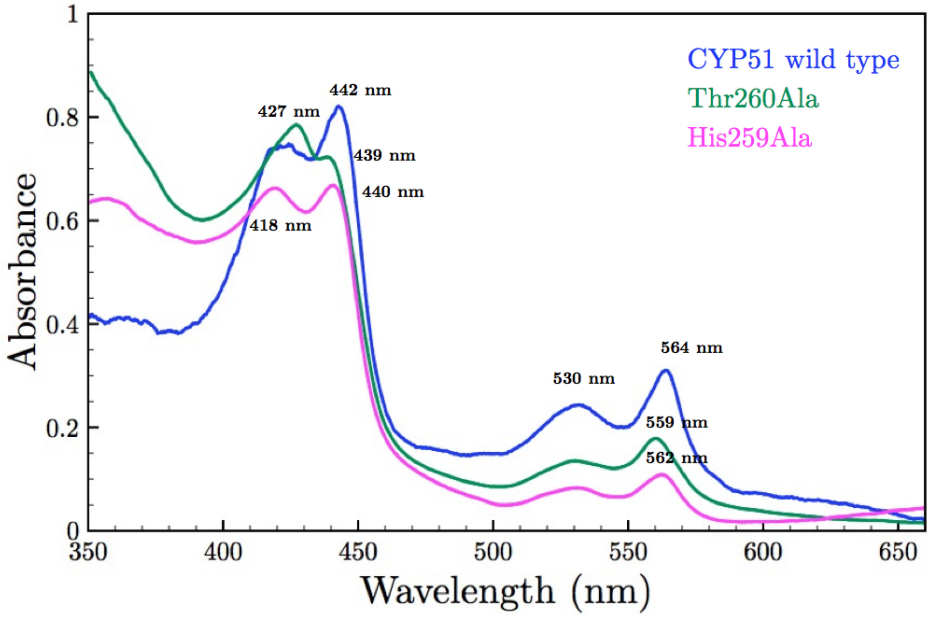

Figure 4.6: UV-vis spectra of Mtb CYP51 wild type, His259Ala and Thr260Ala at 10 K after four weeks of incubation with 10 mCi of ^{32}P-ortho-phosphoric acid.

optical spectra of CYP101 [16, 127, 130]. The broader peak at 421 nm is speculated as being a mixture of ferric and ferrous protein, based on the rapid autoxidation that may have occured in Mtb CYP51 on the addition of ferrous protein to oxygenated buffer.

After decreasing the temperature from 77 K to 4 K followed by annealing the temperature upward in increments of 10 K, the 442 nm peak begins to decrease at temperatures above 160 K and is no longer present at 180 K (Figure 4.7 A). As the 442 nm peak decreases there is an increase in a peak at 419 nm consistent with the formation of low spin ferric Mtb CYP51. SVD Analysis of annealed spectra, yields a basis spectra with a distinct Soret at 442 nm (Figure 4.7 B) consistent with literature [127] for a peroxo species. Conclusive assignment of this species will require an orthogonal spectroscopic method such as resonance Raman or electron paramagnetic

resonance. The optical spectra of the hydroperoxo and peroxo species are said to be only 2-3 nm apart in their Sorets [16, 17]. The peroxo and hydroperoxo species have been confirmed in CYP101 by EPR [15, 161] and resonance Raman [17] studies using the same cryoradiolytic techniques. Through the means of EPR it was seen that the Asp251Asn mutant of CYP101 was able to form the peroxoanion and through annealing of the sample formed the hydroperoxo species which decayed to ferric species on further annealing [15, 17, 162]. The Asp251Asn mutant of CYP101 is unable to transfer protons to the peroxoanion and hence at lower cryogenic temperatures there is no formation of hydroperoxo.

The His259Ala mutant of Mtb CYP on initial inspection shows characteristics of the wild type protein with a split Soret at 441 nm and 418 with Q-bands at 562 nm and 531 nm (Figure 4.8. Although the Soret of this mutant is slightly blue shifted, 441 nm (His259Ala) vs 442 nm (wild type), this may be a result of a number of population of states. However after annealing and SVD analysis, two spectra of interest are found. As shown in Figure 4.8 B, the basis spectra results show very similar spectra with two different Sorets, one at 441 nm and the other at 439 nm. Although small, the blue shift of the Soret by 2 nm may be indicative of a protonation step that is occurring as temperature is increased. The role of the His259 is thought to be similar to that of Asp251 of CYP101, and as such may be important in proton transfer. In the wild type protein at 77 K during cryoradiolysis, the protonation of the peroxoanion species may be barrier-less or at least occur a time scale shorter than the 4 week incubation period. This would result in only one state being observed, that of hydroperoxo. In the His259Ala mutant, the proton transfer may be disrupted which would result in the accumulation of the peroxoanion species. In the Asp251Asn CYP101 mutant the peroxo species is stable between 77 K and 120 K and as the temperature is raised above this point, the peroxo species is protonated. This was observed using EPR

[15] as well as resonance Raman [17], where the protonated and unprotonated states are unambiguous in their spectra. As with the Asp251Asn mutant of CYP101, the His259Ala mutant of CYP51 may exhibit this protonation when temperature is raised (although not directly observed in the optical spectra). At lower temperatures the His259Ala mutant may form the peroxoanion species and as temperature is increased, the lack of the His in this position might not hinder the protonation of the peroxoanion species from another source such as active site water molecules. This speculation could be made based on the SVD basis set of the annealing of this His259Ala sample showing two peroxo species (Figure 4.8 B).

The Thr260Ala mutant exhibited a similar spectrum to that of the wild type with peaks appearing at the same wavelengths as that of the wild type protein (419 nm, 441 nm, 531 nm and 562 nm) as seen in Figure 4.9 A. Temperature annealing of the sample and subsequent SVD analysis and spectrum calculation exhibited results much like that of the wild type protein (Figure 4.9 B). Although this mutation occurs in the active site and plays a role in oxyferrous stability, its role in peroxo intermediate formation and stabilization is unclear although does not inhibit the formation of such a species. From the SVD basis spectra, and based on the Soret of shown in Figure 4.9 B as well as the similarities of the spectra to the wild type protein, the intermediate seen is assumed to be the peroxoanion species.

4.2.3 Reduced Oxyferrous Intermediate Formation at 4 K

The previous annealing studies were performed by allowing the radiolytic process to occur over a 4 week period at 77 K. As previous work in CYP101 has shown by other spectroscopic techniques such as EPR [15] and resonance Raman [17] the peroxoanion species will accumulate at temperatures below 70 K but above this temperature would slowly decay and essentially not be detectable above 147 K when annealed [127]. It

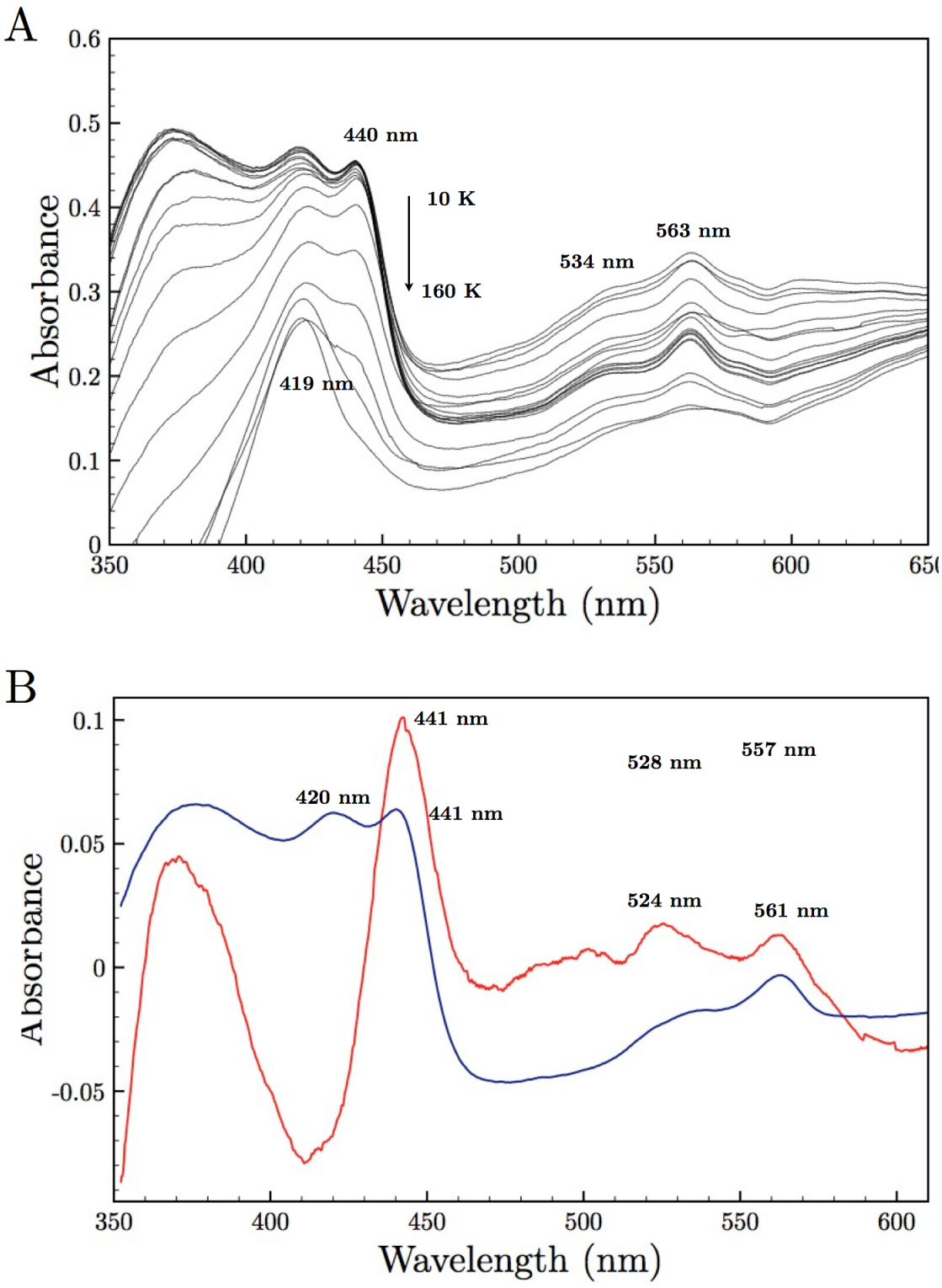

Figure 4.7: Annealing of cryoreduced CYP51 wild type from 10 K - 160 K in 10 K increments A) and SVD basis spectra B)

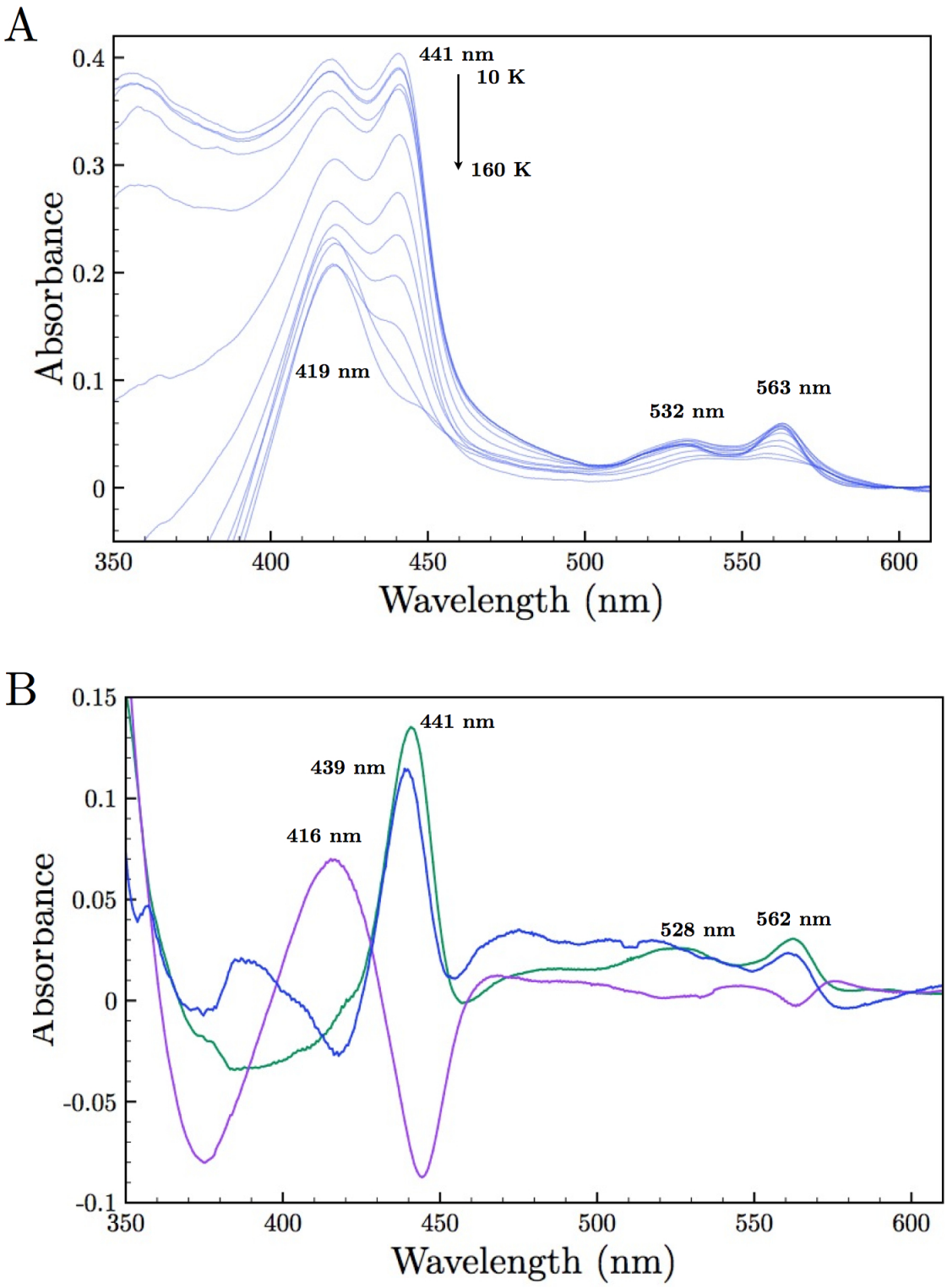

Figure 4.8: Annealing of cryoreduced CYP51 His259Ala from 10 K - 160 K in 10 K increments A) and SVD basis spectra B)

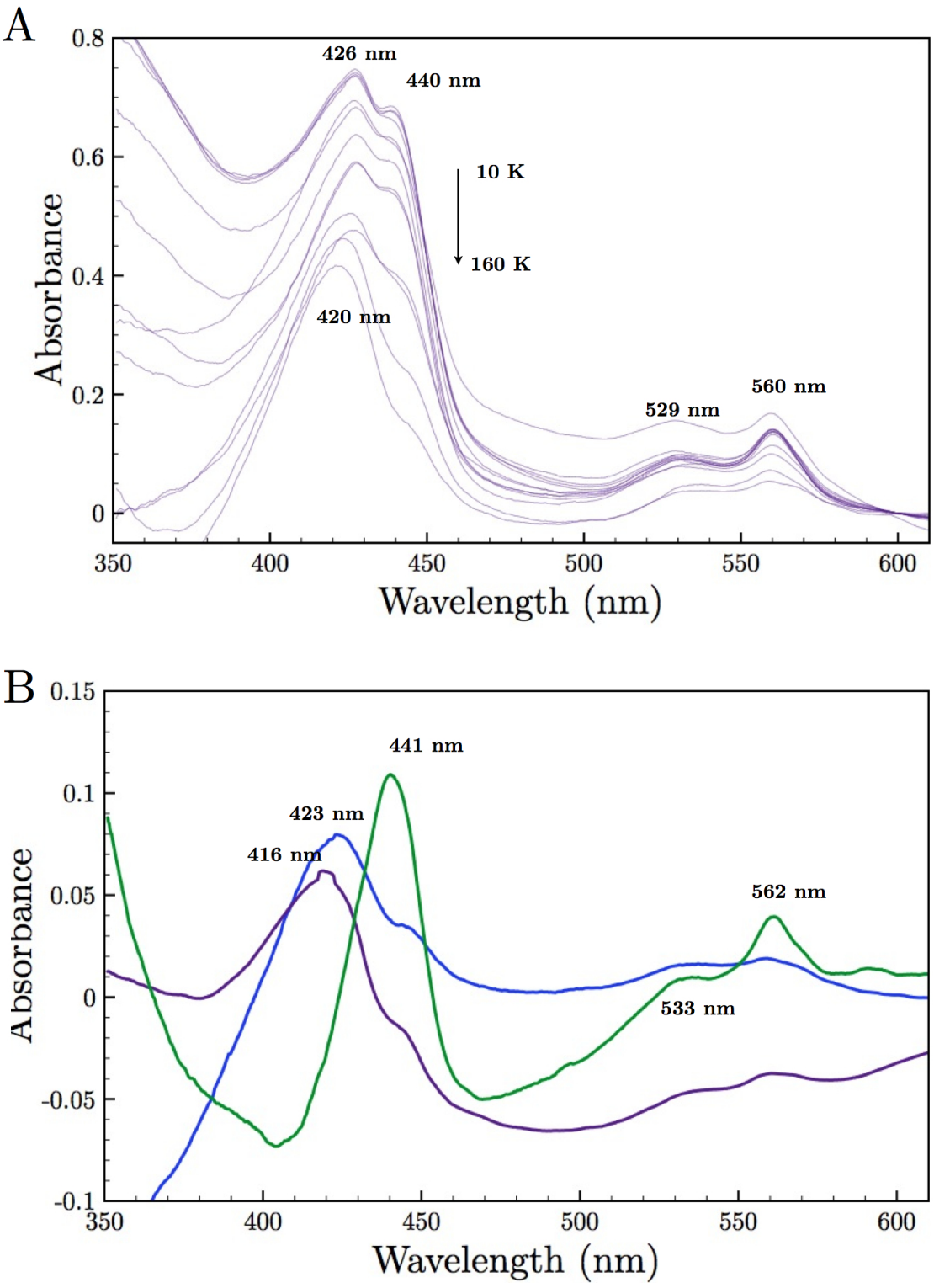

Figure 4.9: Annealing of cryoreduced CYP51 Thr260Ala from 10 K - 160 K in 10 K increments A) and SVD basis spectra B)

became evident that an incubation at 10 K at the start of the cryoradiolysis would yield insight into which peroxo species was being formed in the Mtb CYP51 wild type protein. The radiolytic decay was monitored for 36 hrs in order to observe the formation of the reduced oxyferrous intermediate shown in Figure 4.10 A. These results showed a slight shoulder at 441 nm, the same as at 77 K (Figure 4.10 A). SVD analysis of this step, where time is used as the third dimension instead of temperature, a species with a Soret at 441 nm is observed (Figure 4.10 B). CYP101, whose catalysis is thought to be entirely Cmpd I mediated, is capable of stabilizing the peroxoanion at temperatures lower than 70 K. This would imply that the species formed at 10 K in Mtb CYP51 is the peroxoanion and not hydroperoxo as the final catalytic step involved in C-C bond cleavage is mediated by this intermediate and not hydroperoxo. If this is indeed what is occuring it would stand to reason that the peroxoanion is stable at temperatures higher than that of CYP101 wild type and the spectrum observed at 77 K and above is that of the peroxoanion. This is supported by the observation of the accumulation of peroxoanion in CYP19, another C-C cleaving enzyme, whose catalytic mechanism is also thought to be peroxoanion mediated [163]. In CYP19, Gantt and coworkers also observed that the peroxoanion intermediate is accumulated at 77 K and is stable to temperatures above 180 K. At which point no accumulation of hydroperoxo species is seen [163]. This is significant in that CYP19 is capable of stabilizing the peroxoanion intermediate at temperatures of which there is no accumulation of the peroxoanion in CYP101. Since the proposed reactive intermediate of CYP19 mediated C-C cleavage is the peroxoanion, the ability of the enzyme to stabilize this intermediate strengthens the argument of its mechanism.

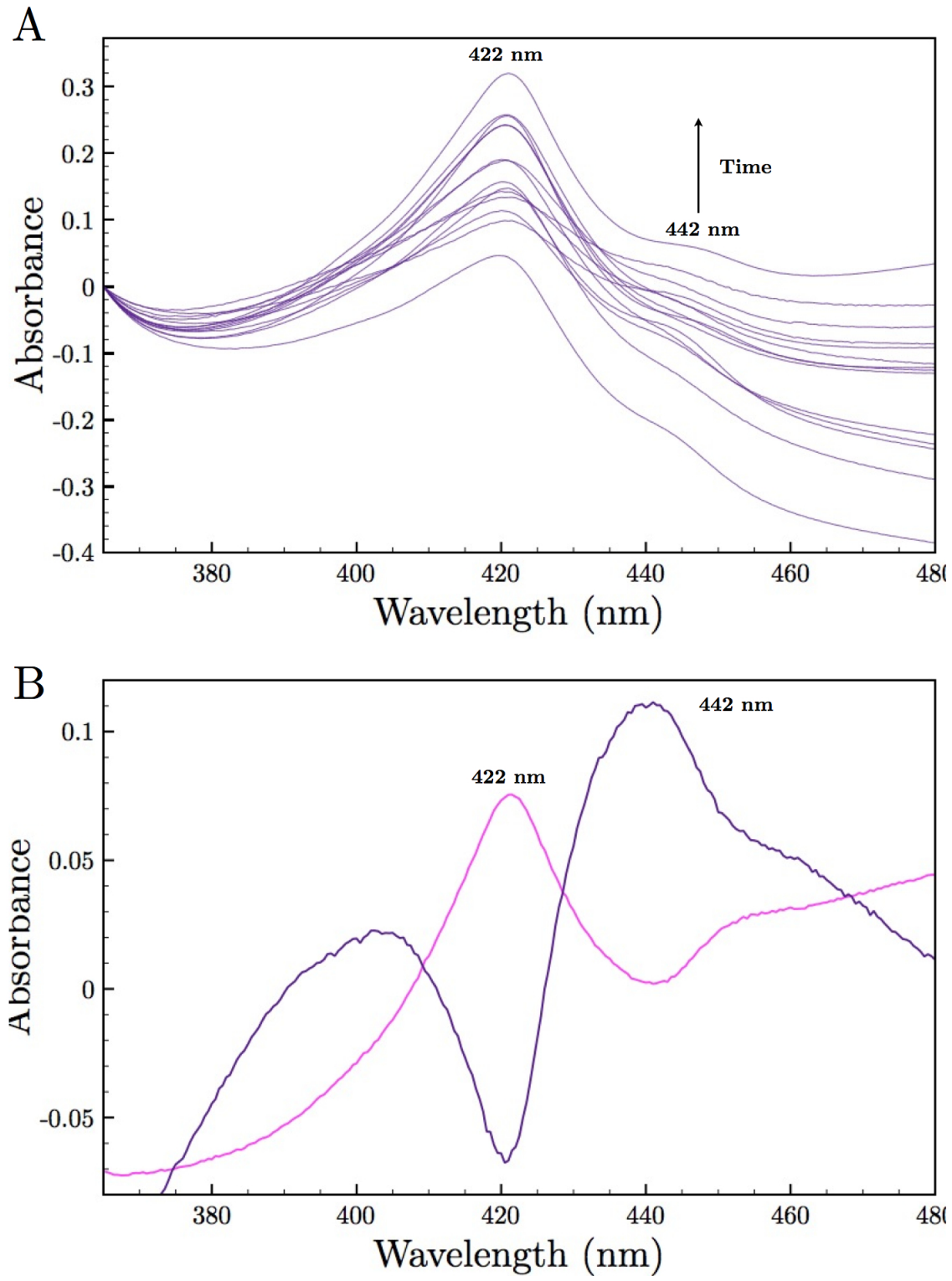

Figure 4.10: A)Time course over 36 hrs of cryoreduction of Mtb CYP51 wild type at 4 K. B) SVD basis spectra of the cryoradiolytic time course.

Conclusion

The cytochromes P450 can be considered some of the most versatile biological catalysts. These monoxygenases play critical roles in the metabolism of xenobiotics and in the biosynthesis of physiologically important molecules. Although there is a postulated and generalized catalytic cycle of these enzymes, the catalytic mechanisms of individual CYPs can vary significantly from another due to the myriad of reactions catalyzed by the CYP superfamily. As CYP101 was the first easily expressed CYP, the vast majority of studies pertaining to CYPs and their catalytic intermediates have been based on this enzyme. Unfortunately, the catalytic mechanism of this relatively "simple" model, can not always be generalized to all members of the CYP superfamily. Being unique in their catalytic mechanisms, the C-C bond cleaving enzymes and in particular CYP51 from *Mycobacterium tuberculosis* are thought to be capable of utilizing diverse catalytic intermediates. During the process of C-C cleavage, CYP51 will perform two passes of the catalytic cycle resulting in two straight forward hydroxylation reactions, but on a third pass is capable catalyzing the C-C cleavage through a catalytic intermediate which is not the classical Cmpd I. This implies CYP51 is capable of tuning its active site in order to use multiple reactive oxygen species in catalysis. CYP51 is also distinct from most CYPs owing to the fact that the acid functionality of the conserved acid-alcohol pair found in most CYPs, is instead a His. This study aimed to trap and characterize dioxygen reactive intermediates, and elucidate the role of the unique acid-alcohol pair in the formation and stabilization of these intermediates.

5.1 The Role of the Acid-Alcohol Pair in *Mycobacterium tuberculosis* CYP51 Oxyferrous Formation and Stability

To date, no reported studies have been performed on the formation and characterization of oxygen intermediates in Mtb CYP51. In order to characterize reactive oxygen intermediates of Mtb CYP51, the isolation and characterization of the oxyferrous intermediate was necessary. This characterization was performed using stopped flow rapid scanning UV/Vis spectroscopy studies on Mtb CYP51 wild type and His259Ala, Thr260Ala and Thr260Val mutants in the presence and absence of saturating concentrations of DHL. In the absence of substrate the rate constants for binding of oxygen to the wild type ferrous protein is faster than that of the mutants. Oxyferrous stability however, is not altered between the wild type and the mutants. In the presence of saturating concentrations of substrate, the wild type protein shows a two fold decrease in the oxygen binding rate constant, however both the His259Ala and Thr260Val mutant show a two fold increase in their oxygen binding rate constants. The rate constants of autoxidation in the wild type and His259Ala mutant are unaffected by the presence of substrate. This is not the case in Thr260Val, where the auto-oxidation rate constant is tripled. Potentially on the binding of substrate, the lack of a suitable hydroxyl group destabilizes the oxyferrous intermediate, increasing the enzymes rate of uncoupling. Unfortunately the inability of the Thr260Ala mutant to bind the substrate used in the studies could not confirm whether the increased rate of autoxidation was as a result of a lack of a hydroxyl group, or that the Val side chain induced enough of a conformational change within the active site to result in increased uncoupling of the catalytic cycle.

As this studied employed the rapid mixing of the reduced CYP protein with oxygenated buffer in order to observe the rates of oxyferrous formation and decay,

future studies could include the mixing of the ferric protein in the presence of oxygen, with its reduced ferredoxin. As studies have shown in some cases the associated redox partner of a CYP is capable of influencing the electron transfer, oxygen binding as well as oxyferrous stability. This experiment would help highlight the roles of the ferredoxin as well as the acid-alcohol pair of Mtb CYP51 in the reduction of the protein from ferric to ferrous, the binding of oxygen to the ferrous protein as well as the auto-oxidation of the oxyferrous intermediate. Another study that could help understand the role of protonation of the His259 residue and its role during catalysis, particularly in the early stages of the catalytic cycle would be pH dependent studies where oxyferrous formation is monitored at pHs above and below the pKa of the His259.

This study reports the successful use of stopped-flow rapid-scanning spectrophotometry in order to observe the formation and decay of the important oxyferrous bound form of Mtb CYP51 and its His259Ala, Thr260Ala and Thr260Val mutants, in the presence and absence of substrate, for the first time.

5.2 *In situ* Generation of Early Oxygen Intermediates in *Mycobacterium Tuberculosis* CYP51

The cryogenic trapping of oxygen intermediates was performed in this study. The characterization of the oxyferrous intermediates at cryogenic temperatures of each protein in the presence and absence of substrate was in agreement with the calculated spectra of the oxyferrous intermediate observed in the stopped flow studies. The ability to isolate the oxyferrous intermediate as well as its stability at 77 K was critical in order to perform cryoradiolytic studies.

The cryoradiolytic technique performed in the absence of substrate yielded the

distinct formation of a red shifted Soret (in agreement with the literature) which was the result of a reduced oxyferrous intermediate (either the ferric peroxoanion or the ferric hydroperoxo intermediate). This peak was seen to decay in all mutants between the temperatures of 160 K and 170 K. The optical spectra of the two peroxo intermediates are almost indistinguishable except for a slight (2-3 nm) blue shift in the Soret of the ferric peroxoanion as it is protonated to the ferric hydroperoxo intermediate. In CYP101 this lack of a blue shift in Soret of the wild type protein is due to the very small energetic barrier associated with the protonation of the peroxoanion, resulting in only an accumulation of the hydroperoxo intermediate at the temperature of 77 K. The peroxoanion however would accumulate in when cryoradiolysis was performed at 6 K [15]. CYP19, another C-C bond cleaving enzyme thought to utilize a peroxoanion catalytic intermediate, is capable of accumulating the peroxoanion at 77 K which decays at temperatures above 160 K without the accumulation of hydroperoxo. This provides support that intermediate accumulating in Mtb CYP51 could in fact be the peroxoanion intermediate. Further evidence to support this fact would be that the same visible spectrum was calculated when the formation of the reduced oxyferrous intermediate was generated over 36 hr at 10 K. Annealing experiments of the reduced oxyferrous intermediate in the His259Ala mutant yielded two distinct spectra indicating a slight blue shift in the Soret (of approximately 2 nm). The two Soret peaks correspond to that of the intermediate observed in the wild type protein and a Soret which is blue shifted. This could imply that the His259Ala mutant is capable of stabilizing the peroxoanion intermediate but not over the entire temperature range used during the annealing step. As the temperature is increased, there is a protonation of the peroxoanion to form the hydroperoxo, which as the protein is further annealed will decay to form the ferric protein.

The inability to unambiguously assign which reduced oxyferrous intermediate was

present in each protein will direct future studies to include resonance Raman and EPR spectroscopy to be performed on each sample. All three techniques will be able to distinguish which reduced oxyferrous species is present in Mtb CYP51 and its mutants. As this data was generated with proteins in the absence of substrate, a more relevant study would include the presence of substrate, which may act to stabilize particular intermediates especially since different substrate intermediates are present during each turn of the CYP51 catalytic cycle. Substrates can include DHL as well as the aldehyde intermediate of DHL. The aldehyde intermediate of DHL is the substrate of the final turn of the catalytic cycle of Mtb CYP51, which is implicated in utilizing the peroxoanion as its catalytic intermediate.

5.3 **Implications**

This study showed the ability to generate, stabilize and characterize reactive dioxygen intermediates in Mtb CYP51. As the life-time of the oxyferrous intermediate in Mtb CYP51 is extremely short at ambient temperatures, this work has shown the laboratory's expertise in being able to generate reduced oxyferrous intermediates at cryogenic temperatures. These intermediates have only been generated in a handful of Cytochromes P450 and as such this work adds critical information to the small body of work currently reported.

This work highlighted chemical and biophysical properties of the Mtb CYP51 catalytic cycle, giving insight into the catalytic mechanism which could be used to rationalize properties of other C-C bond cleaving enzymes. This is critical as the catalytic mechanisms of relatively "simplistic" monoxygenating enzymes such as CYP101 can not be generalized to the C-C bond cleavage step of enzymes such as CYP51 and CYP19. The fact that CYP51 is a target of available drugs in the

treatment of diseases such and Chaga's disease as well as Anti-fungal agents, highlights the importance of understanding the catalytic intermediates of these enzymes. The understanding of the catalytic mechanism of Mtb CYP51 is not only important in the fact that it can give insight into other C-C bond cleaving enzyme catalysis, but could be used to develop highly selective and irreversible inhibitors in the treatment and eradication of Tuberculosis.

Bibliography

Bibliography

[1] P. De Montellano, *Cytochrome P450: structure, mechanism, and biochemistry*, Springer, **2005**.

[2] T. Omura, R. Sato. The carbon monoxide-binding pigment of liver microsomes. *Journal of Biological Chemistry* **1964**, *239*, 2370–2378.

[3] G. Palmer, J. Reedijk. Nomenclature of electron-transfer proteins. *European Journal of Biochemistry* **1991**, *200*, 599–611.

[4] D. Nebert, M. Adesnik, M. Coon, R. Estabrook, F. Gonzalez, F. Guengerich, I. C. Gunsalus, E. Johnson, B. Kemper, W. Levin, et al.. The P450 gene superfamily: recommended nomenclature. *DNA* **1987**, *6*, 1–11.

[5] D. Nebert, D. Nelson, M. Coon, R. Estabrook, R. Feyereisen, Y. Fujii-Kuriyama, F. Gonzalez, F. Guengerich, I. C. Gunsalus, E. Johnson, et al.. The P450 superfamily: update on new sequences, gene mapping, and recommended nomenclature. *DNA and cell biology* **1991**, *10*, 1–14.

[6] R. Bernhardt. Cytochromes P450 as versatile biocatalysts. *Journal of biotechnology* **2006**, *124*, 128–145.

[7] S. Rendic. Summary of information on human CYP enzymes: human P450 metabolism data. *Drug metabolism reviews* **2002**, *34*, 83–448.

[8] F. Guengerich. Mechanisms of cytochrome P450 substrate oxidation: MiniReview. *Journal of biochemical and molecular toxicology* **2007**, *21*, 163–168.

[9] S. Sligar. Coupling of spin, substrate, and redox equilibriums in cytochrome P450. *Biochemistry* **1976**, *15*, 5399–5406.

[10] T. Makris, R. Davydov, I. Denisov, B. Hoffman, S. Sligar. Mechanistic enzymology of oxygen activation by the cytochromes P450. *Drug metabolism reviews* **2002**, *34*, 691–708.

[11] K. McLean, A. Warman, H. Seward, K. Marshall, H. Girvan, M. Cheesman, M. Waterman, A. Munro. Biophysical characterization of the sterol demethylase P450 from *Mycobacterium tuberculosis*, its cognate ferredoxin, and their interactions. *Biochemistry* **2006**, *45*, 8427–8443.

[12] N. Veitch, R. Williams. The molecular basis of electron transfer in redox enzyme systems. *Frontiers in Biotransformation* **1992**, *7*, 279–320.

[13] P. Champion, I. Gunsalus, G. Wagner. Resonance Raman investigations of cytochrome P450cam from Pseudomonas putida. *Journal of the American Chemical Society* **1978**, *100*, 3743–3751.

[14] I. D. G. Macdonald, S. G. Sligar, J. F. Christian, M. Unno, P. M. Champion. Identification of the Fe-O-O Bending Mode in Oxycytochrome P450cam by Resonance Raman Spectroscopy. *Journal of the American Chemical Society* **1999**, *121*, 376–380.

[15] R. Davydov, T. Makris, V. Kofman, D. Werst, S. Sligar, B. Hoffman. Hydroxylation of camphor by reduced oxy-cytochrome P450cam: mechanistic implications of EPR and ENDOR studies of catalytic intermediates in native and mutant enzymes. *Journal of the American Chemical Society* **2001**, *123*, 1403–1415.

[16] S. Sligar, T. Makris, I. Denisov. Thirty years of microbial P450 monooxygenase research: peroxo-heme intermediates–the central bus station in heme oxygenase catalysis. *Biochemical and biophysical research communications* **2005**, *338*, 346–354.

[17] I. Denisov, P. Mak, T. Makris, S. Sligar, J. Kincaid. Resonance Raman Characterization of the Peroxo and Hydroperoxo Intermediates in Cytochrome P450. *The Journal of Physical Chemistry A* **2008**, *112*, 13172–13179.

[18] J. Rittle, J. M. Younker, M. T. Green. Cytochrome P450: The Active Oxidant and Its Spectrum. *Inorganic Chemistry* **2010**, *49*, 3610–3617.

[19] J. Rittle, M. T. Green. Cytochrome P450 Compound I: Capture, Characterization, and C-H Bond Activation Kinetics. *Science* **2010**, *330*, 933–937.

[20] J. Groves, G. McClusky. Aliphatic hydroxylation via oxygen rebound. Oxygen transfer catalyzed by iron. *Journal of the American Chemical Society* **1976**, *98*, 859–861.

[21] S. Sligar, J. Lipscomb, P. Debrunner, I. Gunsalus. Superoxide anion production by the autoxidation of cytochrome P450cam. *Biochemical and biophysical research communications* **1974**, *61*, 290–296.

[22] I. Denisov, T. Makris, S. Sligar, I. Schlichting. Structure and chemistry of cytochrome P450. *Chemical reviews* **2005**, *105*, 2253–2278.

[23] I. Denisov, Y. Grinkova, B. Baas, S. Sligar. The Ferrous-Dioxygen Intermediate in Human Cytochrome P450 3A4. *Journal of Biological Chemistry* **2006**, *281*, 23313–23318.

[24] A. Luthra, I. G. Denisov, S. G. Sligar. Temperature Derivative Spectroscopy To Monitor the Autoxidation Decay of Cytochromes P450. *Analytical Chemistry* **2011**, *83*, 5394–5399.

[25] T. Poulos, B. Finzel, I. Gunsalus, G. Wagner, J. Kraut. The 2.6-A crystal structure of Pseudomonas putida cytochrome P-450. *Journal of Biological Chemistry* **1985**, *260*, 16122–16130.

[26] C. Hasemann, R. Kurumbail, S. Boddupalli, J. Peterson, J. Deisenhofer. Structure and function of cytochromes P450: a comparative analysis of three crystal structures. *Structure* **1995**, *3*, 41–62.

[27] S. Graham, J. Peterson. How similar are P450s and what can their differences teach us? *Archives of biochemistry and biophysics* **1999**, *369*, 24–29.

[28] T. Poulos, Y. Meharenna. Structures of P450 proteins and their molecular phylogeny. *The Ubiquitous Roles of Cytochrome P450 Proteins* **2007**, *3*, 57–96.

[29] A. Sigel, H. Sigel, R. Sigel, *The Ubiquitous Roles of Cytochrome P450 Proteins: Metal Ions in Life Sciences*, of *Metal Ions in Life Sciences*, John Wiley & Sons, **2007**.

[30] O. Gotoh. Substrate recognition sites in cytochrome P450 family 2 (CYP2) proteins inferred from comparative analyses of amino acid and coding nucleotide sequences. *Journal of Biological Chemistry* **1992**, *267*, 83–90.

[31] O. Pylypenko, I. Schlichting. Structural aspects of ligand binding to and electron transfer in bacterial and fungal P450s. *Annual review of biochemistry* **2004**, *73*, 991–1018.

[32] M. Schuler, S. Sligar. Diversities and similarities in P450 systems: an introduction. *The Ubiquitous Roles of Cytochrome P450 Proteins* **2007**, *3*, 1–26.

[33] R. Lindberg, M. Negishi. Alteration of mouse cytochrome P450coh substrate specificity by mutation of a single amino-acid residue. *Nature* **1989**, *339*, 632 – 634.

[34] M. Iwasaki, T. Darden, L. Pedersen, D. Davis, R. Juvonen, T. Sueyoshi, M. Negishi. Engineering mouse P450coh to a novel corticosterone 15 alpha-hydroxylase and modeling steroid-binding orientation in the substrate pocket. *Journal of Biological Chemistry* **1993**, *268*, 759–762.

[35] M. Negishi, M. Iwasaki, R. Juvonen, T. Sueyoshi, T. Darden, L. Pedersen. Structural flexibility and functional versatility of cytochrome P450 and rapid evolution. *Mutation Research/Fundamental and Molecular Mechanisms of Mutagenesis* **1996**, *350*, 43–50.

[36] E. Johnson, C. Stout. Structural diversity of human xenobiotic-metabolizing cytochrome P450 monooxygenases. *Biochemical and biophysical research communications* **2005**, *338*, 331–336.

[37] J. Dawson, R. Holm, J. Trudell, G. Barth, R. Linder, E. Bunnenberg, C. Djerassi, S. Tang, et al.. Oxidized cytochrome P-450. Magnetic circular dichroism evidence for thiolate ligation in the substrate-bound form. Implications for the catalytic mechanism. *Journal of the American Chemical Society* **1976**, *98*, 3707–3709.

[38] N. Ueyama, N. Nishikawa, Y. Yamada, T. Okamura, A. Nakamura. Cytochrome P-450 Model (Porphinato)(thiolato) iron (III) Complexes with Single and Double NH S Hydrogen Bonds at the Thiolate Site. *Journal of the American Chemical Society* **1996**, *118*, 12826–12827.

[39] R. Langen, G. M. Jensen, U. Jacob, P. J. Stephens, A. Warshel. Protein control of iron-sulfur cluster redox potentials. *Journal of Biological Chemistry* **1992**, *267*, 25625–25627.

[40] F. Ogliaro, S. Cohen, S. de Visser, S. Shaik. Medium polarization and hydrogen bonding effects on compound I of cytochrome P450: What kind of a radical is it really? *Journal of the American Chemical Society* **2000**, *122*, 12892–12893.

[41] N. Suzuki, T. Higuchi, Y. Urano, K. Kikuchi, H. Uekusa, Y. Ohashi, T. Uchida, T. Kitagawa, T. Nagano. Novel Iron Porphyrin-Alkanethiolate Complex with Intramolecular NH S Hydrogen Bond: Synthesis, Spectroscopy, and Reactivity. *Journal of the American Chemical Society* **1999**, *121*, 11571–11572.

[42] M. Filatov, N. Harris, S. Shaik. A theoretical study of electronic factors affecting hydroxylation by model ferryl complexes of cytochrome P-450 and horseradish peroxidase. *J. Chem. Soc., Perkin Trans. 2* **1999**, 399–410.

[43] I. Schlichting, J. Berendzen, K. Chu, A. Stock, S. Maves, D. Benson, R. Sweet, D. Ringe, G. Petsko, S. Sligar. The catalytic pathway of cytochrome P450cam at atomic resolution. *Science* **2000**, *287*, 1615–1622.

[44] L. Podust, T. Poulos, M. Waterman. Crystal structure of cytochrome P450 14α-sterol demethylase (CYP51) from *Mycobacterium tuberculosis* in complex with azole inhibitors. *Proceedings of the National Academy of Sciences* **2001**, *98*, 3068–3073.

[45] D. R. Nelson, H. W. Strobel. On the membrane topology of vertebrate cytochrome P-450 proteins. *Journal of Biological Chemistry* **1988**, *263*, 6038–6050.

[46] M. Imai, H. Shimada, Y. Watanabe, Y. Matsushima-Hibiya, R. Makino, H. Koga, T. Horiuchi, Y. Ishimura. Uncoupling of the cytochrome P-450cam monooxygenase reaction by a single mutation, threonine-252 to alanine or valine: possible

role of the hydroxy amino acid in oxygen activation. *Proceedings of the National Academy of Sciences* **1989**, *86*, 7823–7827.

[47] S. Martinis, W. Atkins, P. Stayton, S. Sligar. A conserved residue of cytochrome P-450 is involved in heme-oxygen stability and activation. *Journal of the American Chemical Society* **1989**, *111*, 9252–9253.

[48] H. Shimada, Y. Watanabe, M. Imai, R. Makino, H. Koga, T. Horiuchi, Y. Ishimura. The Role of Threonine 252 in the Oxygen Activation by Cytochrome P-450cam : Mechanistic Studies by Site-directed Mutagenesis. *Studies in Surface Science and Catalysis* **1991**, *66*, 313–319.

[49] H. Shimada, R. Makino, M. Unno, T. Horiuchi, Y. Ishimura, *Proton and electron transfer mechanism in dioxygen activation by cytochrome P450cam* in *Cytochrome P450: biochemistry, biophysics, and molecular biology: 8th international conference, Lisbon, Portugal, 24-28 October 1993*, John Libbey Eurotext, p. 299.

[50] Y. Kimata, H. Shimada, T. Hirose, Y. Ishimura. Role of Thr-252 in cytochrome P450cam: a study with unnatural amino acid mutagenesis. *Biochemical and biophysical research communications* **1995**, *208*, 96–102.

[51] K. Von König, I. Schlichting. Cytochromes P450–Structural Basis for Binding and Catalysis. *The Ubiquitous Roles of Cytochrome P450 Proteins* **2007**, *3*, 235–265.

[52] J. Cupp-Vickery, T. Poulos. Structure of cytochrome P450eryF involved in erythromycin biosynthesis. *Nature Structural & Molecular Biology* **1995**, *2*, 144–153.

[53] S. Nagano, J. Cupp-Vickery, T. Poulos. Crystal Structures of the Ferrous Dioxygen Complex of Wild-type Cytochrome P450eryF and Its Mutants, A245S and A245T INVESTIGATION OF THE PROTON TRANSFER SYSTEM IN P450eryF. *Journal of Biological Chemistry* **2005**, *280*, 22102–22107.

[54] J. Andersen, K. Tatsuta, H. Gunji, T. Ishiyama, C. Hutchinson. Substrate specificity of 6-deoxyerythronolide B hydroxylase, a bacterial cytochrome P450 of erythromycin A biosynthesis. *Biochemistry* **1993**, *32*, 1905–1913.

[55] J. Cupp-Vickery, O. Han, C. Hutchinson, T. Poulos. Substrate-assisted catalysis in cytochrome P450eryF. *Nature Structural & Molecular Biology* **1996**, *3*, 632–637.

[56] H. Xiang, R. Tschirret-Guth, P. de Montellano. An A245T mutation conveys on cytochrome P450eryF the ability to oxidize alternative substrates. *Journal of Biological Chemistry* **2000**, *275*, 35999–36006.

[57] N. Gerber, S. Sligar. Catalytic mechanism of cytochrome P-450: evidence for a distal charge relay. *Journal of the American Chemical Society* **1992**, *114*, 8742–8743.

[58] M. Vidakovic, S. Sligar, H. Li, T. Poulos. Understanding the role of the essential Asp251 in cytochrome P450cam using site-directed mutagenesis, crystallography, and kinetic solvent isotope effect. *Biochemistry* **1998**, *37*, 9211–9219.

[59] R. Kraaipoel, H. Degenhart, J. Leferink, V. Van Beek, H. De Leeuw-Boon, H. Visser. Pregnenolone formation from cholesterol in bovine adrenal cortex mitochondria: proposal of a new mechanism. *FEBS letters* **1975**, *50*, 204–209.

[60] E. Simpson, G. Boyd. The cholesterol side-chain cleavage system of the adrenal cortex: a mixed-function oxidase. *Biochemical and biophysical research communications* **1966**, *24*, 10.

[61] S. Burstein, B. Middleditch, M. Gut. Mass spectrometric study of the enzymatic conversion of cholesterol to (22R)-22-hydroxycholesterol,(20R, 22R)-20, 22-dihydroxycholesterol, and pregnenolone, and of (22R)-22-hydroxycholesterol to the lgycol and pregnenolone in bovine adrenocortical preparations. Mode of oxygen incorporation. *Journal of Biological Chemistry* **1975**, *250*, 9028–9037.

[62] N. Orme-Johnson, D. Light, R. White-Stevens, W. Orme-Johnson. Steroid binding properties of beef adrenal cortical cytochrome P-450 which catalyzes the conversion of cholesterol into pregnenolone. *Journal of Biological Chemistry* **1979**, *254*, 2103–2111.

[63] R. C. Tuckey, H. Kamin. Kinetics of O_2 and CO Binding to adrenal cytochrome P-450scc. Effect of cholesterol, intermediates, and phosphatidylcholine vesicles. *Journal of Biological Chemistry* **1983**, *258*, 4232–4237.

[64] J. De Voss, M. Cryle. Carbon-Carbon Bond Cleavage by P450 Systems. *The Ubiquitous Roles of Cytochrome P450 Proteins* **2007**, *3*, 397–435.

[65] H. Barnes, M. Arlotto, M. Waterman. Expression and enzymatic activity of recombinant cytochrome P450 17 alpha-hydroxylase in Escherichia coli. *Proceedings of the National Academy of Sciences* **1991**, *88*, 5597.

[66] M. Zuber, E. Simpson, M. Waterman. Expression of bovine 17 α-hydroxylase cytochrome P-450 cDNA in nonsteroidogenic (COS 1) cells. *Science* **1986**, *234*, 1258–1261.

[67] M. Akhtar, D. Corina, S. Miller, A. Shyadehi, J. Wright. Incorporation of label from $^{18}O_2$ into acetate during side-chain cleavage catalysed by cytochrome P-45017α (17α-hydroxylase-17, 20-lyase). *J. Chem. Soc., Perkin Trans. 1* **1994**, *271*, 263–267.

[68] P. Lee-Robichaud, M. Akhtar, M. Akhtar. An analysis of the role of active site protic residues of cytochrome P-450s: mechanistic and mutational studies on 17α-hydroxylase-17, 20-lyase (P-450$_{17\alpha}$ also CYP17). *Biochemical Journal* **1998**, *330*, 967–974.

[69] C. Sohl, F. Guengerich. Kinetic analysis of the three-step steroid aromatase reaction of human cytochrome P450 19A1. *Journal of Biological Chemistry* **2010**, *285*, 17734–17743.

[70] E. Thompson Jr, P. Siiteri. The involvement of human placental microsomal cytochrome P-450 in aromatization. *Journal of Biological Chemistry* **1974**, *249*, 5373–5378.

[71] J. Kellis Jr, L. Vickery. Purification and characterization of human placental aromatase cytochrome P-450. *Journal of Biological Chemistry* **1987**, *262*, 4413–4420.

[72] R. Brueggemeier, J. Hackett, E. Diaz-Cruz. Aromatase inhibitors in the treatment of breast cancer. *Endocrine reviews* **2005**, *26*, 331–345.

[73] A. Brodie, L. Wing, P. Goss, M. Dowsett, R. Coombes. Aromatase inhibitors and their potential clinical significance. *Journal of Steroid Biochemistry* **1986**, *25*, 859–865.

[74] M. Akhtar, M. Calder, D. Corina, J. Wright. Mechanistic studies on C-19 demethylation in oestrogen biosynthesis. *Biochemical Journal* **1982**, *201*, 569–580.

[75] K. Sen, J. Hackett. Coupled Electron Transfer and Proton Hopping in the Final Step of CYP19-Catalyzed Androgen Aromatization. *Biochemistry* **2012**, *51*, 3039–3049.

[76] F. Guengerich, C. Sohl, G. Chowdhury. Multi-step oxidations catalyzed by cytochrome P450 enzymes: Processive vs. distributive kinetics and the issue of carbonyl oxidation in chemical mechanisms. *Archives of Biochemistry and Biophysics* **2011**, *507*, 126–134.

[77] D. Ghosh, J. Griswold, M. Erman, W. Pangborn. Structural basis for androgen specificity and oestrogen synthesis in human aromatase. *Nature* **2009**, *457*, 219–223.

[78] J. Alvarez-Idaboy, N. Mora-Diez, R. Boyd, A. Vivier-Bunge. On the importance of prereactive complexes in molecule-radical reactions: Hydrogen abstraction from aldehydes by OH. *Journal of the American Chemical Society* **2001**, *123*, 2018–2024.

[79] G. Garssen, J. Vliegenthart, J. Boldingh. An anaerobic reaction between lipoxygenase, linoleic acid and its hydroperoxides. *Biochemical Journal* **1971**, *122*, 327–332.

[80] X. Liu, Y. Wang, K. Han. Systematic study on the mechanism of aldehyde oxidation to carboxylic acid by cytochrome P450. *Journal of Biological Inorganic Chemistry* **2007**, *12*, 1073–1081.

[81] Y. Yoshida, Y. Aoyama, M. Noshiro, O. Gotoh. Sterol 14-demethylase P450 (CYP51) provides a breakthrough for the discussion on the evolution of cytochrome P450 gene superfamily. *Biochemical and biophysical research communications* **2000**, *273*, 799–804.

[82] D. Nelson. Cytochrome P450 and the individuality of species. *Archives of biochemistry and biophysics* **1999**, *369*, 1–10.

[83] Y. Aoyama, M. Noshiro, O. Gotoh, S. Imaoka, Y. Funae, N. Kurosawa, T. Horiuchi, Y. Yoshida. Sterol 14-demethylase P450 (P45014DM*) is one of the most ancient and conserved P450 species. *Journal of biochemistry* **1996**, *119*, 926–933.

[84] A. Shyadehi, D. Lamb, S. Kelly, D. Kelly, W. Schunck, J. Wright, D. Corina, M. Akhtar. The mechanism of the acyl-carbon bond cleavage reaction catalyzed by recombinant sterol 14α-demethylase of Candida albicans (other names are: lanosterol 14α-demethylase, P-450$_{14DM}$, and CYP51). *Journal of Biological Chemistry* **1996**, *271*, 12445–12450.

[85] J. Fishman, M. S. Raju. Mechanism of estrogen biosynthesis. Stereochemistry of C-1 hydrogen elimination in the aromatization of 2 beta-hydroxy-19-oxoandrostenedione. *Journal of Biological Chemistry* **1981**, *256*, 4472–4477.

[86] S. Cole, R. Brosch, J. Parkhill, T. Garnier, C. Churcher, D. Harris, S. Gordon, K. Eiglmeier, S. Gas, C. Barry, et al.. Deciphering the biology of Mycobacterium tuberculosis from the complete genome sequence. *Nature* **1998**, *393*, 537–544.

[87] S. Cole. Learning from the genome sequence of *Mycobacterium tuberculosis* H37Rv. *FEBS letters* **1999**, *452*, 7–10.

[88] S. Kelly, D. Lamb, A. Corran, B. Baldwin, D. Kelly. Mode of action and resistance to azole antifungals associated with the formation of 14α-methylergosta-8, 24 (28)-dien-3β, 6α-diol. *Biochemical and biophysical research communications* **1995**, *207*, 910–915.

[89] S. Kelly, D. Lamb, D. Kelly, N. Manning, J. Loeffler, H. Hebart, U. Schumacher, H. Einsele. Resistance to fluconazole and cross-resistance to amphotericin B

in Candida albicans from AIDS patients caused by defective sterol [Delta] 5, 6-desaturation. *FEBS letters* **1997**, *400*, 80–82.

[90] C. Hitchcock, K. Dickinson, S. Brown, E. Evans, D. Adams. Interaction of azole antifungal antibiotics with cytochrome P-450-dependent 14 α-sterol demethylase purified from Candida albicans. *Biochemical Journal* **1990**, *266*, 475.

[91] G. Lepesheva, M. Waterman. CYP51—the omnipotent P450. *Molecular and cellular endocrinology* **2004**, *215*, 165–170.

[92] L. Podust, L. Yermalitskaya, G. Lepesheva, V. Podust, E. Dalmasso, M. Waterman. Estriol bound and ligand-free structures of sterol 14α-demethylase. *Structure* **2004**, *12*, 1937–1945.

[93] K. Sen, J. Hackett. Molecular oxygen activation and proton transfer mechanisms in lanosterol 14α-demethylase catalysis. *The Journal of Physical Chemistry B* **2009**, *113*, 8170–8182.

[94] K. Sen, J. C. Hackett. Peroxo–Iron Mediated Deformylation in Sterol 14-Demethylase Catalysis. *Journal of the American Chemical Society* **2010**, *132*, 10293–10305.

[95] A. Wright, M. Zignol, A. Van Deun, D. Falzon, S. Gerdes, K. Feldman, S. Hoffner, F. Drobniewski, L. Barrera, D. Van Soolingen, et al.. Epidemiology of antituberculosis drug resistance 2002-07: an updated analysis of the Global Project on Anti-Tuberculosis Drug Resistance Surveillance. *The Lancet* **2009**, *373*, 1861–1873.

[96] H. Boshoff, C. Barry. Tuberculosis—metabolism and respiration in the absence of growth. *Nature Reviews Microbiology* **2005**, *3*, 70–80.

[97] V. Snewin, G. Stewart, D. Young, *Genetic strategies for vaccine development*, ASM Press, **2000**.

[98] M. Fenton, M. Vermeulen. Immunopathology of tuberculosis: roles of macrophages and monocytes. *Infection and immunity* **1996**, *64*, 683–690.

[99] M. Glickman, W. Jacobs Jr. Microbial Pathogenesis Review of Mycobacterium tuberculosis: Dawn of a Discipline. *Cell* **2001**, *104*, 477–485.

[100] S. Sturgill-Koszycki, P. Schlesinger, P. Chakraborty, P. Haddix, H. Collins, A. Fok, R. Allen, S. Gluck, J. Heuser, D. Russell. Lack of acidification in Mycobacterium phagosomes produced by exclusion of the vesicular proton-ATPase. *Science* **1994**, *263*, 678–681.

[101] W. Ober. Ghon but not forgotten: Anton Ghon and his complex. *Pathology annual* **1983**, *18*, 79–85.

[102] L. Wayne, C. Sohaskey. Nonreplicating Persistence of *Mycobacterium tuberculosis*. *Annual Reviews in Microbiology* **2001**, *55*, 139–163.

[103] L. Wayne, H. Sramek. Metronidazole is bactericidal to dormant cells of *Mycobacterium tuberculosis*. *Antimicrobial agents and chemotherapy* **1994**, *38*, 2054–2058.

[104] J. Brooks, S. Furney, I. Orme. Metronidazole therapy in mice infected with tuberculosis. *Antimicrobial agents and chemotherapy* **1999**, *43*, 1285–1288.

[105] L. Podust, J. Von Kries, A. Eddine, Y. Kim, L. Yermalitskaya, R. Kuehne, H. Ouellet, T. Warrier, M. Altekös ter, J. Lee, et al.. Small-molecule scaffolds for CYP51 inhibitors identified by high-throughput screening and defined by X-ray crystallography. *Antimicrobial agents and chemotherapy* **2007**, *51*, 3915–3923.

[106] K. McLean, K. Marshall, A. Richmond, I. Hunter, K. Fowler, T. Kieser, S. Gurcha, G. Besra, A. Munro. Azole antifungals are potent inhibitors of cytochrome P450 mono-oxygenases and bacterial growth in mycobacteria and streptomycetes. *Microbiology* **2002**, *148*, 2937–2949.

[107] Z. Ahmad, S. Sharma, G. Khuller. Azole antifungals as novel chemotherapeutic agents against murine tuberculosis. *FEMS microbiology letters* **2006**, *261*, 181–186.

[108] Z. Ahmad, S. Sharma, G. Khuller. The potential of azole antifungals against latent/persistent tuberculosis. *FEMS microbiology letters* **2006**, *258*, 200–203.

[109] S. Hudson, K. Mclean, A. Munro, C. Abell. Mycobacterium tuberculosis cytochrome P450 enzymes: a cohort of novel TB drug targets. *Biochemical Society Transactions* **2012**, *40*, 573–579.

[110] F. Odds, A. Brown, N. Gow. Antifungal agents: mechanisms of action. *TRENDS in Microbiology* **2003**, *11*, 272–279.

[111] K. Shakeri-Nejad, R. Stahlmann, et al.. Drug interactions during therapy with three major groups of antimicrobial agents. *Expert opinion on pharmacotherapy* **2006**, *7*, 639–651.

[112] A. Bellamine, A. Mangla, W. Nes, M. Waterman. Characterization and catalytic properties of the sterol 14-demethylase from *Mycobacterium tuberculosis*. *Proceedings of the National Academy of Sciences* **1999**, *96*, 8937.

[113] G. I. Lepesheva, L. M. Podust, A. Bellamine, M. R. Waterman. Folding Requirements Are Different between Sterol 14-Demethylase (CYP51) from *Mycobacterium tuberculosis* and Human or Fungal Orthologs. *Journal of Biological Chemistry* **2001**, *276*, 28413–28420.

[114] A. Bellamine, G. Lepesheva, M. Waterman. Fluconazole binding and sterol demethylation in three CYP51 isoforms indicate differences in active site topology. *Journal of lipid research* **2004**, *45*, 2000–2007.

[115] A. Pingoud, A. Jeltsch. Structure and function of type II restriction endonucleases. *Nucleic Acids Research* **2001**, *29*, 3705–3727.

[116] C. Chen, S. Leung, C. Guilbert, M. Jacobson, J. McKerrow, L. Podust. Structural characterization of CYP51 from *Trypanosoma cruzi* and *Trypanosoma brucei* bound to the antifungal drugs posaconazole and fluconazole. *PLoS neglected tropical diseases* **2010**, *4*, e651.

[117] R. Stewart, A. Roth, F. Dahlquist. Mutations that affect control of the methylesterase activity of CheB, a component of the chemotaxis adaptation system in Escherichia coli. *Journal of bacteriology* **1990**, *172*, 3388–3399.

[118] J. Gegner, F. Dahlquist. Signal transduction in bacteria: CheW forms a reversible complex with the protein kinase CheA. *Proceedings of the National Academy of Sciences* **1991**, *88*, 750.

[119] D. Muchmore, L. McIntosh, C. Russell, D. Anderson, F. Dahlquist. Expression and nitrogen-15 labeling of proteins for proton and nitrogen-15 nuclear magnetic resonance. *Methods in enzymology* **1989**, *177*, 44–73.

[120] H. De Boer, L. Comstock, M. Vasser. The tac promoter: a functional hybrid derived from the trp and lac promoters. *Proceedings of the National Academy of Sciences* **1983**, *80*, 21.

[121] C.-K. Chen, P. S. Doyle, L. V. Yermalitskaya, Z. B. Mackey, K. K. H. Ang, J. H. McKerrow, L. M. Podust. *Trypanosoma cruzi* CYP51 Inhibitor Derived from a *Mycobacterium tuberculosis* Screen Hit. *PLoS Negl Trop Dis* **2009**, *3*, 372.

[122] B. Unger, I. Gunsalus, S. Sligar. Nucleotide sequence of the Pseudomonas putida cytochrome P-450cam gene and its expression in Escherichia coli. *Journal of Biological Chemistry* **1986**, *261*, 1158–1163.

[123] W. Atkins, S. Sligar. The roles of active site hydrogen bonding in cytochrome P-450cam as revealed by site-directed mutagenesis. *Journal of Biological Chemistry* **1988**, *263*, 18842–18849.

[124] J. Schenkman, I. Jansson, *Spectral analyses of cytochromes P450, Vol. 107*, Springer, **1998**.

[125] V. Linek, J. Mayrhoferova. The kinetics of oxidation of aqueous sodium sulphite solution. *Chemical Engineering Science* **1970**, *25*, 787–800.

[126] L. Podust, J. Stojan, T. Poulos, M. Waterman. Substrate recognition sites in 14-sterol demethylase from comparative analysis of amino acid sequences and X-ray structure of Mycobacterium tuberculosis CYP51. *Journal of inorganic biochemistry* **2001**, *87*, 227–235.

[127] I. Denisov, T. Makris, S. Sligar. Cryotrapped reaction intermediates of cytochrome P450 studied by radiolytic reduction with phosphorus-32. *Journal of Biological Chemistry* **2001**, *276*, 11648–11652.

[128] J. Spinks, R. Woods, *An introduction to radiation chemistry*, New York, NY (USA); John Wiley and Sons Inc., **1990**.

[129] M. Kołodziejski, H. Abramczyk. Spectroscopy of an excess electron in 1-propanol-methylcyclohexane system. *Journal of molecular structure* **1997**, *436*, 543–553.

[130] I. Denisov, T. Makris, S. Sugar. Cryoradiolysis for the study of P450 reaction intermediates. *Methods in enzymology* **2002**, *357*, 103–115.

[131] I. Denisov, M. Ikeda-Saito, T. Yoshida, S. Sligar. Cryogenic absorption spectra of hydroperoxo-ferric heme oxygenase, the active intermediate of enzymatic heme oxygenation. *FEBS letters* **2002**, *532*, 203–206.

[132] L. Winkler. Die Bestimmung des im Wasser gelösten Sauerstoffes. *Berichte der Deutschen Chemischen Gesellschaft* **1888**, *21*, 2843–2854.

[133] G. Barnett, E. Hurwitz. The use of sodium azide in the Winkler method for the determination of dissolved oxygen. *Sewage Works Journal* **1939**, *11*, 781–787.

[134] M. Sono, R. Perera, S. Jin, T. Makris, S. Sligar, T. Bryson, J. Dawson. The influence of substrate on the spectral properties of oxyferrous wild-type and T252A cytochrome P450-CAM. *Archives of biochemistry and biophysics* **2005**, *436*, 40–49.

[135] J. Dawson, S. Cramer. Oxygenated cytochrome P-450cam: evidence against axial histidine ligation of iron. *FEBS letters* **1978**, *88*, 127.

[136] M. Sharrock, P. Debrunner, C. Schulz, J. Lipscomb, V. Marshall, I. Gunsalus. Cytochrome P450cam and its complexes, Mö ssbauer parameters of the heme iron. *Biochimica et Biophysica Acta (BBA)-Protein Structure* **1976**, *420*, 8–26.

[137] L. Andersson, A. Johnson, J. Peterson. Active site analysis of P450 enzymes: Comparative magnetic circular dichroism spectroscopy. *Archives of biochemistry and biophysics* **1997**, *345*, 79–87.

[138] J. Dawson, L. Andersson, M. Sono. Spectroscopic investigations of ferric cytochrome P-450-CAM ligand complexes. Identification of the ligand trans to cysteinate in the native enzyme. *Journal of Biological Chemistry* **1982**, *257*, 3606–3617.

[139] M. Sono, L. Andersson, J. Dawson. Sulfur donor ligand binding to ferric cytochrome P-450-CAM and myoglobin. Ultraviolet-visible absorption, magnetic circular dichroism, and electron paramagnetic resonance spectroscopic investigation of the complexes. *Journal of Biological Chemistry* **1982**, *257*, 8308–8320.

[140] K. Uchida, T. Shimizu, R. Makino, K. Sakaguchi, T. Iizuka, Y. Ishimura, T. Nozawa, M. Hatano. Magnetic and natural circular dichroism of L-tryptophan 2, 3-dioxygenases and indoleamine 2, 3-dioxygenase. I. Spectra of ferric and ferrous high spin forms. *Journal of Biological Chemistry* **1983**, *258*, 2519–2525.

[141] J. Dawson, M. Sono. Cytochrome P-450 and chloroperoxidase: thiolate-ligated heme enzymes. Spectroscopic determination of their active-site structures and mechanistic implications of thiolate ligation. *Chemical Reviews* **1987**, *87*, 1255–1276.

[142] J. Dawson, M. Sono, L. Hager. The active sites of chloroperoxidase and cytochrome P-450-CAM: Comparative spectroscopic and ligand binding properties. *Inorganica Chimica Acta* **1983**, *79*, 184–186.

[143] J. Peterson, Y. Ishimura, B. Griffin, et al.. Pseudomonas putida cytochrome P-450: characterization of an oxygenated form of the hemoprotein. *Archives of biochemistry and biophysics* **1972**, *149*, 197.

[144] C. Tyson, J. Lipscomb, I. Gunsalus. The roles of putidaredoxin and P450cam in methylene hydroxylation. *Journal of Biological Chemistry* **1972**, *247*, 5777–5784.

[145] M. Purdy, L. Koo, P. de Montellano, J. Klinman. Steady-state kinetic investigation of cytochrome P450cam: interaction with redox partners and reaction with molecular oxygen. *Biochemistry* **2004**, *43*, 271–281.

[146] L. Eisenstein, P. Debey, P. Douzou. P450cam: Oxygenated complexes stabilized at low temperature. *Biochemical and biophysical research communications* **1977**, *77*, 1377–1383.

[147] N. Gerber, S. Sligar. A role for Asp-251 in cytochrome P-450cam oxygen activation. *Journal of Biological Chemistry* **1994**, *269*, 4260–4266.

[148] T. Hishik, H. Shimada, S. Nagano, T. Egawa, Y. Kanamori, R. Makino, S. Park, S. Adachi, Y. Shiro, Y. Ishimura. X-ray crystal structure and catalytic properties of Thr252Ile mutant of cytochrome P450cam: roles of Thr252 and water in the active center. *Journal of biochemistry* **2000**, *128*, 965–974.

[149] T. Poulos. Intermediates in P450 catalysis. *Philosophical Transactions of the Royal Society A: Mathematical, Physical and Engineering Sciences* **2005**, *363*, 793–806.

[150] E. Whittle, D. Dows, G. Pimentel. Matrix isolation method for the experimental study of unstable species. *The Journal of Chemical Physics* **1954**, *22*, 1943–1943.

[151] J. Turner, G. Pimentel. Krypton fluoride: preparation by the matrix isolation technique. *Science See Saiensu* **1963**, *140*.

[152] J. Bragger, R. Dunn, R. Daniel. Enzyme activity down to- 100 C. *Biochimica et Biophysica Acta (BBA)-Protein Structure and Molecular Enzymology* **2000**, *1480*, 278–282.

[153] V. Réat, J. Finney, A. Steer, M. Roberts, J. Smith, R. Dunn, M. Peterson, R. Daniel. Cryosolvents useful for protein and enzyme studies below- 100 ° C. *Journal of Biochemical and Biophysical Methods* **2000**, *42*, 97–103.

[154] J. Dashnau, N. Nucci, K. Sharp, J. Vanderkooi. Hydrogen bonding and the cryoprotective properties of glycerol/water mixtures. *The Journal of Physical Chemistry B* **2006**, *110*, 13670–13677.

[155] I. G. Denisov, D. C. Victoria, S. G. Sligar. Cryoradiolytic reduction of heme proteins: Maximizing dose-dependent yield. *Radiation Physics and Chemistry* **2007**, *76*, 714 – 721.

[156] K. Kobayashi, M. Amano, Y. Kanbara, K. Hayashi. One-electron reduction of the oxyform of 2, 4-diacetyldeuterocytochrome P-450cam. *Journal of Biological Chemistry* **1987**, *262*, 5445–5447.

[157] R. Davydov, R. Kappl, J. Huettermann, J. Peterson. EPR-spectroscopy of reduced oxyferrous-P450cam. *FEBS letters* **1991**, *295*, 113–115.

[158] B. Griffin, J. Peterson, R. Estabrook. Cytochrome P-450: Biophysical properties and catalytic function. *The Porphorins* **1979**, 333–375.

[159] P. Privalov, *Cold denaturation of protein*, *Vol. 25*, Informa UK Ltd UK, **1990**.

[160] N. Prabhu, K. Sharp. Heat capacity in proteins. *Annu. Rev. Phys. Chem.* **2005**, *56*, 521–548.

[161] R. Davydov, T. Yoshida, M. Ikeda-Saito, B. Hoffman. Hydroperoxy-heme oxygenase generated by cryoreduction catalyzes the formation of α-meso-hydroxyheme as detected by EPR and ENDOR. *Journal of the American Chemical Society* **1999**, *121*, 10656–10657.

[162] R. Davydov, B. Hoffman. Active intermediates in heme monooxygenase reactions as revealed by cryoreduction/annealing, EPR/ENDOR studies. *Archives of Biochemistry and Biophysics* **2011**, *507*, 36–43.

[163] S. Gantt, I. Denisov, Y. Grinkova, S. Sligar. The critical iron–oxygen intermediate in human aromatase. *Biochemical and biophysical research communications* **2009**, *387*, 169–173.